Effect of Nanomaterial Dopants on the Physical Properties of Liquid Crystals

THESIS

Submitted in partial fulfilment
of the requirements for the degree of

DOCTOR OF PHILOSOPHY

by

JITENDRA KUMAR

Under the Supervision of

Prof. V. Manjuladevi

BITS Pilani
Pilani | Dubai | Goa | Hyderabad

BIRLA INSTITUTE OF TECHNOLOGY AND SCIENCE, PILANI

2016

BIRLA INSTITUTE OF TECHNOLOGY & SCIENCE PILANI - 333 031 (RAJASTHAN) INDIA

CERTIFICATE

This is to certify that the research work presented in the thesis entitled "**Effect of Nanomaterial Dopants on the Physical Properties of Liquid Crystals**" by **JITENDRA KUMAR**, ID No. 2011PHXF026P at Department of Physics, BITS Pilani, Pilani campus for the award of the degree of Doctor of Philosophy (Ph.D.), is carried out under my guidance and supervision and is fit to be considered for the award of the Ph.D. No part of the present thesis work has ever been submitted in part or in full to any other university or institution for the award of any other degree or diploma.

_____

Signature of the Supervisor
Dr. V. Manjuladevi

Associate Professor,
Department of Physics,
BITS-Pilani, Pilani Campus

Date: _____

Dedicated to My parents ….

Acknowledgements

I wish to express my deep sense of gratitude and indebtedness to my supervisor **Prof. V. Manjuladevi,** Associate Professor in physics department, BITS pilani, for her valuable guidance, encouragement, continuous inspiration and helpful suggestion throughout my research work. Her wide knowledge and logical way of thinking on critical scientific problems have been of great value for me. I am also grateful to her for being patient while critically reviewing this thesis.

I am immensely thankful to the Vice-Chancellor, Directors, Deputy Directors, Deans and Unit Chiefs of Birla Institute of Technology & Science (BITS), Pilani for providing me the opportunity to pursue my doctoral studies by providing necessary facilities and financial support.

I am indebted to Prof. Raj Kumar Gupta for imparted his priceless and meticulous supervision at each and every phase of research work whenever needed. He inspired me in innumerable ways in accomplishing this research work. Thanks are due to him not only for the academic guidance but also for the moral support, consistent kindness and never ending encouragement given by him.

My deepest gratitude to Prof. S. K. Verma, Dean, Academic Research Division (ARD), BITS Pilani, for and to Prof. Hemant Jadhav Associate Dean ARD, for their co-operation and encouragement at every step during my Ph. D. program. My sincere thanks to Dr. Navin Singh Convenor, Departmental Research Committee (DRC), Department of Physics, BITS Pilani, Pilani Campus for his official support and encouragement. I would also like to thank to Prof. D. D. Pant and to Prof. Rakesh Choubisa for their motivation. I overwhelmingly acknowledge the office staff of ARD, whose secretarial assistance helped me in submitting the various evaluation documents in time.

It gives me immense pleasure to thank Prof. Anshuman Dalvi, Head of Physics Department and my Doctoral Advisory Committee (DAC) members, Prof. Anshuman Dalvi and Prof. Raj Kumar Gupta for their support, critical review and suggestions during the progress review and to review my draft thesis. Also, I wish to express my gratitude to all the faculty members of physics department for their kind support time-to time. I would also like to thank to Prof. Sandeep Kumar from Raman Research Institute, Bengaluru for his help and encouragement. I would like to thank all my dear friends and co-scholars, in particular Amar Singh, C. Karthik, Keerti Naresh

Choudhary, Munesh, Ravi, Monika, Devnarayanan V. P., Sunita Joshi and all others for moral support, diversified help, good wishes and several funs which will always be remembered. I thank the technical staff of physics department for their support.

I deeply acknowledge BITS Pilani and UGC BSR for the financial assistance provided during my Ph.D tenure.

I am privileged to fulfill my parents ambition and greatly indebted to them for providing me moral support and good wishes in the completion of research study. I express an appreciation to my wife, Amresh Bhalothiya, for her understanding, and supporting me through the ups and downs inevitable in the completion of a doctoral program. I would like to express my thanks to my sweet daughter, Priyanshi Bhalothiya for being such a good girl always cheering me up.

Finally, I owe my heartfelt gratitude and indebtness to my grandparents, my mummy, my papa, my elder brother Rakesh, and elder sister Sulochana Poonia who have always encouraged me to follow my heart and inspired my inquisitive mind throughout my childhood and study career. It is their inspiration, encouragement, blessings and support that helped me to achieve what I am today. Lastly, I wish to apologize if I forgot the names of persons who had helped me in any way.

Finally, I wish to express my gratitude to all those who are directly or indirectly assisted me & whose help & cooperation made this research work accomplished

JITENDRA KUMAR

Date:_____

Abstract

Liquid crystals (LCs) are the fourth state of matter whose order lies between that of 3-dimensioanlly ordered solids and completely disordered isotropic fluids. The LC materials are mainly used in display technology. The performance characteristics of nematic liquid crystal (NLC) based devices (e.g. liquid crystal displays) depend mainly on some physical parameters such as threshold voltage (V_{th}), voltage holding ratio (VHR), birefringence and dielectric anisotropy. The value of these physical parameters can be tuned by doping with nanomaterials. To alter the physical properties of LCs, nanomaterials viz., functionalized carbon nanotubes (CNT) and nanoparticles have been used as dopants. This thesis mainly focuses on the physical properties such as dielectric constant, elastic constants, as well as optical response time of thermotropic LC which are doped with nanomaterials such as functionalized CNT and nanoparticles. Self-organizing NLC impart their orientational order onto dispersed CNT and obtain CNT self-assembly on a macroscopic dimension. The long axes of nanotubes, being coupled to the nematic director, enables orientational manipulation via the LC nematic reorientation. Electric field induced director rotation of a NLC doped with CNT system is of interest due to its possible application as display devices. Electric field and temperature dependence of dielectric properties of LC and its CNT nanocomposites system have been investigated. We have measured the dielectric anisotropy and optical response time of octadecylamine functionalized single walled CNT (ODA-SWCNT) doped n-octyl cyanobiphenyl (8CB). We found that the dielectric anisotropy as a function of reduced temperature decreases with an increase in the concentration of ODA-SWCNT. The electro-optic response rise time decreases and decay time increases with addition of higher concentrations of ODA-SWCNT. Due to a strong LC-CNT anchoring energy and structural symmetry matching, long axis of CNT follows the director field cause in the enhancement of the order parameter of the NLC media. In order to see the effect of functionalized CNT as the alignment layer on the optical response time and dielectric permittivity of 4-trans-pentylcyclohexylcyanobenzene (5PCH), LC cells were prepared with mixture of small amount of ODA-SWCNT and polyimide (PI). We found that the total response time of 5PCH in twisted nematic (TN) cell treated with mixture of PI and ODA-SWCNT reduced by 55% as compared to cell treated with pure PI. Our studies on TN cells prepared using mixture of ODA-SWCNT and PI alignment layer indicates that the increase in threshold electric field (E_{th}) might be due to strong

anchoring between LC and ODA-SWCNT. The π-π interaction between the ODA-SWCNT, NLC and the PI alignment layer leads to enhanced surface anchoring of the NLC molecules at the substrate. This strong surface anchoring gives rise to increase in elastic constant which gets reflected as a reduction in the optical response time of NLC. The effect of alignment layer of ODA-SWCNT deposited using spin coating and Langmuir-Blodgett (LB) technique on the V_{th} and response time of pure 4-heptyl-4′-cyanobiphenyl (7CB) has been investigated. We observed that the dielectric anisotropy in the cell treated with LB film of ODA-SWCNT is found to be reduced as compared to pure PI treated cell. The response time of 7CB enclosed in LC cells prepared with substrates treated with only ODA-SWCNT is comparable to the one prepared with substrate treated with pure PI. Assembling semiconductor quantum dots (QDs) into nanoscale configurations over macroscopic dimensions is an important goal for realizing their electro-optical potential. The measurement on dielectric permittivity and V_{th} of octadecylamine capped cadmium selenide quantum dots (CdSe QDs) and titanium dioxide (TiO_2) doped NLC as a function of an applied electric field has been carried out to understand the interaction and alignment of QDs in LC matrix. Doping QDs into 5PCH leads to increase in the dielectric anisotropy in comparison with that of pure 5PCH. Improved dielectric anisotropy in CdSe QD doped 5PCH indicates the self-assembly of QDs which can align themselves along with the average direction of NLC molecules (director). In addition to QDs, we investigated the electro-optical and physical properties of nanocomposites of semiconducting TiO_2 nanoparticles and PEG-SWCNT with 5PCH. The effect of doping ODA-SWCNT on the dielectric permittivity of a LC, 10OHF (10OHFBBB1M7), which exhibits unusual smectic phase sequence is investigated. The stability of SmC^* variant phases is checked by doping them with ODA-SWCNT. Dielectric measurements carried out on 10OHF for the cooling cycle confirm that SmC^*_{FI2} phase exists over a higher temperature range than Sm*C** phase. The dielectric measurement carried out at an applied 1 volt confirms that the temperature range of SmC^*_{FI2} phase decreases in the nanocomposites of 10OHF and ODA-SWCNT. For the sample with highest concentration of ODA-SWCNT, SmC^*_{FI2} almost disappears at 1 volt whereas at 5 volt there is no change in the temperature range of SmC^*_{FI2} phase. The study on dielectric permittivity and conductivity of the thermotropic columnar liquid crystalline phases formed by triphenylene based discotic liquid crystal (DLC) and its zinc sulfide (ZnS) nanoparticle & ionic liquid nanocomposites is investigated. The significant change in the conductivity were observed on addition of ZnS

nanoparticles as well as ionic liquid in the pure DLC system. The addition of ZnS nanoparticles lead to enhancement of the dielectric constant of DLC. The electrical conductivity of these nanocomposites was observed to be enhanced by ~ 90% compared to the pure DLC. These nanocomposites of NLC provide an opportunity to develop LC based optoelectronic devices with improved electro-optic switching.

List of abbreviations

Symbol	Abbreviation
AFM	Atomic force microscopy
BMIB-BF_4	1-butyl-3-methylimidazolium tetrafluoroborate
CdSe	Cadmium selenide
CNT	Carbon nanotube
Col	Columnar
Cr	Crystalline
DLC	Discotic liquid crystal
DSC	Differential Scanning Calorimetery
HAT5	Hexakis(pentyloxy)triphenylene
He-Ne	Helium-Neon
ITO	Indium tin oxide
Iso	Isotropic
IL	Ionic liquid
LC	Liquid crystal
LCD	Liquid crystal display
LB	Langmuir-Blodgett
NLC	Nematic liquid crystal
N_D	Discotic nematic
NW	Normally white
ODA-SWCNT	Octadecylamine single walled carbon nanotube
ODSE	Octadecyl triethoxy silane
PI	Polyimide
PEG	Polyethelene glycole
PID	Proportional integral derivative
POM	Polarizing optical microscopy

Symbol	Abbreviation
RTD	Resistance temperature detector
SmA	SmecticA
SRI	Spreading resistance imaging
MWCNT	Multi walled carbon nanotube
STM	Scanning tunneling microscopy
TP10	Hexakis(decycloxy)triphenylene
NP	Nanoparticle
PEG-SWCNT	Polyethelene glycole single walled carbon nanotube
QDs	Quantum dots
TN	Twisted nematic
TiO_2	Titanium dioxide
TP10	Hexakis(decycloxy)triphenylene
ZnS	Zinc sulfide
10OHF	10OHFBBB1M7
2D	Two dimensional
3D	Three dimensional
5PCH	4-trans-pentylcyclohexylcyanobenzene
7CB	4-heptyl-4′-cyanobiphenyl
8CB	n-octyl-cyanobiphenyl

List of symbols

λ	Wavelength
ε	Dielectric constant
$\varepsilon_{\perp}$	Perpendicular component of dielectric constant
$\varepsilon_{\parallel}$	Parallel component of dielectric constant
$\Delta\varepsilon$	Dielectric anisotropy
$\hat{n}$	Nematic director
μ_0	Ordinary refractive index
μ_e	Extraordinary refractive index
τ_0	Decay time
τ_r	Rise time
$\Delta\mu$	Birefringence
γ	Rotational viscosity
V_{th}	Threshold voltage
W	Polar anchoring energy
E_{th}	Threshold electric field
ϕ	Tilt angle
S	Order parameter
F_e	Frank-Free energy
K_{11}	Splay elastic constant
K_{22}	Twist elastic constant
K_{33}	Bend elastic constant
V_0	Amplitude of the output signal
C	Capacitance
φ_m	Phase of output signal
Rs	Series resistance
N*	Chiral Nematic
T_{NI}	Nematic to isotropic transition temperature

CONTENTS

	Table of contents	Page No.
	Certificate	II
	Dedication	III
	Acknowledgements	IV
	Abstract	VI
	List of abbreviations	IX
	List of symbols	XI
	Table of contents	XII
	List of figures	XVII
	List of tables	XXV
1	**Introduction**	**1-26**
	1.1 Liquid Crystals	1
	1.2 Calamitic LC	2
	1.2.1 Nematic (N)	2
	1.2.2 Smectic (Sm)	3
	1.2.2.1 Smectic A (SmA)	4
	1.2.2.2 Smectic C (SmC)	4
	1.2.3 Cholesteric phase (N^*)	5
	1.3 Discotic LCs	6
	1.3.1 Discotic nematic phase (N_D)	7
	1.3.2 Discotic columnar phase (Col)	7
	1.4 Bent core molecules	8
	1.5 Physical properties of NLC	9
	1.5.1 Curvature elasticity	9
	1.5.2 Birefringence	10
	1.5.3 Dielectric constant (ε)	11
	1.5.4 Orientational order parameter (*S*)	12

	Table of contents	Page No.
	1.5.5 Alignment of NLC sample in LC cell	13
	1.5.6 Freedericksz transition in NLCs	15
	1.5.7 Optical response time	16
	1.6 Review of work on liquid crystals and its carbon nanotubes nanocomposites	19
	1.7 Applications of LC	21
	1.8 LC materials	21
	References	24
2	**Experimental techniques**	**27-44**
	2.1 Introduction	27
	2.1.1 Preparation of LC cells	27
	2.1.2 Cell thickness measurement	28
	2.2 Polarizing optical microscopy	29
	2.3 Experimental setup for electro-optic measurements	30
	2.4 Dielectric constant measurement	32
	2.5 Temperature calibration of hot stage using standard LC compound	35
	2.5.1 LabVIEW program to control the temperature of the hot stage	36
	2.6 Elastic constant measurement	37
	2.7 Differential scanning calorimetry (DSC)	41
	2.8 Optical response time	41
	2.9 Atomic force microscopy	42
	2.10 Current-Voltage (*I-V*) characterization technique	44
	References	44
3	**Effect of octadecylamine functionalized SWCNTs on the elastic constants and electro-optic response of a liquid crystal**	**45-52**
	3.1 Introduction	45
	3.2 Materials and methods	46
	3.2.1 Estimation of birefringence	48

	Table of contents	Page No.
	3.3 Results and discussion	49
	3.3.1 Dielectric constant measurement	49
	3.3.2 Order parameter	52
	3.3.3 Elastic constant measurement	53
	3.3.4 Electro-optic response time	57
	3.4 Conclusions	60
	References	61
4	**Fast response in twisted nematic liquid crystal cells: Effect of functionalized carbon nanotubes**	**63-76**
	4.1 Introduction	63
	4.2 Materials and methods	65
	4.3 Results and discussion	66
	4.3.1 Polarizing optical microscopy (POM)	66
	4.4 Effect of ODA-SWCNT in alignment layer on electro-optic response of NLC	69
	4.5 AFM characterization of alignment layer of polyimide and mixture of polyimide and ODA-SWCNT	74
	4.6 Conclusions	75
	References	76
5	**Effect of ODA-SWCNT in alignment layer on the physical properties and optical response time of nematic liquid crystal**	**78-91**
	5.1 Introduction	78
	5.2 Materials and methods	79
	5.3 Results and discussion	80
	5.3.1 Polarizing optical microscopy	80
	5.3.2 Dielectric constant measurement	81
	5.3.3 Elastic constant measurement	83
	5.3.4 Optical response time	85

	Table of contents	Page No.
	5.4 Polarizing optical microscopy	86
	5.5 Conclusions	91
	References	91
6	**Electro-optic and dielectric studies on nanomaterials doped nematic liquid crystal**	**93-104**
	6.1 Introduction	93
	6.2 Materials and methods	95
	6.3 Results and discussion	96
	6.3.1 Effect of CdSe QDs on physical properties of NLC	96
	6.3.2 Effect of TiO_2 nanoparticles on physical properties of NLC	100
	6.4 Conclusions	104
	References	104
7	**Effect of ODA-SWCNT on the dielectric property of a chiral smectic liquid crystal**	**106-114**
	7.1 Introduction	106
	7.2 Materials and methods	108
	7.3 Results and discussion	109
	7.4 Conclusions	113
	References	113
8	**Nanoparticles and ionic liquid in columnar discotic liquid crystalline material**	**115-127**
	8.1 Introduction	115
	8.2 Materials and methods	117
	8.3 Results and discussions	118
	8.3.1 Effect of ZnS nanoparticles on physical properties of TP10	118
	8.3.2 Effect of ionic liquid on the dielectric permittivity and conductivity of TP10	122
	8.4 Conclusions	126
	References	127

	Table of contents	Page No.
9	**Conclusions and future scope of our studies**	**128-133**
	9.1 Conclusions	128
	9.2 Future scope	132
	List of publications	134
	Brief biography of the Candidate	136
	Brief biography of the Supervisor	137

List of Figures

Figure No.	Caption	Page No.
1.1	Schematic diagram of the nematic phase exhibited by rod-like molecules. n̂ is the director which represents the direction of average orientation of the long axes of the rod-like molecules.	3
1.2	Schematic diagram of the molecular arrangement in the layers of the SmA phase. The director n̂ is parallel to the layer normal $\hat{z}$.	4
1.3	Schematic representation of the molecular arrangement in the SmC phase. The molecules are tilted with respect to the layer normal $\hat{z}$.	5
1.4	Schematic representation of molecular arrangement in the cholesteric phase (N*).	6
1.5	Schematic representation of molecular arrangement in (a) nematic and (b) columnar phase formed by disk shaped mesogens.	7
1.6	Chemical structure of banana shaped compound of 5-Cyano-1,3-phenylene bis(3-fluoro-4- benzyloxybenzoate).	9
1.7	A schematic representation of the (a) splay, (b) twist and (c) bend deformations.	10
1.8	Schematic diagrams of the (a) planar and (b) homeotropic alignment of the LC molecules.	13
1.9	Schematic diagrams of the twisted nematic (TN) alignment of the molecules in (a) absence and (b) presence of electric field (NW mode).	15
2.1	Schematic diagram of LC cell.	28
2.2	Schematic diagram of cell thickness measurement using a spectrometer.	29
2.3	Optical texture of nematic liquid crystal between crossed polarizers (a) rubbing direction of the cell making 45° angle with respect to both polarizers and (b) rubbing direction is parallel to polarizer.	30
2.4	Schematic diagram of the electro-optic measurement setup. P and A are polarizer and analyzer, respectively.	31

Figure No.	Caption	Page No.
2.5	Schematic diagram of (a) electrical circuit equivalent of the LC cell and (b) the dielectric constant measurement set up.	32
2.6	Temperature variation of the dielectric constants ($\varepsilon_{\parallel}$ and $\varepsilon_{\perp}$) of 8CB (filled o and Δ symbols correspond to data measured from our experimental set up and reference [8], respectively).	34
2.7	Transition temperatures observed using hot stage *Vs* transition temperatures of known sample.	36
2.8	The LabVIEW program for measuring the temperature of the hot stage.	37
2.9	Schematic diagram of Freedericksz transition in the splay geometry.	38
2.10	Variation of ratio of capacitance $(C-C_{\perp})/C_{\perp}$ as a function of inverse of applied voltage.	40
2.11	Bend elastic constant (K_{33}) value of 8CB estimated using the data obtained from our experimental set up and value from the reference [8] as a function of reduced temperature.	40
2.12	DSC data for 8OCB in heating and cooling mode.	41
2.13	Oscillogram of the response time of NLC molecules in TN cell.	42
2.14	Schematic diagram of AFM.	43
3.1	Molecular structure of 8CB and its phase transition temperatures (a). Chemical structure of ODA-SWCNT (b).	46
3.2	Photograph of solution of ODA-SWCNT dispersed in chloroform at (a) 0.3 mg/ml and (b) 0.03mg/ml.	47
3.2	(a) The temperature variation of the transmitted intensity of 8.5 μm thick sample of 8CB and (b) transmitted intensity as a function of applied voltage.	48
3.4	Variation of birefringence ($\Delta\mu$) as a function of reduced temperature ($T-T_{NI}$) for pure 8CB and its ODA-SWCNT nanocomposites.	49
3.5	Variation of dielectric constant (ε) as a function of reduced temperature ($T-T_{NI}$) for pure 8CB and its ODA-SWCNT nanocomposites.	50

Figure No.	Caption	Page No.
3.6	Variation of the dielectric anisotropy (Δε) as a function of reduced temperature (T-T_{NI}) for 8CB (*and o symbols correspond to Δε from our measurements and reference [22] respectively).	51
3.7	Variation of dielectric anisotropy (Δε) as a function of reduced temperature (T-T_{NI}) for pure 8CB and its ODA-SWCNT nanocomposites.	51
3.8	Temperature variation of Δε fitted using Haller's extrapolation method for pure 8CB.	52
3.9	Order parameter (S) as a function of reduced temperature (T-T_{NI}) for pure 8CB and its ODA-SWCNT nanocomposites.	53
3.10	(a) Splay elastic constant (K_{11}) as a function of reduced temperature (T-T_{NI}) for pure 8CB and its ODA-SWCNT nanocomposites and (b) estimated K_{11} for pure 8CB and reference [22, 23].	54
3.11	Variation of bend elastic constant (K_{33}) as a function of reduced temperature (T-T_{NI}) for pure 8CB and its ODA-SWCNT nanocomposites.	54
3.12	Elastic constant ratio (K_{33}/K_{11}) as a function of concentration of ODA-SWCNT in the nanocomposites of 8CB at various temperatures	55
3.13	Splay elastic constant (K_{11}) as a function of square of order parameter (S^2) in the nematic phase for pure 8CB and its ODA-SWCNT nanocomposites.	56
3.14	Bend elastic constant (K_{33}) as a function of square of order parameter (S^2) in the nematic phase for pure 8CB and its ODA-SWCNT nanocomposites.	57
3.15	Threshold voltage (V_{th}) as a function of reduced temperature (T-T_{NI}) for pure 8CB and its ODA-SWCNT nanocomposites.	57
3.16	Rise time (a) and (b) decay time as a function of applied voltage peak-to-peak (V_{PP}) in the nematic phase at a reduced temperature T-T_{NI}= -2^0C for 8CB as well as its ODA-SWCNT nanocomposites.	58
3.17	Rise time (a) and (b) decay time as a function of applied voltage peak-to-peak (V_{PP}) in the nematic phase at a reduced temperature T-T_{NI}= - 3°C for 8CB as well as its ODA-SWCNT nanocomposites.	59

Figure No.	Caption	Page No.
3.18	A schematic model representing the orientation of ODA-SWCNT nanocomposites of LC in the planar aligned LC cell: at lower concentration of ODA-SWCNT ($\leq$ 0.05 wt%) (a) without and (b) with electric field, and at higher concentration of ODA-SWCNT (c) without and (d) with electric field.	60
4.1	Molecular structure of 5PCH (4-trans-pentylcyclohexylcyanobenzene).	65
4.2	Optical textures of pure 5PCH and its ODA-SWCNT nanocomposites in TN cells as observed between the cross polarizers of a polarizing optical microscope.	66
4.3	Transmitted intensity as a function of applied voltage for pure 5PCH and its ODA-SWCNT nanocomposites at a reduced temperature (T_{NI}-T) of 3.7°C.	67
4.4	Threshold electric field (E_{th}) as a function of reduced temperature (T_{NI}-T) for pure 5PCH and its ODA-SWCNT nanocomposites.	67
4.5	(a) Rise time and (b) decay time of the TN cells as a function of applied electric field for pure 5PCH and its ODA-SWCNT nanocomposites.	68
4.6	Transmittance as a function of applied voltage for pure 5PCH in TN cell fabricated using mixtures of PI and ODA-SWCNT as alignment layers.	70
4.7	Threshold electric field (E_{th}) as a function of reduced temperature (T_{NI}-T) for pure 5PCH in TN cell fabricated using mixtures of PI and ODA-SWCNT as an alignment layer.	70
4.8	Dielectric constant as a function of applied voltage for pure 5PCH in TN cell fabricated using mixtures of PI and ODA-SWCNT as alignment layers.	71
4.9	Measured oscillograms for 5PCH in TN cells prepared with pure PI and mixtures of PI and ODA-SWCNT as alignment layers at an applied voltage of 10V	72
4.10	(a) Rise time and (b) decay time as a function of applied electric field for pure 5PCH in TN cell fabricated using mixtures of PI and ODA-SWCNT as alignment layer.	72

Figure No.	Caption	Page No.
4.11	AFM images of ITO substrates treated with pure PI and mixtures of ODA-SWCNT and PI.	74
4.12	Roughness of ITO coated glass plates treated with pure PI and its mixture with different concentration of ODA-SWCNT.	75
5.1	Chemical structure of 4-heptyl-4′-cyanobiphenyl (7CB).	79
5.2	POM images of 7CB confined in LC cells prepared with pure PI (A) and (B), mixture of PI and ODA-SWCNT with 0.16 μg/ml concentration (C) and (D), 0.33 μg/ml concentration (E) and (F) 0.66 μg/ml concentration (G) and (H). Rubbing direction is at 45° to the polarizer in Figure 5.2(A), (C), (E) and (G) while those are parallel to the polarizer shown in Figure 5.2 (B), (D), (F) and (H).	81
5.3	Dielectric constant ($\varepsilon_{\perp}, \varepsilon_{\parallel}$) as a function of reduced temperature (T_{NI}-T) for pure7CB in planar cell fabricated using pure PI as well as mixtures of PI and ODA-SWCNT as the alignment layer.	82
5.4	Dielectric anisotropy as a function of reduced temperature (T_{NI}-T) for pure 7CB in planar cell fabricated using pure PI as well as mixtures of PI and ODA-SWCNT as the alignment layer.	82
5.5	(a) Threshold voltage (V_{th}) and (b) splay elastic constant (K_{11}) as a function of reduced temperature (T_{NI}-T) for pure 7CB in planar cell fabricated using pure PI as well as mixtures of PI and ODA-SWCNT.	83
5.6	Bend elastic constant (K_{33}) as a function of reduced temperature (T_{NI}-T) for pure 7CB in planar cell fabricated using pure PI as well as mixtures of PI and ODA-SWCNT.	84
5.7	(a) Rise time and (b) decay time as a function of applied voltage for pure 7CB in planar cell fabricated using pure PI as well as mixtures of PI and ODA-SWCNT as an alignment layer.	85

Figure No.	Caption	Page No.
5.8	POM images of 7CB in LC cells treated with alignment layer polyimide (A) mixture of polyimide and ODA-SWCNT using spin coating (B) ODA-SWCNT using LB technique (C) ODA-SWCNT using spin coating technique (D).	86
5.9	Dielectric constant as a function of reduced temperature (T_{NI}-T) for pure 7CB in planar cell fabricated using pure PI, mixture of PI and ODA-SWCNT and only ODA-SWCNT deposited by spin coating as well as LB techniques.	87
5.10	Dielectric anisotropy as a function of reduced temperature (T_{NI}-T) for pure 7CB in planar cell fabricated using pure PI, mixture of PI and ODA-SWCNT and only ODA-SWCNT deposited by spin coating as well as LB techniques.	88
5.11	(a) Threshold voltage (V_{th}) and (b) splay elastic constant (K_{11}) as a function of reduced temperature (T_{NI}-T) for pure 7CB in planar cell fabricated using pure PI, mixture of PI and ODA-SWCNT and only ODA-SWCNT deposited by spin coating as well as LB techniques.	89
5.12	Bend elastic constant (K_{33}) as a function of reduced temperature for pure 7CB in planar cell fabricated using pure PI, mixture of PI and ODA-SWCNT and only ODA-SWCNT deposited by spin coating as well as LB techniques.	89
5.13	(a) Rise time and (b) decay time as a function of applied voltage for pure 7CB in planar cell fabricated using pure PI, mixture of PI and ODA-SWCNT and only ODA-SWCNT deposited by spin coating as well as LB techniques.	90
5.14	Rotational viscosity as a function of reduced temperature for pure 7CB in planar cell fabricated using pure PI, mixture of PI and ODA-SWCNT and only ODA-SWCNT deposited by spin coating as well as LB techniques.	91
6.1	Chemical structure of 4-trans-pentylcyclohexylcyanobenzene (5PCH) and its phase transition temperatures.	95
6.2	Dielectric constant ($\varepsilon_{\perp}, \varepsilon_{\parallel}$) for pure and CdSe QDs doped NLC as a function of reduced temperature (T_{NI}-T).	97
6.3	Dielectric anisotropy for pure and CdSe QDs doped NLC as a function of reduced temperature (T_{NI}-T).	97

Figure No.	Caption	Page No.
6.4	Threshold voltage (V_{th}) for pure and CdSe QDs doped NLC as a function of reduced temperature (T_{NI}-T).	98
6.5	Splay elastic constant (K_{11}) for pure and CdSe QDs doped NLC as a function of reduced temperature (T_{NI}-T).	99
6.6	Dielectric constant ($\varepsilon_{\parallel}, \varepsilon_{\perp}$) for pure 5PCH and its nanocomposites of TiO_2 nanoparticles and PEG-SWCNT as a function of temperature.	101
6.7	Dielectric anisotropy ($\Delta\varepsilon$) for pure 5PCH and its nanocomposites of TiO_2 nanoparticles and PEG-SWCNT as a function of temperature.	102
6.8	Threshold voltage (V_{th}) for pure 5PCH and its nanocomposites of TiO_2 nanoparticles and PEG-SWCNT as a function of temperature.	103
6.9	Splay elastic constant (K_{11}) for pure 5PCH and its nanocomposites of TiO_2 and PEG-SWCNT as a function of temperature.	103
7.1	The five chiral smectic-C^*_{tilted} subphases drawn in the same order as usually observed upon heating. Ellipses, numbered by layer indices, represent the projections of the molecules onto the smectic layer plane [7].	107
7.2	Chemical structure of the compound 10OHF and its phase transition temperature.	108
7.3	Temperature dependence of the dielectric permittivity at 1 and 5 volt at a frequency of 1 kHz for pure 10OHF in the cooling mode.	109
7.4	Temperature dependence of dielectric permittivity at 1 volt with 1 kHz for pure 10OHF and its ODA-SWCNT nanocomposites in the cooling mode.	110
7.5	Temperature dependence of dielectric permittivity at 5 volt at 1 kHz for pure 10OHF and its ODA-SWCNT nanocomposites in the cooling mode.	111
7.6	Dielectric permittivity for the pure 10OHF and its ODA-SWCNT nanocomposites at a frequency of 1 kHz as a function of applied voltage at a temperature of 72°C. Open and closed symbols represent the decreasing and increasing voltage, respectively.	112

Figure No.	Caption	Page No.
8.1	Chemical structure of TP10 [hexakis(decyloxy)triphenylene] and 1-Butyl-3-methylimidazolium tetrafluoroborate (BMIM-BF_4).	117
8.2	DSC curves for pure TP10 and its nanocomposites with 2 and 5 *w*t% of ZnS.	118
8.3	Variation of dielectric constant for TP10 and its ZnS nanocomposites as a function of temperature.	119
8.4	Conductivity of pure TP10 and its ZnS nanocomposites as a function of temperature.	120
8.5	*I-V* characteristics of pure TP10 and its ZnS nanocomposites in columnar phase in plane geometery.	121
8.6	Conductance of pure TP10 and its ZnS nanocomposites in columnar phase.	121
8.7	DSC curves for pure TP10 and its nanocomposites with 2.5 and 4.5 *w*t% of ionic liquid (IL) BMIM-BF_4.	122
8.8	Variation of dielectric constant for TP10 and its BMIM-BF_4 nanocomposites as a function of temperature.	123
8.9	Conductivity of pure TP10 and its BMIM-BF_4 nanocomposites as a function of temperature.	124
8.10	Variation of dielectric constant for TP10 and its BMIM-BF4 nanocomposites as a function of temperature in the cells treated with mixture of HAT5 and graphene.	125
8.11	Conductivity of pure TP10 and its BMIM-BF4 nanocomposites as a function of temperature in the cells treated with mixture of HAT5 and graphene.	126
9.1	Measured oscillogram for 5PCH in TN cells prepared with pure PI and mixtures of PI and ODA-SWCNT as the alignment layers at an applied voltage of 10V. AL1, AL2, AL3 and AL4 correspond to LC cell prepared with pure PI, 0.16, 0.33 and 0.66 μg of ODA-SWCNT in 1 ml PI solution, respectively.	129

List of Tables

Table No.	Caption	Page No.
1.1	LC materials and their phase transition temperatures.	22
2.1	LC materials and their phase transition temperatures	35

Chapter 1

Introduction

1.1 Liquid Crystals

The molecules in highly ordered crystalline state occupy specific sites in a three dimensional lattice or regular periodic structure, i.e., they have long range three dimensional (3D) positional and orientational order. When a crystalline solid is heated to the melting point, it transforms into isotropic liquid with random orientation of molecules. Some organic compounds, when they are heated, the formation of one or more phases with molecular ordering less than the crystalline state and more than the isotropic liquid state is observed. Such organic compounds are known as mesogens. These intermediate phases are known as liquid crystal (LC) phase. The LC phases also known as mesophases since their properties lie between an isotropic liquid and a 3D ordered solid crystal phase [1, 2]. The LC phase was first observed by Reinitzer in 1888 [3]. Later, Lehman [4] identified liquid crystalline phases in some cholesteryl compounds.

The LCs are classified into two categories viz., thermotropic and lyotropic. The transition in thermotropic LC phases can be driven as a function of temperature. The LC phase can be obtained either by heating a crystalline solid or by cooling an isotropic liquid. The mesogens exhibit mesophases either only on heating the crystalline solid or only on cooling an isotropic liquid are known as monotropic LCs and when the mesophases are observed on both heating and cooling, the mesogens are called enantiotropic LCs [1, 2]. Thermotropic LCs find widespread applications in electro-optic devices e.g. liquid crystal displays (LCD), smart windows [5], temperature and pressure sensors [6].

Lyotropic LC materials exhibit mesophase when amphiphilic molecules are dissolved in a solvent at an appropriate concentration. The phases of lyotropic LCs are dependent on concentration, temperature, pH and salt content. Lyotropic LCs can be observed in biological system, paints and colloids etc.

Classification of LC based on shape

Thermotropic LCs are most widely used and extensively studied for their linear as well as nonlinear optical properties. In general, mesogens should possess some shape anisotropy for exhibiting LC phases. Therefore, a large number of LC molecules possessing different degree of shape anisotropy have been synthesized. The thermotropic LCs are classified into three categories depending on the shape anisotropy of the molecule,

(i) Calamitic
(ii) Discotic
(iii) Banana

These LCs are composed of rod-like, disc-like and bent-core molecules, respectively.

1.2 Calamitic LC

Molecules with cylindrical symmetry are known as calamitic LCs. Most of the rod-shaped meosgenic compounds consist of a rigid core of two or more aromatic ring systems, which are linked together directly or through connecting groups and one or two flexible chains are attached at the end. The rigid core is often made of phenyl- or cyclohexane-rings, and sometimes heterocyclic aromatic organic compound such as pyrimidine. These rigid units induce orientational arrangement of molecules by providing strong intermolecular interactions. Formation of the mesophase is a consequence of a delicate interaction between rigid and flexible moieties in these molecules. Regardless of the molecular shape and structure, LC phases can be classified based on symmetry and the degree of ordering of LC molecules. In this chapter, we have described some common LC phases, which are employed for our studies.

1.2.1 Nematic (N)

Nematic is one of the fundamental LC phases. In nematic phase, the molecules have a long range orientational order but no translational order. This is the least ordered LC phase. The long axes of the molecules are on an average oriented along a specific direction, which is denoted by a unit vector ($\hat{n}$), called the director. The molecules in this phase can rotate freely about the long molecular axes but maintain their original orientation. The nematic liquid crystals (NLC) are uniaxial, i.e. there exists rotational symmetry around director $\hat{n}$. In this phase, even if the individual molecules possess permanent electric dipoles, they will assemble in such a way that the net electric

polarization is zero hence the nematic director $\hat{n}$ is a dimensionless apolar vector i.e. ($\hat{n} \equiv -\hat{n}$) [1]. NLCs reorient easily along the applied electric field and hence are used in LC device applications such as LCD. The schematic diagram of molecular arrangement in nematic phase is shown in Figure 1.1.

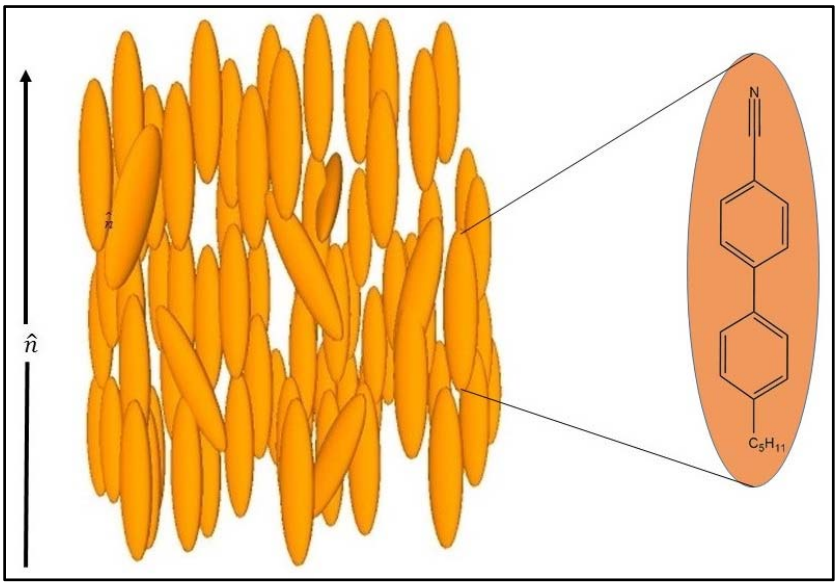

Figure 1.1: Schematic diagram of the nematic phase exhibited by rod-like molecules. n̂ is the director which represents the direction of average orientation of the long axes of the rod-like molecules.

1.2.2 Smectic (Sm)

In addition to long range orientational order, there exists 1D or 2D translational order in smectic phase (Sm) which arises from a layered arrangement of the molecules [1]. There are several type of smectic phases, which are characterized by a variety of molecular arrangements within the layers. Based on the moleculer arrangement and orientation of molecules within the layers, the smectic phases are further classified into SmA, SmB, SmC, SmE, SmF, SmG, SmH, SmI and SmJ. The SmB, SmF and SmI phases are more ordered in which the molecules are arranged in hexagonal order within the layers. Disordered crystals having layer-like structures are often referred to as SmE, SmH, SmK, SmG and SmJ phases and they are more properly defined as lamellar plastic crystals. Among these smectic phases, two most commonly observed smectic phases are the smectic-A (SmA) and the smectic-C phase (SmC).

1.2.2.1 Smectic-A (SmA)

In the SmA phase, the molecules are positionally random in layers, but orientationally ordered with their long axis normal to the plane of the layer. The interlayer attractions are relatively weak and the layers can slide over one another relatively easily and each layer behaves as a two dimensional liquid [2]. Hence, this phase has fluid properties, though it is much more viscous than nematic. The LC molecules in the SmA phase are optically uniaxial similar to nematics i.e, there is a rotational symmetry around the director axis. The schematic diagram of molecular arrangement in SmA phase is shown in Figure 1.2.

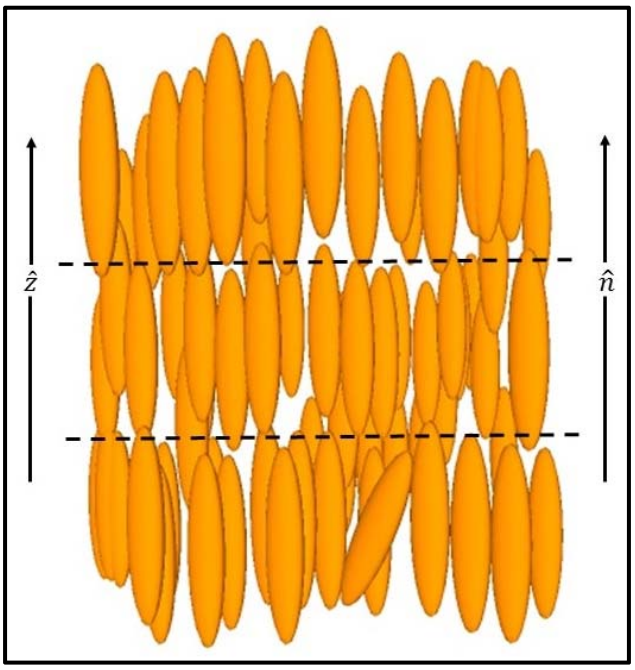

Figure 1.2: Schematic diagram of the molecular arrangement in the layers of the SmA phase. The director $\hat{n}$ is parallel to the layer normal $\hat{z}$.

1.2.2.2 Smectic-C (SmC)

The SmC phase has the layer structure similar to SmA, but the molecular arrangement is such that the long axes of molecules is tilted with respect to the layer normal. The SmC phase is optically biaxial unlike the SmA and nematic phase. Because of the anisotropic polarizability, SmC becomes optically biaxial [2]. The schematic diagram of molecular arrangement in SmC phase is shown in Figure 1.3.

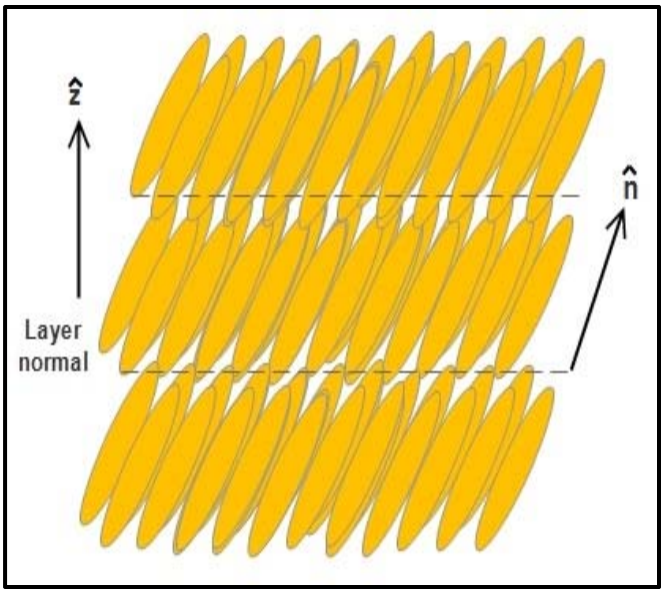

Figure 1.3: Schematic representation of the molecular arrangement in the SmC phase. The molecules are tilted with respect to the layer normal $\hat{z}$.

1.2.3 Cholesteric phase (N*)

The first chiral nematic phase (N*) was discovered in 1888 by Austrian botanist, Reinitzer. The chiral nematic phase is also called the cholesteric phase. The cholesteric LC phase (N*) is exhibited by mesogenic molecules which are optically active or by NLCs doped with small quantity of chiral molecules. When a chiral molecule is incorporated into the nematic mesophase, the complete structure can be visualized as a stack of very thin 2D nematic layers with the director in each layer twisted with respect to consecutive layers [2]. This further induces a helical director configuration in which the director rotates throughout the sample and hence termed as twisted nematic (Nt) or chiral nematic (N*). An important characteristic of the cholesteric mesophase is its pitch (p), which can be defined as the distance travelled by the director to rotate one full turn in the helix. The helical structure has the ability to selectively reflect light, if the pitch length is equal to the wavelength of light in visible spectrum. For this reason, the chiral nematic materials can be used in thermochromic thermometer devices. The schematic diagram of molecular arrangement in cholesteric phase is shown in Figure 1.4.

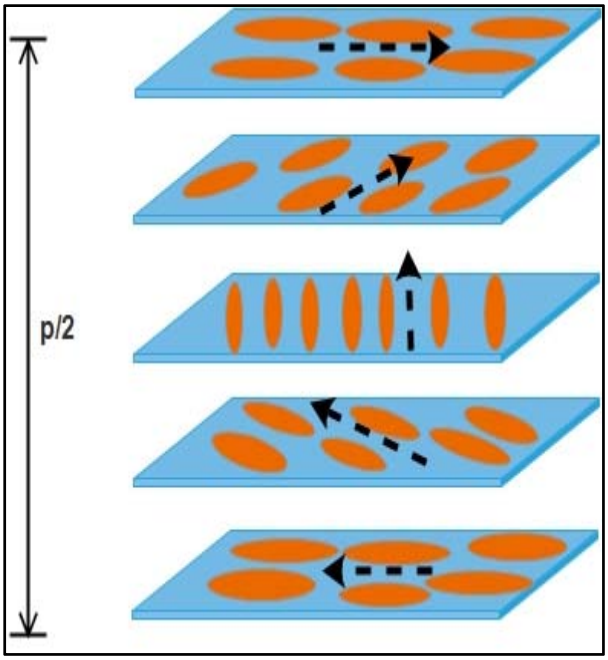

Figure 1.4: Schematic representation of molecular arrangement in the cholesteric phase (N*).

LC made up of disk shape molecules

In addition to calamitic molecules, there are different shape anisotropic molecules, which exhibit LC phases. In 1977, the disc shaped mesogen was first discovered by Chandrasekhar *et al* [5]. These LCs are of great interest from many applications point of view.

1.3 Discotic LCs

The LC phases exhibited by disc shaped mesogens are called as discotic LCs. The DLC molecules are composed of π–conjugated central core with covalently attached 6-8 side groups. These discotic material form a new class of LC, in which molecules are stacked on one top of other to build columnar phases with long-range two-dimensional order of the columns. The self-organization of the molecules due to strong π–π interaction between the discotic cores, leads to the formation of various LC phases. The strong π–π interaction between the cores results in the high charge mobility along the column axis. The high anisotropy in the charge mobility results in quasi-one dimensional conductivity along the columns [7]. Due to anisotropy in conductivity, discotic LCs find applications in devices like field effect transistor, light emitting diode, photovoltaic solar cell, sensors and memory devices [8-10]. The discotic molecules also exhibit various LC phases like calamitic molecules, depending on the organization of molecules. The

molecular arrangement of discotic mesogens in nematic and columnar phases are shown in Figure 1.5(a) and 1.5(b), respectively.

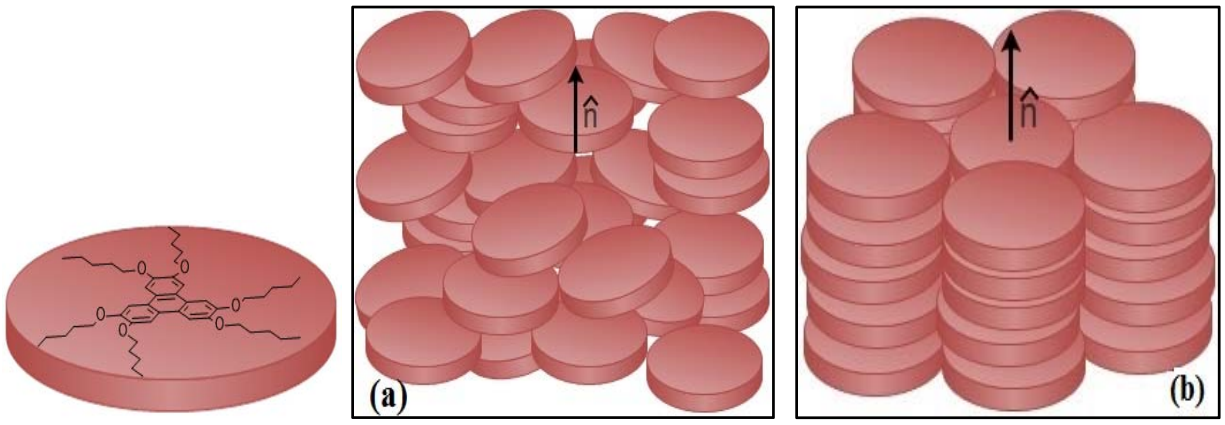

Figure 1.5: Schematic representation of molecular arrangement in (a) nematic and (b) columnar phase formed by disk shaped mesogens.

1.3.1 Discotic nematic phase (N_D)

The simplest, least-ordered mesophase formed by disc-like molecules is the discotic nematic (N_D) phase (Figure 1.5 (a)). This phase is similar to the nematic phase exhibited by the calamitic LCs. In the N_D phase, the molecular axis perpendicular to disc-plane align on average in one particular direction, known as director $\hat{n}$. In this phase, the molecules have only the long range orientational order but no positional order. If the discotic molecules are chiral in nature or if chiral dopant is added into discotic LC materials, the material may exhibit chiral discotic nematic phase. Similar to the cholesteric phase, there is a gradual change in the direction of orientation of the short axis.

1.3.2 Discotic columnar phase (Col)

In this phase, the molecules are stacked on one top of other to form column like structures (Figure 1.5(b)). The columns are arranged in a two dimensional (2D) lattice. Depending on the 2D lattice formation of the columns, the columnar phases are classified as hexagonal, rectangular and oblique phases.

Columnar hexagonal phase is characterized by a hexagonal packing of the molecular columns. Hexagonal mesophases are often denoted as Col_{ho} or Col_{hd} where h stands for hexagonal and o or d for ordered or disordered stacking of the molecules. The columnar rectangular mesophase consists of the stacking of the aromatic cores of the molecules in columns surrounded

by the disordered aliphatic chains, and the columns are packed in a rectangular fashion. Columnar rectangular phase is denoted by Col_r. In the columnar oblique mesophase, the columns are arranged with an oblique unit cell.

1.4 Bent core molecules

In addition to calamitic and discotic mesogens, the mesogens, which are bent shaped also exhibit LC phases. The mesogen with bent-shaped molecules was first synthesized by Vorlander in 1929 [11]. In the formation of mesophases by bent-core molecules, the central bent-core, side arms, their linking to each other, as well as the linking of various organic fragments in the side arms play significant role [12]. Various mesophases are exhibited by bent core molecules like B1, B2….B8 phases, where B stands for bent core. In addition to B phase, they also exhibit nematic and smectic phases.

Niori *et al*. [13], have reported ferroelectric properties exhibited by achiral compound namely 1, 3-phenylene bis [4-(4-noctyliminomethyl) benzoate]. It was shown that due to their bent shape, the molecules can preferably be packed in bent direction giving rise to a long-range correlation of the dipole moments leading to macroscopic polarization in the smectic layers. Hence, bent core molecule exhibits antiferroelectric switching although the molecule is non-chiral. The LC phase in which molecules are arranged perpendicular to the layers like in SmA phases but they possess a polar packing (in bent direction) within the layer plane are known as SmAP phase. Depending on the direction of the polar axes in adjacent layers, the SmAP phase can behave as ferroelectric (polar axes parallel in adjacent layer, $SmAP_F$) or antiferroelectric (polar axes antiparallel in adjacent layer, $SmAP_A$). A chemical structure of banana shaped compound of 5-cyano-1,3-phenylene bis(3-fluoro-4- benzyloxybenzoate) (5CN) is shown in Figure 1.6.

Due to polar order and the macroscopic chiral superstructures, the bent core LCs can be used in nonlinear optics, flexoelectricity and photoconductivity applications. Bent-core NLC has been extensively studied for various physical properties such as dielectric properties, optical properties, rheological and elastic properties, ferroelectric, and antiferroelectric properties [8].

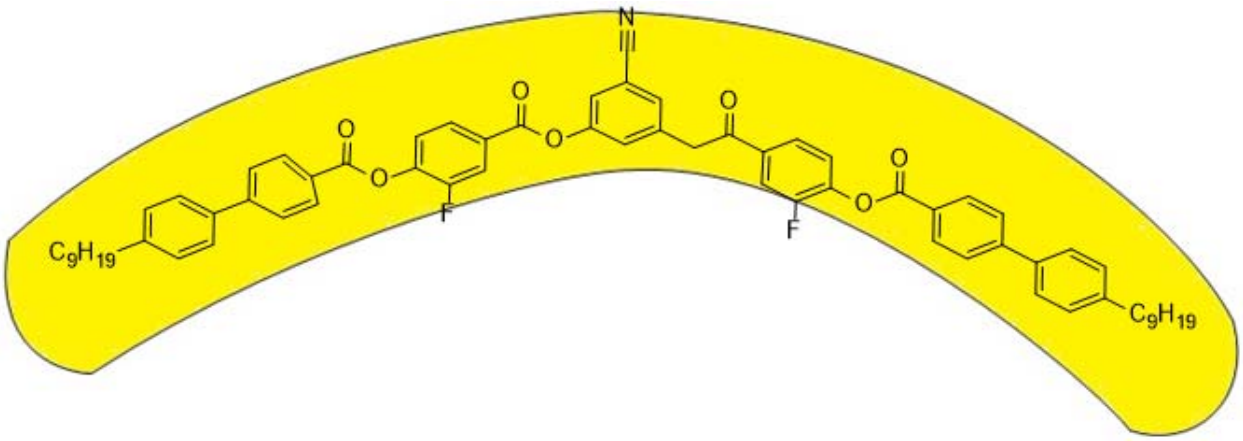

Figure 1.6: Chemical structure of banana shaped compound of 5-Cyano-1,3-phenylene bis(3-fluoro-4-benzyloxybenzoate) (5CN).

1.5 Physical properties of NLC

Due to the molecular shape anisotropy and preferential orientation of the molecules, NLC medium exhibit anisotropic physical properties. NLCs exhibit anisotropy in the refractive indices, dielectric constants, and diamagnetic susceptibilities, which make them suitable candidates for their applications in display devices. In order to use the NLCs in LCD technology, a uniform alignment of LC material is important. The performance characteristics of LC based devices like operating voltage, viewing angle and contrast ratio depends on physical properties such as elastic constants, dielectric anisotropy, birefringence, and viscosity of liquid crystalline materials [14]. The study on physical parameters such as threshold voltage (V_{th}), dielectric permittivity parallel and perpendicular to molecular long axes ($\varepsilon_{\parallel}$, $\varepsilon_{\perp}$), dielectric anisotropy ($\Delta\varepsilon$), elastic constants (splay and bend), and response time (rise time and decay time) are mainly focused in this thesis.

1.5.1 Curvature elasticity

In a well aligned nematic, the molecules on average are oriented along the direction of director. Due to externally applied field (electric and magnetic) or mechanical stress from the boundary surfaces, the direction of director will vary spatially. The distortions of the director from uniform alignment occur over microscopic length. The deformation of LCs can be considered as a combination of three basic curvature deformations. Each of these deformations cost positive

energy. The theory of describing elasticity in terms of the director distortions was initiated by Oseen [15] and Zocher [16]. It was further developed by Frank [17] and Ericksen [18].

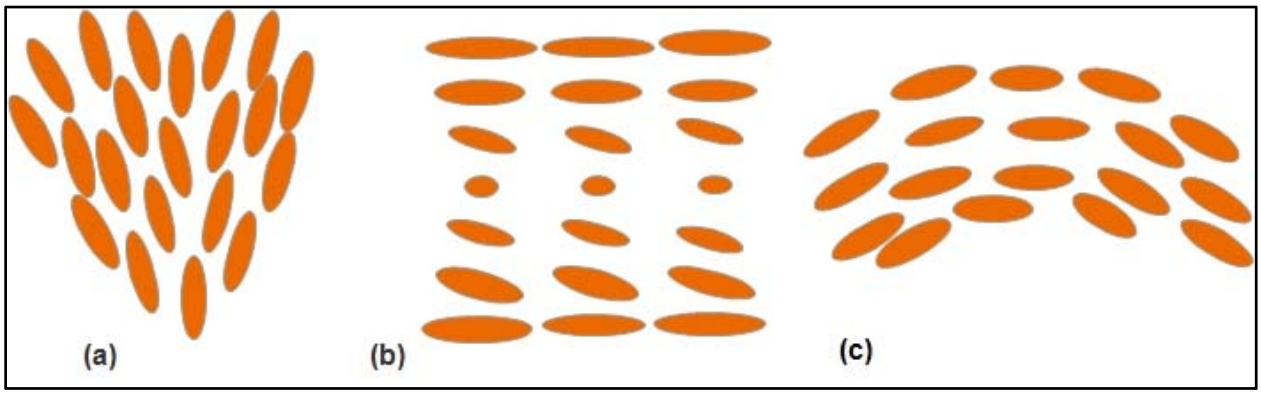

Figure 1.7: A schematic representation of the (a) splay, (b) twist and (c) bend deformations.

The elasticity of NLC can be described in terms of the free energy density due to these deformations. This free energy is referred to as Frank free energy.

$$F_e = \frac{1}{2}K_{11}[\nabla.\hat{n}]^2 + \frac{1}{2}K_{22}[\hat{n}.(\nabla \times \hat{n})]^2 + \frac{1}{2}K_{33}[\hat{n} \times (\nabla \times \hat{n})]^2 \qquad (1.1)$$

where K_{11}, K_{22} and K_{33} are referred to as splay, twist and bend elastic constants respectively. The schematic representation of splay, twist and bend deformation is shown in Figure 1.7. The typical magnitudes of these constants are about 10^{-12}N. The elastic constants are positive and usually the magnitude of elastic constants has the following order: $K_{33} > K_{11} > K_{22}$.

1.5.2 Birefringence

In case of uniaxial NLC, the electric vector of incident plane polarized light entering a LC phase splits into two components called ordinary and extraordinary rays. If the polarization axis of light is parallel to the LC director, then the light experiences the extraordinary refractive index (n_e). If the polarization is perpendicular to the LC director, then the light experiences the ordinary refractive index (n_o). The difference between n_e and n_o is called birefringence, defined as $\Delta n = n_e - n_o$. Refractive indices are dependent on the wavelength and temperature. As the temperature increases the birefringence decreases, and typically it varies from 0.01 to 0.2.

The long-range intermolecular interactions in LC phase cause the long axes of molecules to align preferentially parallel over microscopic distances. The distribution of long molecular axes around the nematic director ($\hat{n}$), is characterized by an order parameter (S). From the birefringence

value, we can estimate the approximate orientational order parameter of NLCs. Haller approximation method is used to determine the *S* at temperature slightly away from the clearing point [19].

$$\Delta n = \Delta n_0 (1 - \frac{T}{T_C})^{\alpha} \qquad (1.2)$$

where Δn_0 is the birefringence of perfectly aligned NLC. T_c is the clearing temperature of LC and α is a constant. The order parameter *S* can be estimated using following relation.

$$S = \frac{\Delta n}{\Delta n_0} \qquad (1.3)$$

1.5.3 Dielectric constant (ε)

For display device, dielectric constant (ε) is a very important material property as it determines the degree of coupling between applied electric field and LC molecules. Dielectric constant depends on the intrinsic properties of the material like distribution of the charges in the molecules and intermolecular interactions. In a material with molecules that have permanent dipoles, there is a contribution to the polarizability of the material from the field-induced partial reorientation of the molecular dipoles in an applied electric field. The orientational polarization in LCs has a major contribution to the dielectric constants. In a NLC material, the dielectric constant parallel ($\varepsilon_{\parallel}$) to the director $\hat{n}$ is different from the dielectric constant perpendicular ($\varepsilon_{\perp}$) to the director $\hat{n}$; thus the dielectric anisotropy $\Delta\varepsilon = \varepsilon_{\parallel} - \varepsilon_{\perp}$ is nonzero. The dielectric constant changes with the temperature and the frequency of the applied electric field. In the isotropic liquid phase, the dielectric anisotropy becomes zero. Maier and Meier have extended the Onsager theory of isotropic dipolar liquids and proposed the theory for static dielectric properties of nematics [20].

Maier and Meier [21] showed that the dielectric anisotropy is proportional to the order parameter i.e. $\Delta\varepsilon \propto S$. The sign and magnitude of $\Delta\varepsilon$ depend upon the polarisabilities and the permanent dipole moments of the molecules. It is positive, if the net dipole moment of the molecule is along the long axis, and is negative if the net dipole moment of the molecule is perpendicular to the long axis.

Maier and Meier's theory showed that the electric permittivity measured parallel ($\varepsilon_{\parallel}$) and perpendicular ($\varepsilon_{\perp}$) to the nematic director $\hat{n}$ are related to the molecular quantities by the following equations.

$$\varepsilon_{\parallel} = 1 + 4\pi \frac{N_A \rho h F}{M} \left\{ \bar{\alpha} + \frac{2}{3} \Delta\alpha_0 S + \frac{F\mu^2}{3k_B T} [1 - (1 - 3\cos^2\beta) S] \right\} \quad (1.4)$$

$$\varepsilon_{\perp} = 1 + 4\pi \frac{N_A \rho h F}{M} \left\{ \bar{\alpha} - \frac{1}{3} \Delta\alpha_0 S + \frac{F\mu^2}{3k_B T} [1 + (1 - 3\cos^2\beta) S] \right\} \quad (1.5)$$

Where $\Delta\alpha_0 = \alpha_{\parallel} - \alpha_{\perp}$, is the anisotropy of polarisability of a perfectly oriented medium, N_A is the Avogadro number, ρ the density, M the molecular weight, $h = \frac{3\bar{\varepsilon}}{2\bar{\varepsilon}+1}$, is the cavity field factor and F is the cavity reaction field factor for the spherical cavity and $\bar{\alpha}$ is the average polarisability [22]. μ is the molecular dipole moment and β is the angle between the direction of dipole moment and the long axis of molecule. The average dielectric constant can be obtained from the equations

$$\bar{\varepsilon} = 1 + \frac{4\pi N_A \rho h F}{M} \left\{ \bar{\alpha} + \frac{F\mu^2}{3k_B T} \right\} \quad (1.6).$$

The dielectric anisotropy is given by

$$\Delta\varepsilon = (\varepsilon_{\parallel} - \varepsilon_{\perp}) = 4\pi \frac{N_A \rho h F}{M} \left\{ \Delta\alpha - F\left(\frac{\mu^2}{2k_B T}\right)(1 - 3\cos^2\beta) \right\} S \quad (1.7)$$

Equation (1.7) defines the temperature dependence of the dielectric anisotropy (Δε).

1.5.4 Orientational order parameter (*S*)

The order parameter (*S*) describes the distribution of long axes of the molecules along the director ($\hat{n}$) direction in a NLC medium. The degree of orientational ordering in a NLC can be quantified by defining an order parameter. For cylindrically symmetric molecules, the *S* is defined as

$$S = \frac{1}{2} < 3\cos^2(\theta) - 1 > \quad (1.8)$$

where θ is the angle made by a molecule with the director ($\hat{n}$). The bracket denotes the average over the orientation of long axis of LC molecules. The order parameter is very sensitive to the variation of temperature. On increasing temperature of a NLC, *S* decreases monotonically in nematic phase and drops discontinuously at the nematic-isotropic transition point (T_{NI}). Equation (1.2) predicts that *S* = 0 at the T_{NI} transition point but experimentally observed value of order parameter in nematic materials is typically in the range *S* = 0.3–0.4 at the transition, which is weakly first order [1].

1.5.5 Alignment of NLC sample in LC cell

The alignment layer on the substrate plays a crucial role in determining the bulk orientation of LC molecules. In a liquid crystal display device, the substrates are treated with certain organic or inorganic film. The interaction between the LC molecules and the surface is strong enough to align the director in a particular direction at the boundaries. In an unaligned liquid crystalline medium the director ($\hat{n}$) varies gradually from point to point. In order to measure physical properties, the director should be homogenously aligned in the cell. In general two basic geometry exist in which the director is aligned either parallel or perpendicular to the plane of the glass substrate, called planar and homeotropic alignment, respectively [22-24]. Without treatment of the surface of the substrate, the molecules tend to orient in different directions forming mesophase characteristic defects. The schematic diagrams of different alignment geometries of LCs are shown in Figure 1.8.

Planar alignment: The LC sample can be aligned in a uniform homogeneous or planar geometry if the glass surfaces are uniformly coated with a polyimide and are rubbed along one direction. A thin layer of polyimide is deposited on the indium tin oxide (ITO) coated glass plate, and cured at 250°C for one hour. Then the plates are rubbed uniaxially along one direction with a soft cloth. The rubbing on polyimide creates micro-grooves. The LC cells are made using such treated substrates. In the case of uniaxial NLC the long axis of molecules will be along the rubbing direction (Figure 1.8(a)). The aligned LC near the substrates induce long range alignment throughout the liquid crystal cell.

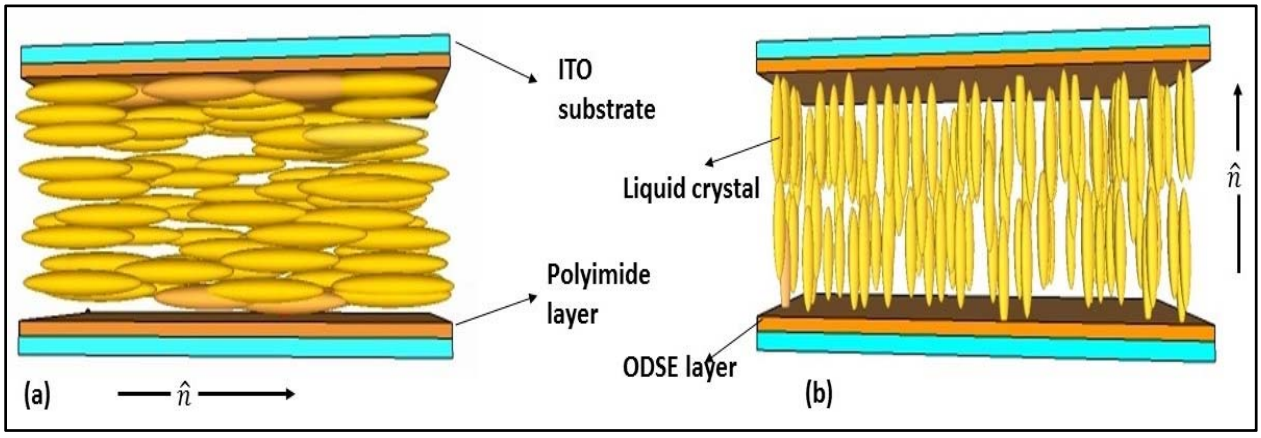

Figure 1.8: Schematic diagrams of the (a) planar and (b) homeotropic alignment of the LC molecules.

Homeotropic alignment: In this geometry the long axis of the LC molecules are arranged perpendicular to the surface of the substrate (Figure 1.8(b)). The ITO plates are coated with a surfactant which are long chain molecules like octadecyl triethoxy silane (ODSE). Such treated ITO plates can give rise to a homeotropic alignment. The surfactant ODSE has a polar head group and a long alkyl chain. The polar head group gets attached to the surface of the glass plate and the long octadecyl chains can induce the perpendicular orientation of the LC molecules with respect to the glass plate.

Twisted nematic alignment: For the twisted nematic (TN) alignment, the ITO plates are coated with polyimide and rubbed unidirectionally with soft cloth similar to the method which is used to prepare LC cells in planar alignment geometry. In TN LC cell, the rubbing direction of alignment layer on top substrate is perpendicular to the alignment layer on the bottom substrate. Hence, the LC molecules undergo 90° twist in the LC cell from bottom to the top layer. In TN alignment mode, two possible configuration are possible called normally white (NW) and normally black (NB) twisted nematic mode. Figure 1.9 shows the TN LC molecules alignment in NW mode with OFF and ON-states. The NW mode is a mode in which light is transmitted through the TN LC cell placed between two crossed polarizers in absence of electrical field (OFF state). In OFF state (Figure 1.9(a)), the polarization state of incoming linearly polarized light follow the molecules twist inside the TN cell and pass through the second polarizer. Hence, bright state is observed.

In ON state (Figure 1.9(b)), the directors are reoriented perpendicular to the substrates, except at the boundary layers. Applied electric field breaks the twisted structure of the LC and fails to re-orient the polarized light passing through the cell. In this case the light is blocked by the second polarizer and the image appears opaque.

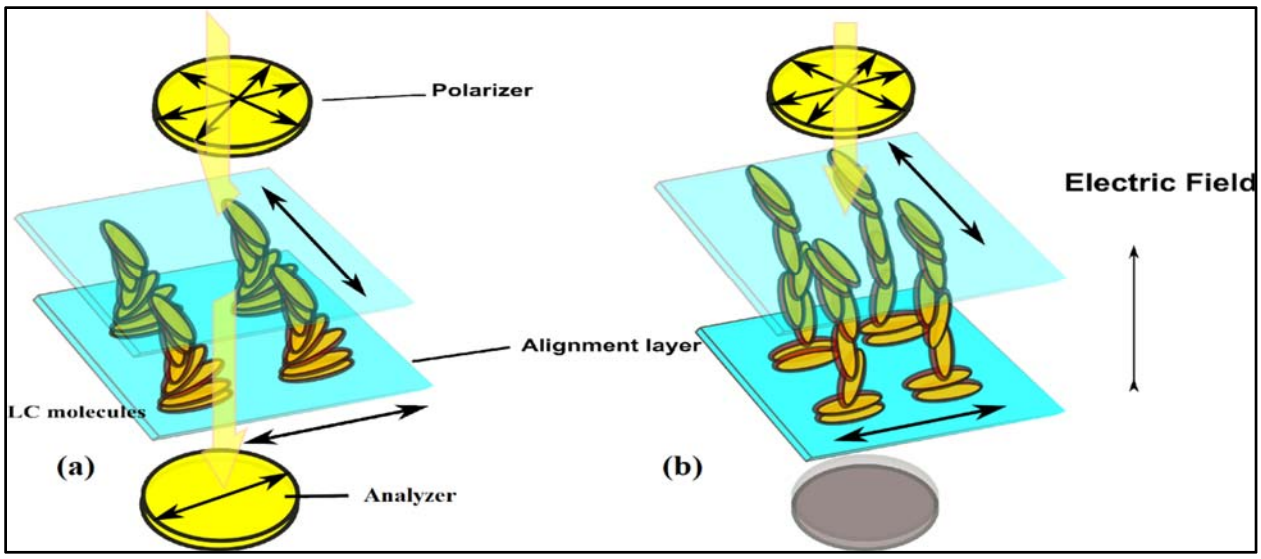

Figure 1.9: Schematic diagrams of the twisted nematic (TN) alignment of the molecules in (a) absence and (b) presence of electric field (NW mode).

1.5.6 Freedericksz transition in NLCs

For LC based display applications, the LC material is sandwiched between two transparent conducting ITO coated glass plates. These conducting plates are treated with alignment layer which determine the orientation of LC at the surface of substrate. NLC molecules can possess permanent or induced dipole moments parallel or perpendicular to the long molecular axis (positive or negative dielectric anisotropy). With the application of external electric field, the direction of the director can be manipulated. In a planar cell, the director of positive dielectric anisotropic NLC sample tends to align parallel to the substrate due to the surface anchoring in the absence of external electric field. When electric field is applied across the LC cell, the molecules experience external torque which results in the reorientation of the director in the macroscopic volume of the material along the electric field direction. As the magnitude of applied electric field increases, at first no change in alignment of the molecules is observed. However, if the voltage exceeds a certain value, the orientation of molecules starts to change from perpendicular to parallel with respect to electric field. The field induced reorientation of NLC is referred to as the Freedericksz transition [1, 2]. The voltage at which Freedericksz transition takes place is called the Freedericksz threshold voltage (V_{th}). The V_{th} value depends on the dielectric anisotropy $\Delta\varepsilon$ and the elastic properties of the NLC. The V_{th} value can be measured by measuring the change in the

transmitted intensity as a function of applied voltage or can be determined by measuring the capacitance change with increasing applied voltage [26]. The value of V_{th} is given by,

$$V_{th} = \pi \sqrt{\frac{K_{11}}{\varepsilon_0 \Delta\varepsilon}} \tag{1.9}$$

where K_{11} is the splay elastic constant and $\Delta\varepsilon$ is the dielectric anisotropy. K_{11} can be estimated using Equation (1.9), if the sample has a positive dielectric anisotropy.

1.5.7 Optical response time

The optical response time is important parameter for the LCD which depends on the V_{th} and rotational viscosity (γ_1) of the NLC. When the magnitude of applied electric field is higher than the Freedericksz transition threshold voltage, a distortion in the bulk LC occurs. The applied electric field disturbs the director orientation leading to generation of the bend or splay deformations in planar aligned samples. In planar LC cell, the total free energy density due to elasticity of LC and applied electric field is given by

$$F = \int_0^d [\frac{1}{2}(K_{11}\cos^2\phi + K_{33}\sin^2\phi)(\frac{\partial\phi}{\partial z})^2 - \frac{1}{2}\varepsilon_0\Delta\varepsilon E^2\sin^2\phi]dz \tag{1.10}$$

where d is the thickness of LC cell. $\varepsilon_0\Delta\varepsilon E^2$ is the electric field energy density and ϕ is the tilt angle of the LC directors with respect to the plane of substrate. Using the Euler-Lagrange method to minimize the energy, we obtain

$$(K_{11}\cos^2\phi + K_{33}\sin^2\phi)\frac{\partial^2\phi}{\partial z^2} + (K_{33} - K_{11})\sin\phi\cos\phi(\frac{\partial\phi}{\partial z})^2 + \varepsilon_0\Delta\varepsilon E^2\sin\phi\cos\phi = 0 \tag{1.11}$$

The dynamics of LC reorientation is described by the Erickson–Leslie equation, when the back flow and inertia effects are ignored [17]. In Erickson–Leslie equation, the strong anchoring and pretilt angle are assumed to be zero. The electric torque and elastic torque is balanced by the viscosity torque which opposes the change of director orientation with applied electric field.

$$(K_{11}\cos^2\phi + K_{33}\sin^2\phi)\frac{\partial^2\phi}{\partial z^2} + (K_{33} - K_{11})\sin\phi\cos\phi(\frac{\partial\phi}{\partial z})^2 + \varepsilon_0\Delta\varepsilon E^2\sin\phi\cos\phi = \gamma_1\frac{\partial\phi}{\partial t} \tag{1.12}$$

γ_1 is the rotational viscosity of LC. When the tilt angle is small, sinϕ ~ ϕ (small angle approximation) and $K_{33} \sim K_{11}$ (single elastic constant approximation) then Erickson–Leslie equation is reduced to Equation (1.13) [27].

$$K_{11}\frac{d^2\phi}{dz^2} + \varepsilon_0 \Delta\varepsilon E^2 \phi = \gamma_1 \frac{\partial\phi}{\partial t} \tag{1.13}$$

When the electric field is switched off, i.e., E=0, Equation (1.13) is further simplified as:

$$K_{11}\frac{d^2\phi}{dz^2} = \gamma_1 \frac{\partial\phi}{\partial t} \tag{1.14}$$

The solution of Equation (1.14) can be expressed as

$$\phi(z,t)=\phi_m \sin(\frac{\pi z}{d})\exp(\frac{\tau}{\tau_0}) \tag{1.15}$$

with decay time $\tau_0 = \dfrac{\gamma_1 d^2}{K_{11}\pi^2}$ (1.16)

where ϕ_m represents the maximum tilt angle in the center of the LC cell. The decay time (τ_0) and the rise time is expressed in Equations (1.16) and (1.17) respectively.

$$\tau_{rise} = \frac{\gamma_1 d^2}{K_{11}\pi^2\left[\left(\dfrac{V}{V_{th}}\right)^2 - 1\right]} \tag{1.17}$$

where d is the cell gap, V is the applied voltage, and V_{th} is the threshold voltage. From these equations, we find that in order to achieve fast response time, the visco-elastic coefficient (γ_1/K) of the NLC and cell gap d need to be reduced. Also, a high voltage helps to shorten the rise time. The rotational viscosity (γ_1) also plays a crucial role in the LC response time. The response time of a NLC device is linearly proportional to γ_1 [28]. The rotational viscosity of an aligned LC depends on the detailed molecular constituents, structure, intermolecular interaction and temperature.

If the anchoring of the LC at the boundary is not infinitely strong, the tilt angle ϕ at the boundary is no longer fixed but changes with the applied field. Now we must consider the surface energy in determining the equilibrium director configuration. The total free energy of a NLC is written as follows:

$$F = \int_0^d [\frac{1}{2}(K_{11}\cos^2\phi + K_{33}\sin^2\phi)(\frac{\partial\phi}{\partial z})^2 - \varepsilon_0\Delta\varepsilon E^2\sin^2\phi]dz + f_s(0) + f_s(d) \qquad (1.18)$$

where $f_s = \frac{1}{2}\sin^2\phi$

and W is polar anchoring energy strength coefficient, also called as the *anchoring energy*. The surface anchoring energy is also crucial parameter for response time [29]. Under strong anchoring condition, the LC directors on the substrates are fixed on their easy axis and the pretilt angle is zero. Here, easy axis stands for the directions of LC directors, which minimize the energy of the surface regions. Under such condition, the boundary conditions expressed as

$$\phi(-d/2) = \phi(+d/2) = 0 \qquad (1.19).$$

However, when the anchoring energy of the LC cell is finite, the simple boundary conditions given in Equation (1.19) are no longer valid and we use the extrapolation length concept to derive the analytical solutions for the LC response time. The extrapolation length (b) can be interpreted as the extension of the LC cell gap [28]. The parameter $b = K/W$ has the dimension of length, which is usually called the extrapolation length. For example, an infinity anchoring means no extension since b=0. For a LC cell with a finite anchoring energy, the LC directors on the physical substrate boundaries $z = \pm d/2$ will still be reoriented by the external electric fields. According to the definition of the extrapolation length, ϕ is zero at $z = \pm d/2+b$. Therefore, $z = \pm d/2 + b$ can be considered as virtual boundaries of the LC cell and the effective cell gap becomes

$d' = d+2b$

We can write Equation (1.16) in term of effective cell gap. The decay time can be expressed with the effective cell gap,

$$\tau'_0 = \frac{\gamma_1 d'^2}{K\pi^2} = \frac{\gamma_1(d+2b)^2}{K\pi^2} = \frac{\gamma_1}{K\pi^2}(d^2 + \frac{4dK}{W} + \frac{4K^2}{W^2}). \qquad (1.20)$$

The term $(\frac{K}{W})^2$ in Equation (1.20) is independent of cell gap and its magnitude is small so this term can be omitted and the LC director response time is reduced to

$$\tau'_0 \approx \frac{\gamma_1}{K\pi^2}(d^2 + \frac{4dK}{W}). \qquad (1.21)$$

The response time of NLC directors is proportional to cell gap d as $\tau_0 \sim d^x$, where the exponent x can vary between 1 and 2, depending on the surface anchoring energy.

1.6 Review of work on liquid crystals and its carbon nanotube nanocomposites

NLCs are widely used in LCDs due to their easy collective reorientation of director on application of electric field. The doping of LCs with nanomaterials has attracted much attention from the scientific community. The introduction of nanomaterials into LC can influence the display parameters such as switching time, diffraction efficiency, contrast ratio and operating voltage of LCs. Carbon nanotube (CNT) is a graphene sheet rolled into a cylindrical form with a diameter in the range of nanometers. CNTs are very interesting materials mainly for devices due to their unique physical properties, namely their high electrical conductivity along the tube length, high chemical stability and high thermal conductivity [30-31]. Generally, CNTs are classified into two categories based on their structure and dimensions: single-walled carbon nanotubes (SWCNT), which consist of one layer of cylindrical graphene and have diameter of few nm and lengths in the range 20–1000 nm. Multi-walled carbon nanotubes (MWCNTs) consist of several concentric graphene sheets with diameter in the range of 10–100 nm and lengths from 1μm to a few microns [32]. The investigation on LC and their composites with CNT, are of growing interest from scientific and technological points of view. One of the main challenges is the homogeneous dispersion of the CNTs into the LC material. Due to the shape compatibility, the CNTs can be doped in the LC matrix. One of the techniques to disperse CNT into mesogens is chemical functionalization, which is proved to be a good method to promote the dispersability of CNTs in organic solvent [33]. CNTs are, generally, not soluble in organic solvent due to strong van der walls interaction between adjacent CNT and they form bundles. We have used functionalised CNTs at low concentration, which can be dispersed in organic solvents such as ethanol and chloroform without aggregation.

The inclusion of CNT in NLC matrix improves the electro-optic switching characteristics and physical properties of NLC such as $\Delta\varepsilon$, V_{th}, K_{ii}, memory effect and response time in twisted as well as planar alignment modes [34-38]. NLC doped with a small amount of CNT showed a remarkable change in the $\Delta\varepsilon$, the elastic constant, and rotational viscosity [34-38]. The introduction of CNTs into the LC affects the threshold voltage as well as conductivity. NLC doped with SWCNT and MWCNT have been studied and found that doping CNT increase the conductivity of the sample due to reorientation of CNT along the director field of NLC. Middha *et al.* [44] observed that doping functionalised SWCNTs into NLC doped with chiral molecules results in an

irreversible electro-optic memory in the material. The π–π interaction between SWCNTs present in the alignment layers and twisted NLC molecules affects the molecular relaxation process.

The screening effect caused by ion charge is one of the biggest problems associated with the LCD technology. As a consequence of the ion impurities present in LC, an electronic double layer (EDL) is generated at the interface of polyimide and LCs. Due to EDL, effective voltage decreases leading to increase in the V_{th} as well as driving voltage, which causes an image sticking problems. CNT was used to trap the impurity charges and reduced the image-sticking problem of the LC display devices [34]. In 2006, Chen *et al*. [38] reported that after doping CNTs in NLC, the charge density as well as driving voltage reduced due to the sufficient ion trapping via charge transfer mechanism.

The self-organizing properties of LCs can be used for the alignment of dispersed CNTs on a macroscopic dimension [39-43]. The long axis of CNTs, can couple to the nematic director, enables orientational manipulation via the LC nematic reorientation. Electric field induced director rotation of a NLC doped with CNT system is of interest due to its various application in display devices. Materials that have low-weight and shape anisotropy can be aligned when dispersed in NLC. This effect is due to the orientational order of the NLC provided the concentration of the dispersed material is low to prevent aggregation. Lynch *et al.* [43] first exploited this property when they deposited a suspension of CNTs and LCs on a porous membrane. After the LC was filtered out, aligned CNTs exhibiting the nematic order were obtained. Lee *et al.* [45] observed that the LC cells fabricated with MWCNT mixed polyimide layer showed the improved electro-optical properties, such as a low V_{th} and fast response time.

Apart from the CNTs, a variety of inorganic and insulating nanoparticles (NPs) have been doped into LCs which lead to change in the properties of LC [46-51]. Cho *et al*. [47] reported the effect of graphene quantum dots (QDs) on the response time of pure NLC. The presence of graphene QDs leads to improved electro-optical properties, such as faster response times and a low threshold voltage for twisted nematic LCDs. The doping of the TN-LCD with graphene QDs reduces the field-screening effect, which is caused by impurity ions. Recently, a study of titanium dioxide (TiO_2) NPs doped LC has been done which reveals that doped NPs can trap the inevitable ion impurities at alignment layers and hence, the screening effect is suppressed [48].

The inherent conductivity and spontaneous self-alignment properties of CNTs make them suitable candidate as an alignment layer. It has been observed that the long axis of CNT was aligned parallel to the LC director and with a bias voltage, the tubes also tried to orient along the LC director [42-43]. The degree of alignment of nanotubes could be controlled in a liquid crystalline solvent and the ordered nanotube films could also enhance alignment in the NLC [40-41]. The CNT films were used to fabricate optical cells in which planar alignment of NLC is achieved and the director orientation can be manipulated on application of electric field. Along with the changes observed in the physical properties, the effect of the CNTs on phase transition has also been observed [30].

1.7 Applications of LC

Due to their self-assembly behavior, LCs are playing significant role in nanoscience and nanotechnology. LC material can be used for synthesis of nanomaterials using LCs as template. The most common application of LC is in display technology such as LCD in watches, calculators, mobile phones and projectors. There are many types of LCDs, each with unique properties. The most common LCD is the TN display. This is achieved with little power consumption and at low operating voltages. The LC is now being explored for optical imaging and recording. In this technology, a LC cell is placed between two layers of photoconductor. Light is focused to the photoconductor, which increases the material's conductivity. This causes an electric field to develop image in the LC corresponding to the intensity of the light. The electric pattern can be transmitted by an electrode, which enables the image to be recorded. This technology is still being developed and is one of the most promising areas of LC research.

LCs can also be used to make a temperature sensor. A chiral nematic material under incident white light reflects light with a wavelength determined by the pitch of the chiral nematic. Thus some chiral NLCs appear highly colored in white light. Since the pitch of a chiral nematic is temperature dependent, the color observed changes as the temperature changes. Thus, the color of the display can be used to determine the temperature.

1.8 LC Materials

A list of LC materials which were used in our investigations are presented in table 1.1.

Table 1.1 LC materials and their phase transition temperatures.

Liquid crystals	Phase sequence
8CB (n-octyl cyanobiphenyl)	**Cr-21.5°C-SmA -33.5°C-N-40.3°C-Iso**
7CB (4-heptyl-4′-cyanobiphenyl)	**Cr-4.5°C-N-42.8°C-Iso**
5CB (4-pentyl-4′-biphenylcarbonitrile)	**Cr-22.5°C-N-35°C-Iso**
8OCB (n-octyloxy-cyanobiphenyl)	**Cr-53.5°C-SmA -67.5°C-N-79.5°C-Iso**
5PCH(4-trans-pentylcyclohexylcyanobenzene)	**Cr-15.5°C-N-55.3°C-Iso**
TP10 (Hexakis(decyloxy)triphenylene)	**Cr-45°C-Col_h-69°C-Iso**
10OHF (10OHFBBB1M7)	**Iso- 120.7°C-SmA-82.5°C-SmC^*_α - 72.9°C-SmC^*_{F12} - 61.4°C-SmC^*-55.5°C- Cr (cooling)**

The contents of the different chapters in this thesis are briefly given below.

A brief introduction of the LCs and the LC phase exhibited by mesogens with different shape is discussed in chapter 1. The application of LCs and their importance in the various fields also discussed. Chapter 2 deals with the experimental methods used to characterize the properties of LC materials. The fabrication of LC cell has been discussed. The methods for measuring the dielectric constant and optical response time have been described. Chapter 3 presents the results of estimation of dielectric constant of pure n-octyl cyanobiphenyl (8CB) and its nanocomposites of octadecylamine functionalized SWCNTs (ODA-SWCNT) as a function of temperature. The dielectric anisotropy as a function of reduced temperature decreases with an increase in the concentration of ODA-SWCNT. The splay and bend elastic constants are also estimated for pure 8CB and its ODA-SWCNT nanocomposites. The electro-optic response rise time decreases and decay time increases with increasing concentration of ODA-SWCNT. The temperature range of smectic phase is increased with an increase in the concentration of ODA-SWCNT.

The effect of ODA-SWCNT mainly on the response characteristics, i.e., rise time and decay time of a NLC in TN alignment geometery is described in chapter 4. On increasing the concentration of ODA-SWCNT, faster response time was observed than pure NLC. The optical response time of a NLC reduces due to incorporation of ODA-SWCNT in the LC host. Such reduction is believed to be due to increase in elastic constant of the nanotubes doped LC system. The effect of ODA-SWCNT as an alignment layer on the response time of NLC has also been investigated. Our

investigation on TN cells prepared using mixture of ODA-SWCNT and PI alignment layer indicates that the increase in threshold electric field (E_{th}) might be due to strong anchoring between LC and ODA-SWCNT. We have observed a reduction in optical response time for the TN cell prepared with PI-ODA-SWCNT mixture compared to that of pure PI alignment layer. One important observation is reduction of optical response time, which may be useful for potential applications as slow optical response time has been a critical issue with the doped system. The results related to the determination of dielectric and electro-optical parameters have been discussed in detail.

The effect of ODA-SWCNT as an alignment layer in planar LC cells on the dielectric anisotropy and electro-optic properties of NLC is discussed in chapter 5. The dielectric anisotropy increases with increasing concentration of ODA-SWCNT into PI alignment layer as compared to that of pure PI treated LC cell. The ODA-SWCNT also influences the switching behavior, splay elastic constant, rotational viscosity and V_{th} of pure LC. The presence of ODA-SWCNT as an alignment layer causes slight reduction of splay elastic constant and rotational viscosity of LC cells. It is also interesting to study the ODA-SWCNT as an alignment layer using different deposition techniques. Aligning the CNTs on the substrate in control way or proper alignment is also important from application point of view. The ODA-SWCNT is deposited on ITO using spin coating and Langmuir-Blodgett techniques. LC cells were fabricated using such alignment layer deposited substrates and the optical response time of NLC was measured.

The splay elastic constant and dielectric properties of nanoparticles, viz., octadecylamine capped cadmium selenide quantum dots (CdSe QDs) and titanim dioxide (TiO_2) doped NLC is presented in chapter 6. The NLC was doped with different concentrations of the semiconducting CdSe QDs. The doped samples were found to have a lower V_{th} than that of pure NLC. The dielectric constants and splay elastic constant were measured to analyze the cause of the V_{th} value reduction. Doping CdSe QDs led to increase in dielectric anisotropy in comparison with that of pure NLC. We have also investigated the effect of semiconducting TiO_2 on the $\Delta\varepsilon$ of NLC. The introduction of TiO_2 into NLC also enhances the value of $\Delta\varepsilon$ as well as splay elastic constant. The result showed that the incorporation of nanoparticles into NLC provides a way to improve the performance of LC based devices.

Chapter 7 describes the effect of ODA-SWCNT on the dielectric permittivity of a LC compound 10OHFBBB1M7 (10OHF), which exhibits unusual smectic phase sequence. The results show

dielectric properties change with the presence of CNTs but the phase sequence of the 10OHF is not altered. Dielectric measurements carried out for the cooling cycle confirm that SmC^*_{FI2} phase exists over a higher temperature range than Sm*C** phase. The dielectric permittivity increases with increasing concentration of ODA-SWCNT.

Chapter 8 deals with the dielectric permittivity and conductivity studies on the thermotropic columnar liquid crystalline phases formed by triphenylene based discotic molecules (DLC) and its zinc sulfide (ZnS) nanoparticle nanocomposites. The conductivity changes effectively, after the addition of nanoparticles in the pure DLC system. The dielectric study indicates the enhancement of dielectric constant for 1% and 2% concentration of ZnS doped mixtures. The in-plane charge transport mechanism for LC sample was studied by recording *I-V* curve at different temperatures. The electrical conductivity of these composites was observed to be enhanced by ~ 90% compared to the pure DLC. The dielectric and conductivity study of DLC doped with ionic liquids is also a part of this chapter.

In the end, I conclude that our experimental findings and explanations presented in the thesis provide an information about the effect of nanomaterial on the electro-optic characteristics and physical properties of LCs.

References:

1. P. G. de Gennes, J. Prost, *The Physics of Liquid Crystals, 2nd ed*. Clarendon Press, Oxford, **1993**.
2. S. Chandrasekhar, *Liquid Crystals, 2nd ed.* Cambridge University Press, Cambridge, **1992**.
3. F. Reinitzer, Wiener Monatsh. Chem. 9, 421, **1888**.
4. O. Z. Lehmann, Phys. Chem. 4, 462, **1889**.
5. D. W. Bruce, J. W. Goodby, J. R. Sambles, H. J. Coles, Phil. Trans. R. Soc. A 364, 2567, **2006**.
6. S. Chandrasekhar, B. K. Sadashiva, K. A. Suresh, Pramana, 9, 471, **1977**.
7. S. Kumar, Chem. Soc. Rev. 35, 83, **2006**.
8. S. Sergeyev, W. Pisula, Y. H. Geerts, Chem. Soc. Rev. 36, 1902, **2007**.
9. S. Kumar, S. K. Varshney, Angew. Chem. Int. Ed. 39, 3140, **2000.**
10. A. B. Shivanandareddy, M Kumar, V. Lakshminarayanan, S. Kumar, RSC adv. 5, 47692, **2015**.
11. D. Vorländer, Ber Dtsch, Chem Ges, 62, 10, **1929**.
12. D. Shen, S. Diele, G. Pelzl, I. Wirth, C. Tschierske, J. Mater. Chem. 9, 661, **1999**.
13. T. Niori, T. Sekine, J. Watanabe, T. Furukawa, H. Takezoe, J. Mater. Chem. 6, 1231, **1996**.

14. S. M. Kelly, M. O. Neill, *In Handbook of Advanced Electronic and Photonic Materials and Devices*, Academic Press, Burlington, pp 10-11, **2001**.
15. C. W. Oseen, Trans. Faraday Soc. 29, 883, **1933**.
16. H. Zocher, Trans. Faraday. Soc. 29, 94. **1933**.
17. F. C. Frank, Disc. Faraday Soc. 25, 19, **1958**.
18. J. L. Ericksen, Arch. ration. tech. Analysis, 23, 266, **1966.**
19. I. Haller, Prog. Solid. State Chem. 10, 103, **1975.**
20. L. Onsager, J. Am. chem. Soc. 58, 1486, **1936**.
21. W. Maier and G. Meier, Z. Natursforsch. 16a, 262, **1961**.
22. V. Manjuladevi, *Experimental Studies on Phase Diagrams of Liquid Crystal* [Ph.D. thesis], Raman Research Institute, Bangalore, **2004**.
23. T. Uchida, H. Seki, *Surface alignment of liquid crystal, in liquid crystal Application and uses,* World scientific singapore. 21, 40, **1991**.
24. K. Takatoh, M. Hasegawa, M. Koden, R. Hasegawa, M. Sakamoto, *Alignment Technologies and Application of Liquid crystals,* CRC Press, 99-105, **2005**.
25. W. Lee, J.-S. Gau, H. Y. Chen, Appl. Phys. B 81, 171, **2005**.
26. S. T. Wu, D. Coates, E. Bartmann, Liq. Cryst. 10, 635, **1991**.
27. E. Jakeman and E. P. Raynes, Phys. Lett., 39A, 69, **1972**.
28. X. Nie, R. Lu, H. Xianyu, T. X. Wu, S. T. Wu, J Appl Phys. 101, 103110, **2007**.
29. D. K. Yang and S. T. Wu, *Fundamentals of Liquid Crystal Devices,* Wiley, New York, 145–154, **2006**.
30. P. J. F. Harris, *Carbon Nanotubes and Related Structures*, Cambridge Univ. Press, Cambridge, UK, **1999**.
31. T.W. Ebbesen, *Carbon Nanotubes: Preparation and Properties*, CRC Press, Inc., Boca Raton, **1997**.
32. L. Lacerda, A. Bianco, M. Prato, K. Kostarelos, Adv. Drug Del. Rev. 58, 1460, **2006.**
33. V. Manjuladevi, R. K. Gupta, S. Kumar, J. Mol. Liq. 171, 60, **2012**.
34. I. S. Baik, S. Y. Jeon, S. H. Lee, K. A. Park, S. H. Jeong, K. H. An, Y. H. Lee, Appl. Phys. Lett. 87, 263110, **2005**.
35. R. Basu, G. S. Iannacchione, Phys. Rev. E 81, 051705, **2010**.
36. H. Lee, S. Yang, J. H. Lee, Y. S. Park, Appl. Phys. Lett. 104, 191601, **2014**.

37. H. Y. Chen, W. Lee, N. A. Clark, Appl. Phys. Lett. 90, 033510, **2007**.

38. H. Y. Chen, W. Lee, Appl. Phys. Lett. 88, 222105, **2006**.

39. I. Dierking, G. Scalia, P. Morales, D. LeClere, Adv. Mat. 16, 865, **2004**.

40. C. Da Cruz, P. Launois, M. Veber, J. of Nanosc. and Nanotech. 4, 86, **2004**.

41. J. M. Russell, O. Soojin, I. LaRue, O. Zhou, E. T. Samulski, Thin Solid Films, 509, 53, **2006**.

42. M. D. Lynch, D. L. Patrick, Nanoletters. 2, 1197, **2002**.

43. I. Dierking, G. Scalia, P. Morales, J. Appl. Phys. 97, 044309, **2005**.

44. M. Middha, Rishi Kumar, K.K. Raina, Liq. Crys. 42, 1028, **2015.**

45. K. J. Lee, H. G. Park, H. C. Jeong, D. H. Kim, D. S. Seo, J. W. Lee, B. M. Moon, Liq. Crys. 41, 25, **2014**.

46. U. B. Singh, R. Dhar, R. Dabrowski, M. B. Pandey. Liq Cryst. 40, 774, **2013**.

47. M. J. Cho, H. G. Park, H. C. Jeong, J. W. Lee, Y. H. Jung, D. H. Kim, J. H. Kim, J. W. Lee, D. S. Seo, Liq. Crys. 41, 6, **2014**.

48. S. P. Yadav, R. Manohar, S. Singh, Liq. Crys. 42, 8, **2015**.

49. H. K. Chung, H. G. Park, Y. S. Ha, J. M. Han, J. W. Lee, D. S. Seo, Liq Cryst. 40, 632, **2013**.

50. P. Goel, P. L. Upadhyay, A. M. Biradar, Liq Cryst. 40, 45, **2013**.

51. H. Qi, T. Hegmann, J. Mater. Chem. 18, 3288, **2008**.

52. M. Schadt, Annu. Rev. Mater. Sci. 27, 305, **1997.**

Chapter 2

Experimental techniques

2.1 Introduction

Liquid crystal (LC) and its nanocomposites should be studied systematically by employing various experimental techniques. In this thesis, we have used predominantly polarizing optical microscopy (POM) for phase identification and textural evaluation, capacitance-voltage (C-V) measurement for estimation of dielectric permittivity & elastic constants of the LC medium and atomic microscopic force (AFM) for studying surface morphology. In this chapter, we describe the major experimental techniques employed for the study of LC and its nanocomposites.

2.1.1 Preparation of LC cells

The LC cells were prepared to study the electro-optic properties such as elastic constants, dielectric anisotropy and optical response time of LC material. The indium tin oxide (ITO) coated glass plates were used to fabricate the cells. The ITO is a conductive transparent layer, which was used to apply electric field across the LC. An effective area of electrode was obtained by making a pattern on ITO and the unwanted portions of the ITO were etched by the appropriate solution of hydrochloric acid (HCL) and zinc dust. After etching the ITO plate, it was rinsed with soap water subsequently followed by cleaning using chloroform and ethanol. The planar and homeotropic alignment of the LC sample was obtained by treating the ITO substrate with polyimide (PI 2303) and octadecyl triethoxy silane (ODSE), respectively. The PI was coated on ITO substrates using spin coating unit (Apex, SCU2007A). Thereafter the PI deposited plates were cured at ~ 250°C for about a 1 hour and such substrates were rubbed using a soft cloth in a uniaxial direction. The rubbing of the PI induces some microscopic physical grooves on the surface of cured substrate leading to orientation of the LC molecules along the groove direction. Typically, commercial

liquid crystal displays (LCDs) use a rubbing process for aligning LCs. In 1972, Berreman has experimented by simply rubbing the glass to align LCs [1]. He found that the LC molecules are aligned in the direction of rubbing. Two ITO plates were assembled in an antiparallel fashion with respect to their rubbing direction for obtaining the planar alignment. After rubbing process, the ITO plates were glued and cured at 100°C for about an hour to obtain the LC cell. The cells of definite thickness were prepared using glass spacers. A schematic diagram of LC cell is shown in Figure 2.1.

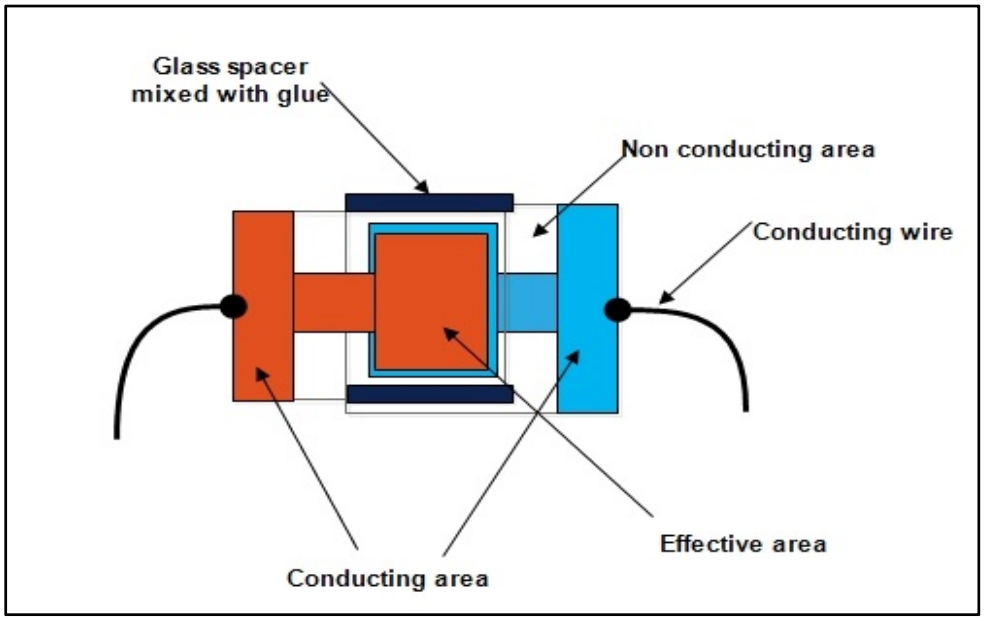

Figure 2.1: Schematic diagram of LC cell.

A uniform and stable alignment of LC molecules is essential for the fabrication of LC based devices because the electro-optic effect depends on the initial orientation of the LC molecules. The orientation of molecules can be manipulated on application of external electric field.

2.1.2 Cell thickness measurement

The thickness of the empty LC cell is measured by using a fiber optic spectrometer (USB 4000XL). The thickness measurement is based on an interferometry technique. Using this technique, we can precisely measure the cell thickness at various positions. The light from a white source (Halogen lamp) passes through the optical fiber and incident on the cell which transmits from the cell and is collected by the second optical fiber. This signal is sensed by the spectrometer. The schematic diagram of cell thickness measurement using the spectrometer is shown in Figure 2.2.

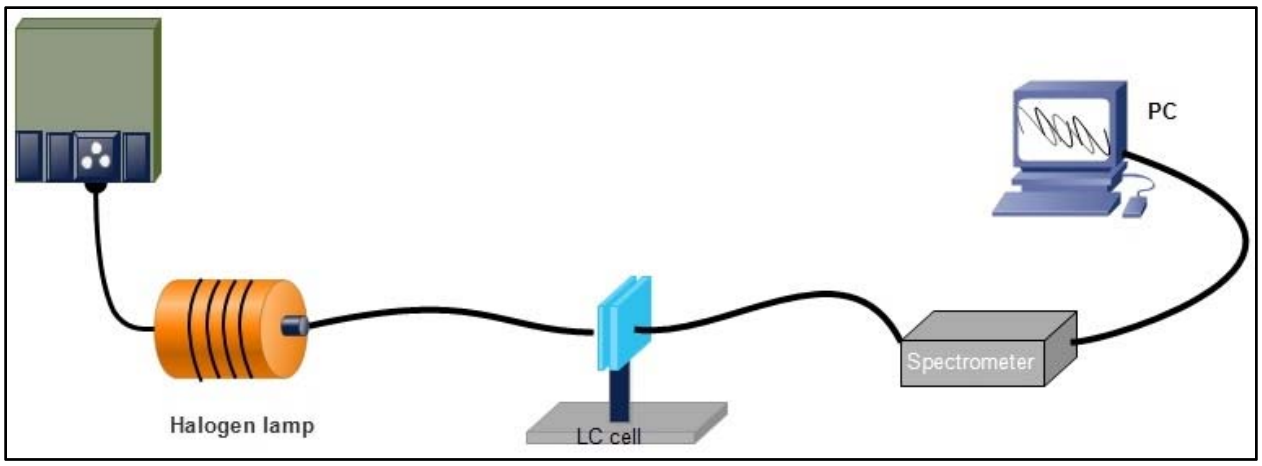

Figure 2.2: Schematic diagram of cell thickness measurement using a spectrometer.

From the intensity *vs* wavelength spectrum, the thickness (*d*) of the LC cell is estimated using the formula.

$$d = \frac{(m-n)(\lambda_m \times \lambda_n)}{2(\lambda_m - \lambda_n)} \qquad (2.1)$$

The values λ_m and λ_n correspond to the wavelengths of the m^{th} & n^{th} maxima or minima measured using the spectrometer. The thickness measurement is performed at several positions of the cell over the overlapped electrode area in order to ascertain that the gap is uniform. The cell, which has uniform thickness (±1% variation) over the entire effective area, is chosen for the further experiments.

2.2 Polarizing optical microscopy

Polarizing optical microscopy (POM) is a powerful tool in LC research and is generally used to identify different LC phases, as each LC phase exhibits its own characteristic textures [2-3]. A POM (OLYMPUS Model BX51) was used to investigate the texture of the LC. The LC cell filled with LC sample is kept on the stage of POM between the crossed polarizers. The microscopic optical textures were captured through a digital camera (AmScope FMA050) attached to POM. A suitable software (Amscope) was used to obtain the images.

Figure 2.3 shows the POM texture of nematic liquid crystal (NLC) in planar aligned cell which appears as uniform bright and complete dark depending on the rubbing direction of LC cell with respect to the polarization axis of polarizer and analyzer. The maximum brightness is

achieved when the rubbing direction of the LC cell is making an angle of 45° with respect to either of the crossed polarizers [Figure 2.3(a)]. The texture is completely dark when the rubbing direction is parallel to the transmission axis of either polarizer or analyzer [Figure 2.3(b)].

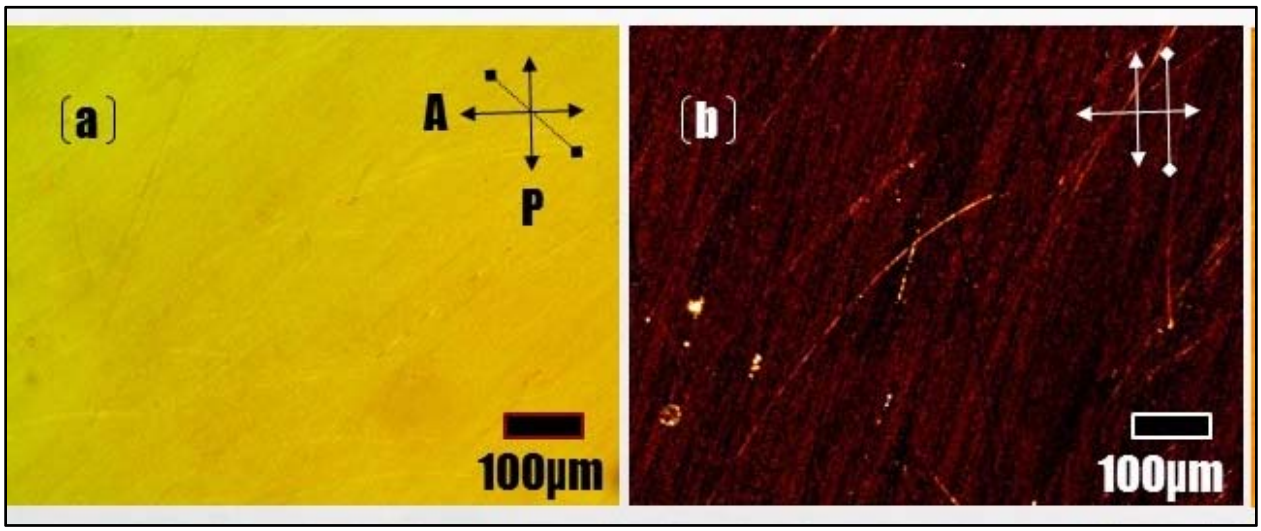

Figure 2.3: Optical texture of nematic liquid crystal between crossed polarizers (a) rubbing direction of the cell making 45° angle with respect to both polarizers and (b) rubbing direction is parallel to polarizer. Rubbing direction is indicated by arrow (◆⟶◆)

2.3 Experimental setup for electro-optic measurements

The electro-optic measurement of the NLC involves application of electric field to induce director reorientation in nematic phase and measuring the optical response of NLC as function of applied voltage at different temperatures. The LC cell was placed between a pair of crossed polarizers such that the rubbing direction of the cell makes an angle of 45° with respect to either of the polarizers. A Helium-Neon (He-Ne) laser of wavelength of 632.8 nm was used as light source. An optical chopper (Signal Recovery 198A) was used to get the light being chopped at a particular frequency and is made incident on the sample. This enables us to measure only the intensity of the beam which is coming through the LC cell and not due to any other stray signal. The transmitted light from the LC cell between crossed polarizers is collected using a photo-diode. The photo-diode is connected to a dual-channel lock-in amplifier (EG&G 7265).The intensity data was collected by using a suitable software (LabVIEW, National Instruments) and the intensity data were plotted using the software origin 6.0. The temperature of LC sample was controlled using a hot stage and was maintained within an accuracy of ±0.1 °C. In order to measure the threshold voltage (V_{th}), an

electric field was applied across the cell using a function generator (Aplab, 33220). The transmitted intensity as a function of temperature is measured in planar aligned sample for measuring the birefringence. The transmitted intensity from the planar aligned cell kept between the two crossed polarizers can be written as

$$I_t = I_0(1-\cos\Delta\phi)/2 \qquad (2.2)$$

where I_0 is the intensity of incident light. The path difference ($\Delta\phi$) is given as

$$\Delta\phi = 2\pi d\Delta\mu/\lambda \qquad (2.3)$$

where $\Delta\mu$ is the birefringence, d, the sample thickness and λ, the wave length of incident light. Using the Equations 2.2 and 2.3, the value of $\Delta\mu$ of the NLC sample enclosed in planar aligned cell is calculated. The V_{th} value is estimated using the transmitted intensity as a function of applied voltage.

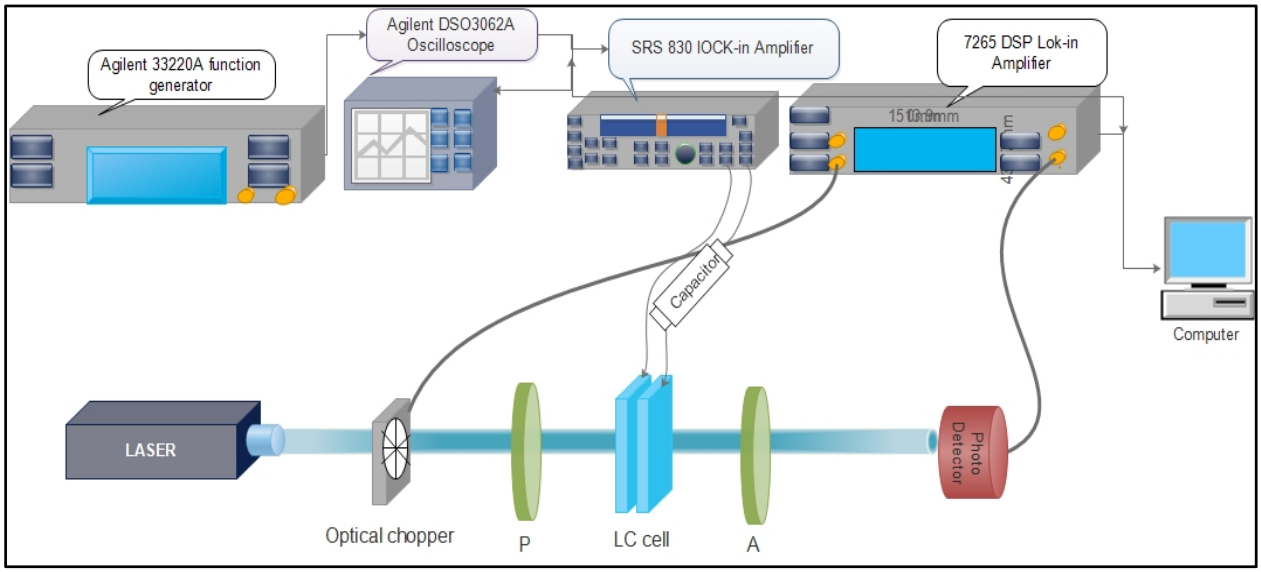

Figure 2.4: Schematic diagram of the electro-optic measurement setup. P and A are polarizer and analyzer, respectively.

A schematic diagram of electro-optic measurement set-up is shown in Figure 2.4. All the instruments are interfaced with computer through LabVIEW program. For birefringence and dielectric measurements, the intensity and capacitance of the LC cell are measured as a function of temperature at fixed voltage. At fixed temperature, the capacitance and intensity variation as a function of applied voltage was also recorded. Using this data, the value of V_{th} and splay elastic constant (K_{11}), and bend elastic constant (K_{33}) were estimated.

2.4 Dielectric constant measurement

Due to the anisotropic shape of LC molecules, the dielectric permittivity measured along the direction of long axis of LC molecules ($\varepsilon_{\parallel}$) is different from that measured perpendicular to the long axis of LC molecules ($\varepsilon_{\perp}$). For the dielectric measurement of LCs, $\varepsilon_{\parallel}$ and $\varepsilon_{\perp}$ represent the dielectric constants measured with an electric field parallel and perpendicular to the director $\hat{n}$, respectively. The dielectric constant (ε) is given by the ratio C_S / C_0, where C_0 is the capacitance of the empty cell, and C_S is the capacitance of the cell filled with LC sample.

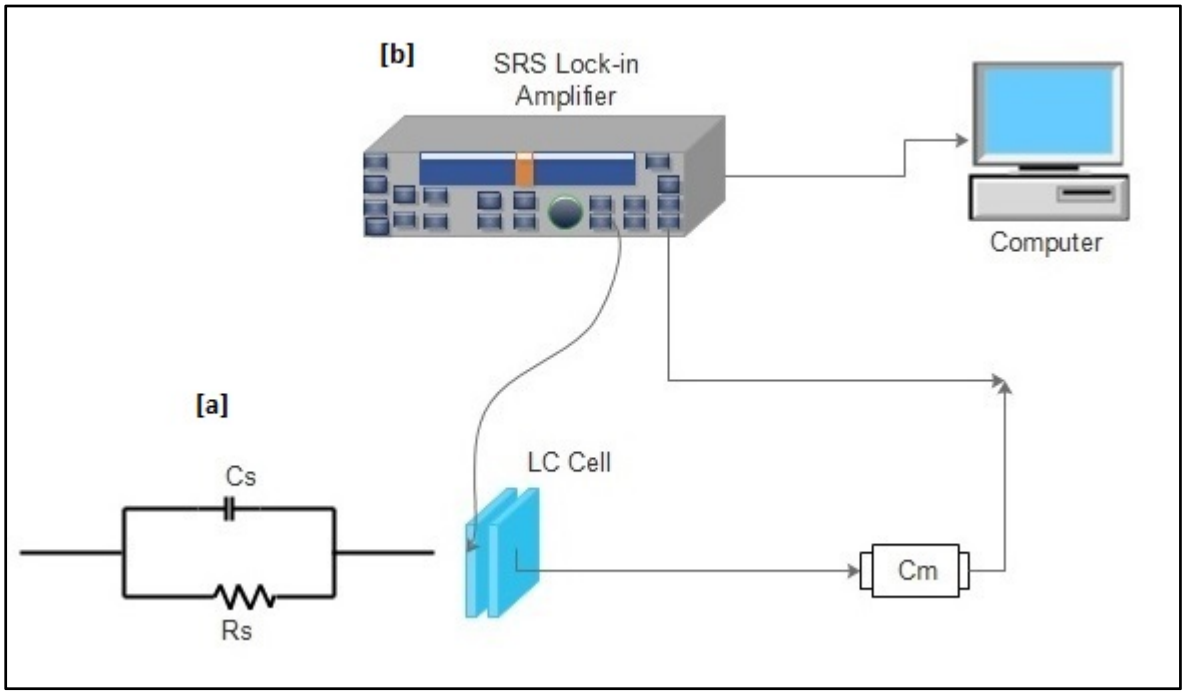

Figure 2.5: Schematic diagram of (a) electrical circuit equivalent of the LC cell and (b) the dielectric constant measurement set up.

Most of LC materials are not free of ionic impurities and exhibit finite resistances. The equivalent electrical circuit of a LC cell can hence be considered to be a capacitor of capacitance (C_S) connected in parallel with resistor of resistance (R_S) (Figure 2.5(a)). A lock-in amplifier (Stanford Research System, SRS 830) is connected to the cell in series with a standard capacitor of capacitance value $C_m \sim 1\mu F$ to measure the impedance of the cell. C_m is chosen to be large, so that a large part of the voltage drops across the cell and only a small voltage is measured by lock-in amplifier. V_0 and φ_0 are the amplitude and phase of the output signal. V_m and φ_m are the voltage

and phase measured across the capacitor C_m. Using impedance analysis, we measure C_S and R_S of the sample. The impedance (Z_S) of cell is given by [4]

$$Z_S = R_S \frac{(1 - i\omega C_S R_S)}{(1 + \omega^2 C_S{}^2 R_S{}^2)} \tag{2.4}$$

where $\omega = 2\pi f$ and f is the frequency of applied field and $i = \sqrt{-1}$.

The total impedance of the circuit Z_t, which is a series combination of Z_S and $Z_m (= 1/i\omega C_m)$ is given by

$$Z_t = \frac{\omega R_S C_m - i[1 + \omega^2 R_S{}^2 C_S (C_m + C_S)]}{\omega C_m (1 + \omega^2 C_S{}^2 R_S{}^2)} \tag{2.5}$$

The total current flowing through the circuit is given by $I_t = \frac{V_0 e^{i(\omega t + \varphi_0)}}{Z_t}$ (2.6)

Hence, $I_t = \frac{V_0 e^{i(\omega t + \varphi_0)} \omega C_m (1 + \omega^2 C_S{}^2 R_S{}^2)}{\omega R_S C_m - i[1 + \omega^2 R_S{}^2 C_S (C_m + C_S)]}$ (2.7)

The voltage drop across C_m which is measured by lock-in amplifier is given by

$$V_m e^{i(\omega t + \varphi_m)} = I_t Z_m \tag{2.8}$$

Comparing real and imaginary part, we get

$$V_m \cos(\omega t + \varphi_m) = V_0 \frac{[1 + \omega^2 C_S (C_m + C_S) R_S^2] \cos(\omega t + \varphi_0) + \omega C_m R_S \sin(\omega t + \varphi_0)}{1 + \omega^2 (C_m + C_S)^2 R_S^2} \tag{2.9}$$

and

$$V_m \sin(\omega t + \varphi_m) = V_0 \frac{[1 + \omega^2 C_S (C_m + C_S) R_S^2] \sin(\omega t + \varphi_m) - \omega C_m R_S \cos(\omega t + \varphi_m)}{1 + \omega^2 (C_m + C_S)^2 R_S^2} \tag{2.10}$$

Solving Equation (2.9) and (2.10) we get

$$C_S = \frac{C_m V_m [V_0 \cos(\varphi_m - \varphi_0) - V_m]}{V_0^2 + V_m^2 - 2V_0 V_m \cos(\varphi_m - \varphi_0)} \tag{2.11}$$

and

$$R_S = \frac{V_0^2 + V_m^2 - 2V_0 V_m \cos(\varphi_m - \varphi_0)}{\omega C_m V_0 V_m \sin(\varphi_m - \varphi_0)} \tag{2.12}$$

According to Maier and Meier theory, the dielectric constant of LC material depends on the molecular structure, temperature and frequency. Determination of dielectric constant from

capacitance measurements is a well-established experimental procedure [5]. The accuracy of the measured capacitance is ~1% and that of the resistance is ~ 4 %. The values for dielectric permittivity obtained using the capacitance measurement method also includes stray capacitance contributions from the wires attached to the electrodes as well as from the edges of the electrode area. We have measured the stray capacitance using standard capacitor. In place of LC cell, a set of standard capacitors and resistors are connected in parallel and the system is calibrated. The value of stray capacitance is found to be ~ 2 *pF*. The dielectric constants $\varepsilon_{\perp}$ and $\varepsilon_{\parallel}$ were measured using planar and homeotropic LC cells, respectively. The dielectric anisotropy ($\Delta\varepsilon = \varepsilon_{\parallel} - \varepsilon_{\perp}$) is estimated using $\varepsilon_{\parallel}$ and $\varepsilon_{\perp}$ values.

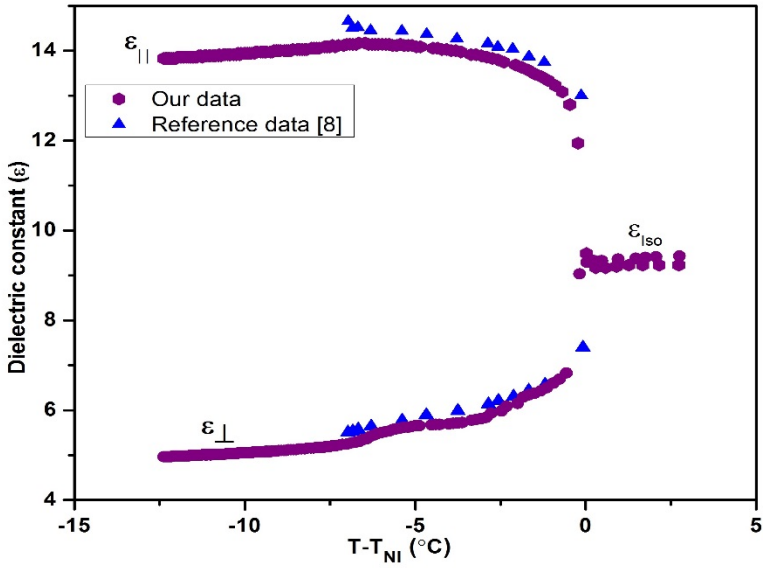

Figure 2.6: Temperature variation of the dielectric constants ($\varepsilon_{\parallel}$ and $\varepsilon_{\perp}$) of 8CB (filled o and Δ symbols correspond to data measured using our experimental set up and reference [8], respectively).

The dielectric constant $\varepsilon_{\perp}$ and $\varepsilon_{\parallel}$ of n-octyl cyanobiphenyl (8CB) are measured with a sinusoidal signal of 0.4V at a frequency of 4.1 kHz in planar and homeotropic LC cell, respectively. The measured values of dielectric constant for 8CB is shown in Figure 2.6 and are in agreement with that reported by Morris *et al.* [8]

2.5 Temperature calibration of hot stage using standard LC compound

The physical properties of LC are studied as a function of temperature. The temperature of the LC cells was controlled using an inhouse built hot stage. A resistance temperature detector (RTD) is

used to measure the temperature of the sample in hot stage. We have used a Proportional Integral Derivative (PID) temperature controller algorithm to vary as well as maintain the temperature of the sample. The PID algorithm is used specifically for precise temperature control of the hot stage. The PID controller can adjust the outputs based on the history and rate of change of the error signal. In PID algorithm, the voltage applied to the hot stage is a summation of three terms. The first, second and third terms are proportional to the error in temperature, the time integration of the error in temperature and the time derivative of the error in temperature, respectively. A proportional controller decreases the average power being supplied to the hot stage as the temperature approaches set point. This has the effect of slowing down the heating so that it will not overshoot the set point, and maintain a stable temperature. The function of the integral control is to reduce the steady state error. The function of derivative control is to reduce the overshoots in the response of the hot stage. A digital multimeter (Keithly 2000) was used to measure the resistance of 2-probe RTD, and a programmable power supply (Aplab PPS 6005) was used to heat the hot stage. Heating or cooling rates can be varied by choosing appropriate P, I and D values. A program was written in LabVIEW 6.0 to control and collect the data from the equipments. We have calibrated the temperature of hot stage using different standard LC materials with known transition temperatures. The LC materials and their corresponding phase transition temperature are showed in the table 2.1.

Table 2.1: LC materials and their phase transition temperatures

LC materials	**Phase transition**	**Temperature (°C)**
8CB (n-octyl cyanobiphenyl)	SmA to N	33.5
8CB	N to Iso	40.5
5PCH (4-trans-pentylcyclohexylcyanobenzene)	N to Iso	55.3
8OCB (n-octyloxy-cyanobiphenyl)	SmA to N	67.3
8OCB	N to Iso	79.5

A plot of observed phase transition temperature of LC materials using inhouse built hot stage and the known transition temperature from literature is shown in Figure 2.7. It shows a linear behavior. Using this data, we have calibrated the temperature of the hot stage.

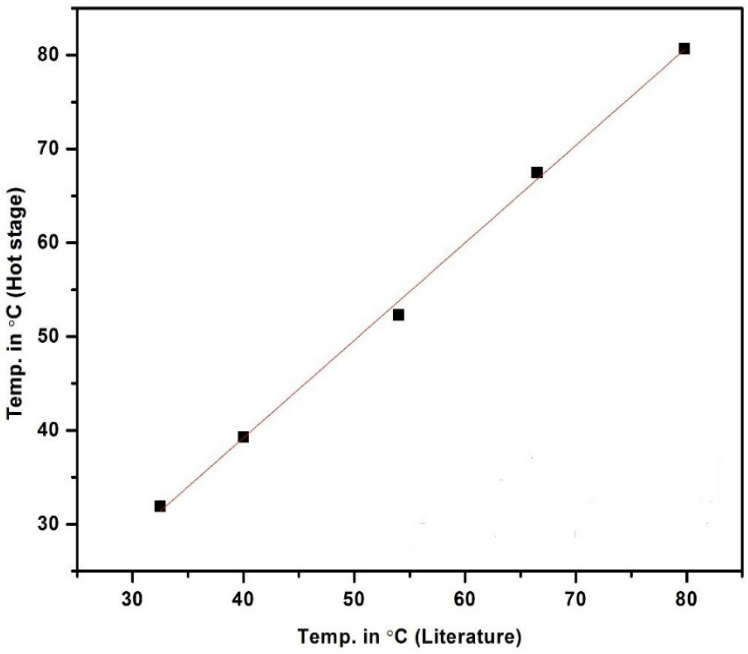

Figure 2.7: Transition temperatures observed using hot stage *Vs* transition temperatures of known sample.

2.5.1 LabVIEW program to control the temperature of the hot stage

LabVIEW stands for Laboratory Virtual Instrument Engineering Workbench and is an important tool for acquiring, analyzing, and presenting data [15]. It is an easy-to-use graphical based program, which is designed to interface with any kind of measurement hardware and automation applications. Each program in LabVIEW is called a Virtual Instrument, or a VI. Each VI is composed of two main components, namely the front panel and the block diagram. The front panel is the graphical user interface of the VI. It contains the controls and indicators such as buttons, slides, dials, tables, graphs etc. which user manipulates to interact with the VI. The block diagram is the graphical code. LabVIEW is a dataflow program meaning that data flows from data sources such as controllers in the front panel or outputs of data acquisition functions (i.e. analog input functions) to sinks such as indicators in the front panel.

A LabVIEW program enables the whole experiment to be automated with different settings, allowing data to be recorded over desired time interval. The example of temperature controller program with PID is shown in Figure 2.8. This program stores all the information; set

target temperature, resistance of cell and time interval or delay for increasing and decreasing temperature. Typically, we have performed the experiment at the rate of 0.2°C per minute.

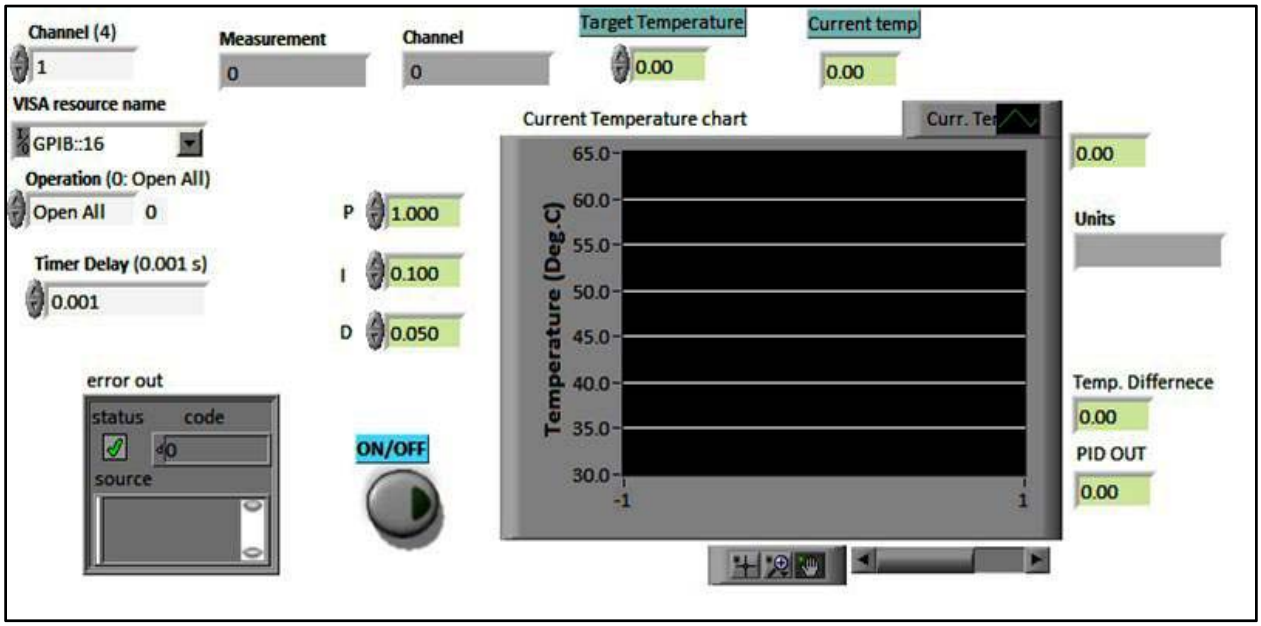

Figure 2.8: The LabVIEW program for measuring the temperature of the hot stage.

2.6 Elastic constant measurement

The splay (K_{11}) and bend (K_{33}) elastic constants of NLC can be determined from the variation of capacitance or optical phase retardation due to applied electric field. The values of elastic constants and $\Delta\varepsilon$ influence the V_{th} and response time of LC device. A smaller value of K_{11} can lead to lower V_{th}, however, viscoelastic coefficient increases [16]. Therefore, a proper balance between V_{th} and response time should be taken into consideration. The value of K_{33} is estimated from the capacitance data at voltages above the V_{th} using the C-V curve method [1]. In planar LC cell, a NLC is enclosed between two ITO plates and direction of $\hat{n}$ is in the rubbing direction of alignment layer in absence of external electric field as shown in Figure 2.9(a). When applied voltage exceeds the V_{th}, the director $\hat{n}$ reorients due to anisotropy in dielectric constant of NLC as shown in Figure 2.9(b). The reorientation of the director causes modifications to the electrical and optical properties of the sample. At the voltage higher than V_{th}, the molecules will be tilted by an angle ϕ relative to the substrate increasing their elastic energy but lowering the electrostatic energy. The angle ϕ will be a function of coordinate z, $\phi(z)$ assuming a maximum value ϕ_{max} at z = d/2 and being 0 at the boundaries.

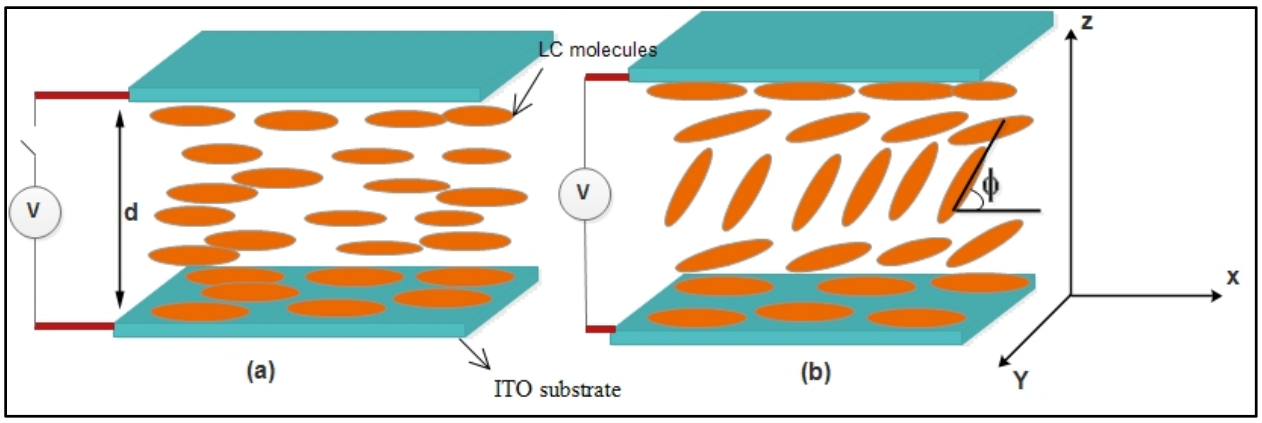

Figure 2.9: Schematic diagram of Freedericksz transition in the splay geometry.

In a LC cell, with a given boundary condition and under the influence of an external applied field, the NLC exhibits a director field configuration $\vec{n}$ that minimizes the total free energy of the system. In case of strong anchoring, the total free energy per unit area

$$F = \int_0^d (f_{elastic} + f_{electric})dz \tag{2.13}$$

where $f_{elastic} = \frac{1}{2}\left[(K_{11}\cos^2\phi + K_{33}\sin^2\phi)(\frac{\partial\phi}{\partial z})^2\right]$ and

$$f_{electric} = -\frac{1}{2}\varepsilon_0\Delta\varepsilon E^2\sin^2\phi$$

$$F = \int_0^d [\frac{1}{2}(K_{11}\cos^2\phi + K_{33}\sin^2\phi)(\frac{\partial\phi}{\partial z})^2 - \frac{1}{2}\varepsilon_0\Delta\varepsilon E^2\sin^2\phi]dz \tag{2.14}$$

Using the Euler- Lagrange method to minimize the free energy, we obtain

$$\sqrt{\varepsilon_0\Delta\varepsilon E^2}\,dz = \sqrt{\frac{K_{11}\cos^2\phi + K_{33}\sin^2\phi}{\sin^2\phi_m - \sin^2\phi}}d\phi$$

Deuling *et al.* [5-6] showed that for the boundary condition $\phi(0)=0=\phi(d)$

$$\frac{V}{V_{th}} = \frac{2}{\pi}\sqrt{1+\gamma\sin^2\phi_m}\int_0^{\phi_m}\left\{\frac{(1+k\sin^2\phi}{(1+\gamma\sin^2\phi)(\sin^2\phi_m - \sin^2\phi)}\right\}^{1/2}\cos\phi d\phi \tag{2.15}$$

where $k = (K_{33}\text{-}K_{11})/K_{11}$, $\gamma = (\varepsilon_{\parallel}\text{-}\,\varepsilon_{\perp})/\varepsilon_{\perp}$, ϕ_m is the maximum tilt angle in the middle of the cell. The value of V_{th} is given by

$$V_{th} = \pi\sqrt{\frac{K_{11}}{\varepsilon_0\Delta\varepsilon}} \tag{2.16}.$$

The value of V_{th} is the voltage required to distort the director which is used to measure the splay elastic constant. The splay elastic constant is measured using equation 2.16. For the planar aligned LC molecules at voltage less than V_{th}, the equation 2.15 can be written as

$$\frac{C}{C_{\perp}} = \frac{\int_0^{\phi_m} \left[\frac{(1+k\sin^2\phi)(1+\gamma\sin^2\phi)}{(\sin^2\phi_m - \sin^2\phi)} \right]^{1/2} d\phi}{\int_0^{\phi_m} \left[\frac{(1+k\sin^2\phi}{(1+\gamma\sin^2\phi)(\sin^2\phi_m - \sin^2\phi)} \right]^{1/2} d\phi} \tag{2.17}$$

At larger voltages compared to the V_{th}, $\phi_m = \pi/2$, and Equation 2.17 can be written as

$$\frac{C(V)-C_{\perp}}{C_{\perp}} = \gamma - \frac{2\gamma}{\pi}\frac{V_{th}}{V}\sqrt{1+\gamma}\int_0^{\frac{\pi}{2}} \left\{ \frac{(1+k\sin^2\phi}{(1+\gamma\sin^2\phi)} \right\}^{1/2} \cos\phi d\phi \tag{2.18}$$

where $C(V)$ is the voltage dependent capacitance and $C_{\perp}$ is the capacitance measured at the voltage below the V_{th}.

$$\frac{C(V)-C_{\perp}}{C_{\perp}} = \gamma - \frac{\alpha}{V} \tag{2.19}$$

where

$$\alpha = \frac{2\gamma}{\pi} V_{th}\sqrt{1+\gamma}\int_0^{\frac{\pi}{2}} \left\{ \frac{(1+k\sin^2\phi}{(1+\gamma\sin^2\phi)} \right\}^{1/2} \cos\phi d\phi$$

The tilt (ϕ) of the long molecular axes of the NLC with respect to the substrate plane varies on application of external electric field. The capacitance at any particular position in the cell is dependent on the applied voltage and the dielectric anisotropy ($\Delta\varepsilon$). Therefore, for $V >> V_{th}$, the plot of $(C(V)- C_{\perp})/ C_{\perp}$ as a function of $(1/V)$ will be linear with a slope α. The plot of $(C-C_{\perp})/C_{\perp}$ as a function of $(1/V)$ fit to a linear curve as shown in the Fig 2.10. The extrapolated value of the ordinate for $1/ V = 0$ corresponds to the intercept γ. From the slope α, the parameters k can be estimated. The value of K_{33} can be estimated from k using the value of K_{11} at that particular temperature. The value of K_{11} is estimated from V_{th} and $\Delta\varepsilon$ values using equation 2.16.

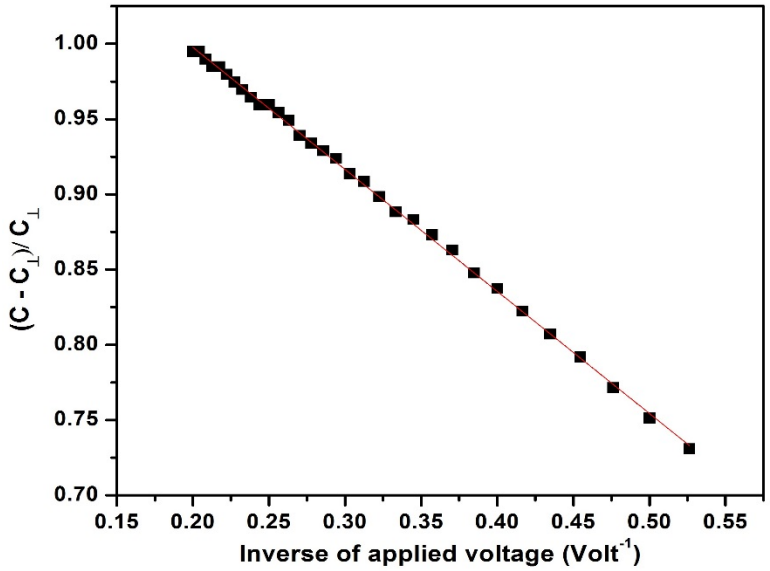

Figure 2.10: Variation of ratio of capacitance $(C-C_{\perp})/C_{\perp}$ as a function of inverse of applied voltage.

Using above mentioned method, we have estimated the value of K_{33} of 8CB. The estimated temperature variation of K_{33} value for 8CB is compared with that of values reported in literature [8] and is shown in Figure 2.11.

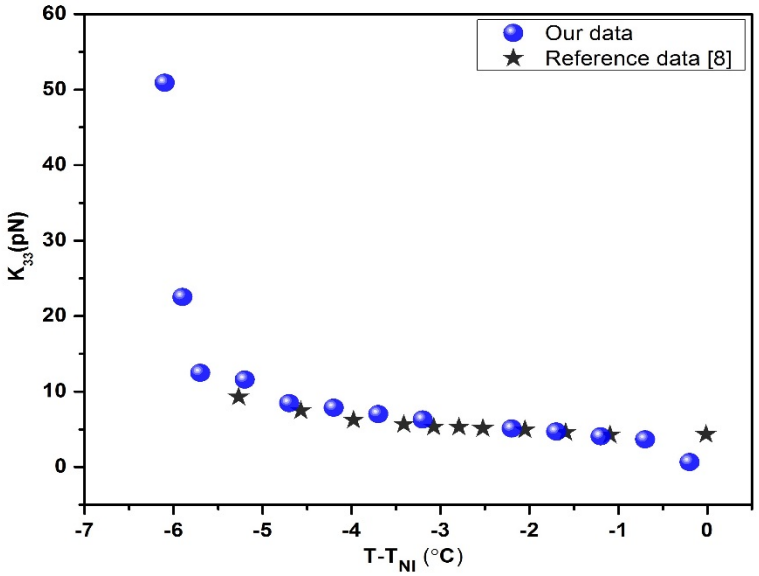

Figure 2.11: Bend elastic constant (K_{33}) value of 8CB estimated using the data obtained from our experimental set up and value from the reference [8] as a function of reduced temperature ($T-T_{NI}$).

2.7 Differential scanning calorimetry (DSC)

Differential scanning calorimetry (DSC) is a thermal analysis technique that measurers heat flow to and from a sample as a function of time and temperature.

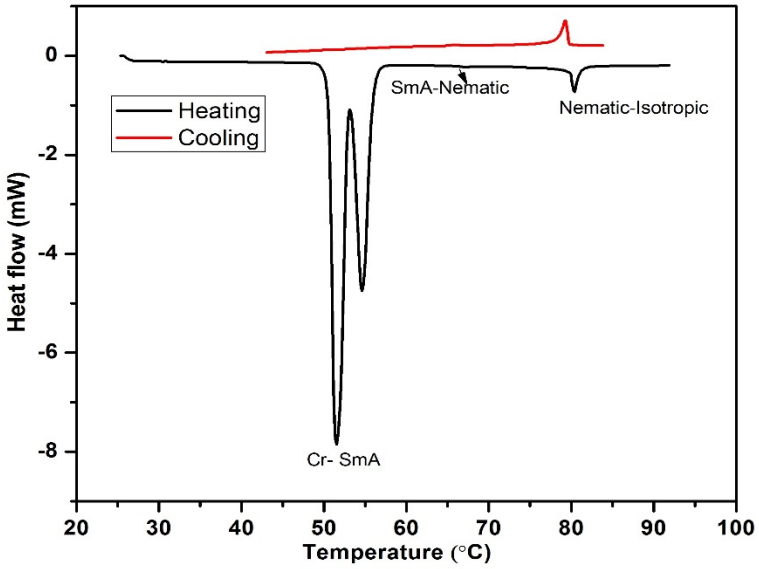

Figure 2.12: DSC data for 8OCB in heating and cooling mode.

DSC is one of the most widely used analytical instrument which can be used to study phase transition temperature, enthalpy, heat capacity and specific heat. Even though the phase transition temperature of the material can also be measured through thermal polarizing microscopy, the DSC can give more precise transition temperature values and the information about the nature of the phase transitions. The differential scanning calorimeter (Shimadzu, DSC60) was used in the experiment to determine transition temperatures.

2.8 Optical response time

Optical response time is one of the most important parameters of a LCD device. Response time of LC depends on cell thickness, applied external electric field strength, surface anchoring and rotational viscosity (γ) [9–10]. The optical response time of LC in planar aligned as well as twisted nematic (TN) geometry is measured. In planar cell, the electro-optic response of LC in nematic phase was recorded on application of modulated 60Hz square signal [11]. An AC voltage is applied across the LC cell through function generator (Agilent 33220A). When the applied AC voltage with sufficiently low frequency exceeds the V_{th} value, the response time is characterized by the rise time and the fall time. A light beam of wavelength of 632 nm is allowed to pass through the LC cell. The output intensity of light as a function of time is recorded using oscilloscope (Agilent, DSO3062A). In planar LC cell, the rise and decay times were measured from the transmittance variation between 10% to 90% and 90% to 10%, respectively [12].

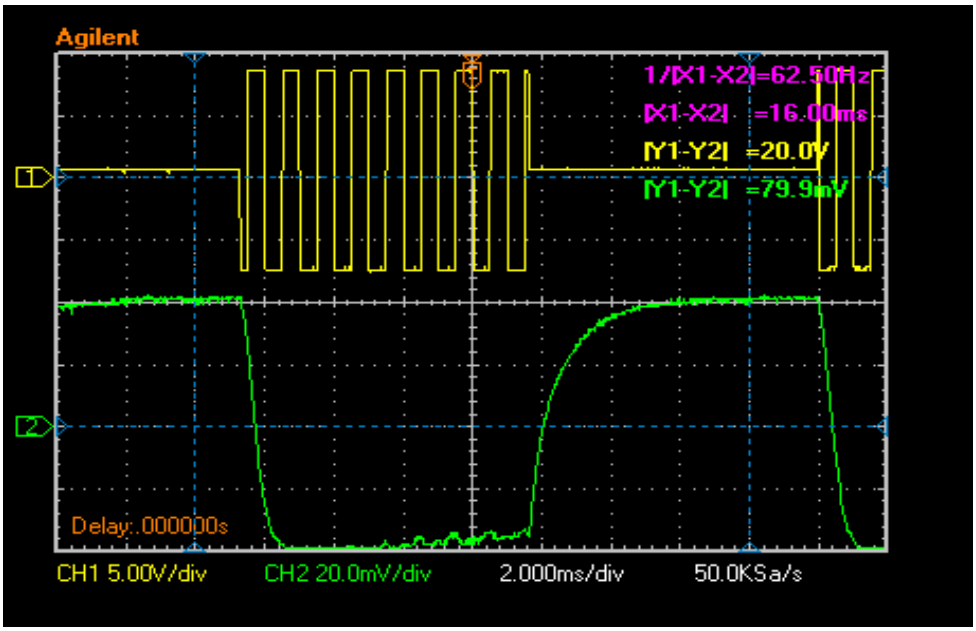

Figure 2.13: Oscillogram of the response time of NLC molecules in TN cell.

In TN cell, response time measurement was carried out by applying a signal of amplitude modulated square wave of frequency of 60 Hz (carrier frequency of 1 kHz) across the cell. The decay and rise times in the normally white TN mode cells were measured from the transmittance variation data. The oscillogram of the TN LC cell with an applied voltage of 10V at frequency of 60 Hz square wave signal (carrier frequency of 1 kHz) for one of the LC samples is shown in the Figure 2.13.

2.9 Atomic force microscopy

After the invention of the scanning tunneling microscope (STM), a number of new scanning probe microscopes (SPM) have been developed that use the key components of the STM [13]. One of the most important SPM techniques is the atomic force microscope (AFM) technique [14]. In AFM, a tip integrated to the end of a spring cantilever is brought within the interatomic separations of a surface such that the atoms of the tip and the surface are influenced by interatomic interaction. AFM techniques yield the topographic images by sensing the atomic forces between the sharp tip and the sample. A schematic diagram of AFM is shown in Figure 2.14. The tip is attached to a cantilever type spring. As the tip and sample interact, forces act on the tip and cause the cantilever (spring) to deflect. The cantilever deflection is monitored by a position detector. The output of the

detector is connected to a feedback controller that regulates the force between the sample and the tip by moving the sample up or down.

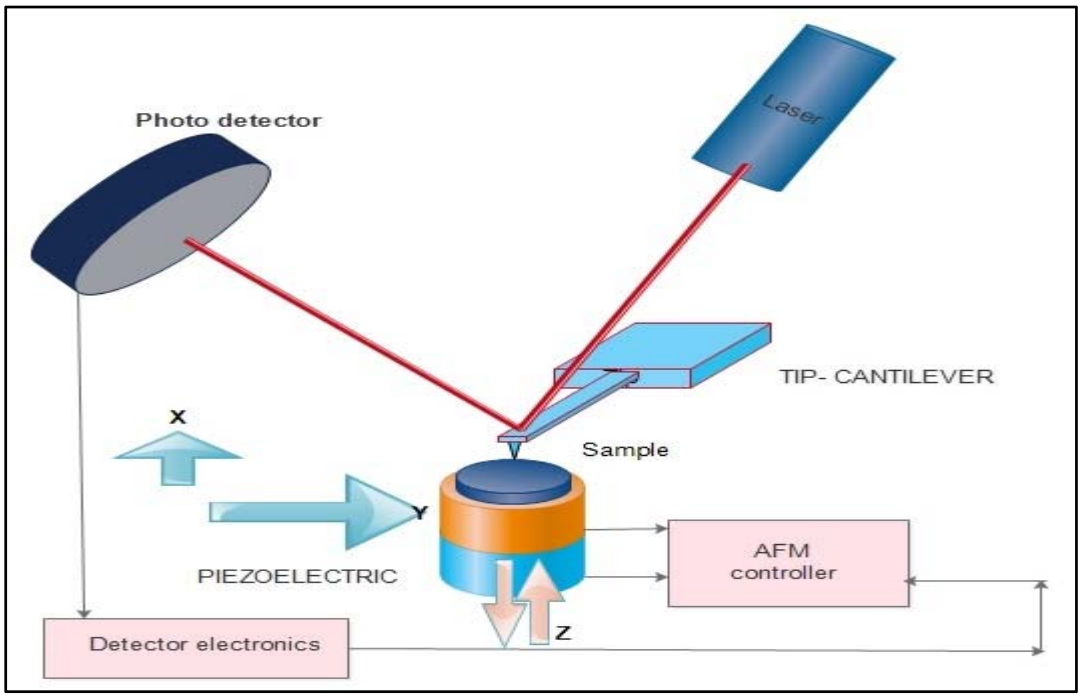

Figure 2.14: Schematic diagram of AFM.

There are numerous modes of operation of AFM. We have utilized contact and spreading resistance imaging (SRI) modes of AFM. In contact mode, the force between the tip and the sample is kept constant and by monitoring the cantilever deflection as a function of (x, y), a topographic image can be obtained. The cantilever must be soft enough to deflect a measurable amount without damaging the surface features of the sample. The amount of deflection is proportional to the force acting on the tip. In spreading resistance imaging mode of operation, a conductive AFM tip is brought in direct contact with the sample surface. A voltage bias is applied to the tip and the resulting current through the sample is measured as a function of the tip position on the surface. There are a large number of applications for the AFM in various systems including biological systems, polymers, and a host of insulator and semiconductor materials.

2.10 Current-Voltage (*I-V*) characterization technique

The *I-V* charcterization of LC sample was carried out using Keithley (Model 2400 Source meter). The in-plane charge transport mechanism for LC material was studied by recording *I-V* curve at different temperatures. For *I-V* measurement, we used gold electrodes fabricated on silicon (Si)

wafer having interelectrode separation of ~15μm. The LC material was placed on to the gold electrode coated Si substrate and mounted in the hot stage. The electric field is applied across the gold electrode and corresponding current is measured using the source meter.

References:

1. D. W. Berreman, Phys. Rev. Lett. 28, 1683, **1972**.
2. I. Dierking, *Textures of Liquid Crystals*, p33, **1999**.
3. A. J. Nicastro, *American Laboratory*, 14, 12, **1982**.
4. G. Basappa, N. V. Madhusudana, Mol. Cryst. Liq. Cryst. 288, 1, **1996**.
5. M. Schadt, J. Chem. Phys. 56, 1494, **1972**.
6. H. Gruler, T. J. Scheffer, G. Meier, Z. Naturforsh, 72n, 27, **1972**.
7. T. Uchida, Y. Takahashi, Mol. Cryst. Liq. Cryst., 72, 133, **1981**.
8. S. W. Morris, P. P. Muhoray, D. A. Balzarini, Mol. Cryst. Liq. Cryst. 139, 263, **1986**.
9. S. Kaur, A. K. Thakur, R. Chauhan, S. S. Bawa, A. M. Biradar, Physica B 352, 347, **2004**.
10. K. Skarp, I. Dahl, S. T. Lagerwall, B. Stebler, Mol. Cryst. Liq. Cryst. 114, 283, **1984**.
11. S. Gauza, X. Zhu, W. Piecek, J. Disp. Tech. 3, **2007**.
12. X. Nie, R. Lu, H. Xianyu, J Appl Phys. 101, 103110, **2007**.
13. G. Binnig, H. Rohrer, Ch. Gerber, E. Weibel, Phys. Rev. Lett. 50, 120, **1983**.
14. Q. Huo, S. Russev, T. Hasegawa, J. Nishijo, J. Umemura, G. Puccetti, K. C. Russell, R. M. Leblanc, J. Am. Chem. Soc. 122, **2002**.
15. LabView, National Instruments Corporation, N Mopac Expwy, Austin, Texas, USA.
16. J. Kumar, V. Manjuladevi, R. K. Gupta, S. Kumar, Liq. Cryst. 42, 3, **2015**.

Chapter 3

Effect of octadecylamine functionalized SWCNTs on the elastic constants and electro-optic response of a liquid crystal

3.1 Introduction

The switching characteristics of liquid crystal display (LCD) devices rely on the physical properties of the liquid crystal (LC) materials used [1]. Particularly, the values of dielectric anisotropy and elastic constants decide the reorientation of LC molecules on application of electric field [1-3]. The LCs with large value of ratio of bend to splay elastic constants are known to exhibit sharp electro-optic response [4]. Many groups have reported interesting results on measurement of the elastic constants in some LCs with longer aromatic backbone [4-6]. Balachandran *et al.* [4] have carried out measurements of elastic constants of a LC dimer exhibiting transition from ordinary nematic to a second nematic phase. They have reported that the value of bend elastic constant (K_{33}) initially increases on cooling from isotropic phase, however on further cooling, the K_{33} value decreases with decrease in temperature. In the vicinity of second nematic phase, the K_{33} reduces by a factor of 3 as compared to the value observed near to the isotropic-nematic transition point. In an oxadiazole bent-core system, the K_{33} was reported to be temperature independent in its nematic phase [5]. Aya *et al*. [4] reported that in a diphenylacetylene-core based compound, K_{33} was found to be of the order of nanonetwons over a wide temperature range compared to K_{11} which is of the order of piconewtons. In general, the display industry employs the calamitic LCs on a large scale. In this era of nanotechnology, nanomaterials are being used in many device fabrication. To alter the physical properties of LCs, efforts have been made by many researchers by doping them with nanoparticles and carbon nanotubes [7-18]. Although carbon nanotubes (CNTs) exhibit similar shape anisotropy as compared to a calamitic LC molecule, namely rod shaped, the CNTs can possess larger length to width (L/W) aspect ratio. Due to the shape

compatibility, the CNTs can be doped in the LC matrix. The *L*/*W* ratio and the organic functionalization of the CNTs can play a key role in altering the physical properties of the LC medium [12-16]. In 2013, Lim *et al.* [17] have reported a decrement in electro-optic response time due to the incorporation of thin multiwalled carbon nanotubes in a negative dielectric anisotropic LC material filled in a patterned vertically aligned cell. Though, there are many studies on determination of elastic constants of calamitic LCs but there is hardly any report on a systematic study of elastic constant of calamitic LCs doped with single-walled carbon nanotubes (SWCNT). Octadecylamine functionalized SWCNTs are soluble in many organic solvents and also at low concentrations, it is found to be dispersible in LCs [15].

In this chapter, we are presenting the results of measurements of elastic constants of nanocomposites of a LC compound, n-octyl cyanobiphenyl (8CB) doped with octadecylamine functionalized SWCNTs (ODA-SWCNT) as a function of temperature. The dielectric anisotropy, birefringence, and optical response time are also measured for pure 8CB as well as its nanocomposites with ODA-SWCNT. The dielectric anisotropy as a function of reduced temperature decreases with an increase in the concentration of ODA-SWCNT. The rise time decreases and decay time increases in the sample with highest concentration of ODA-SWCNT. The temperature range of smectic phase is widen with an increase in the concentration of ODA-SWCNT.

3.2 Materials and methods

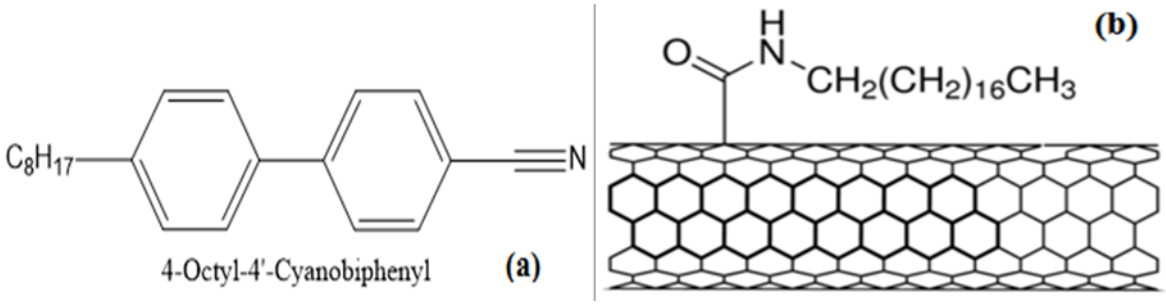

Cr-21.5°C-SmA -33.5°C-N-40.3°C-Iso

Figure 3.1: Molecular structure of 8CB and its phase transition temperatures (a). Chemical structure of ODA-SWCNT (b).

The LC n-octyl cyanobiphenyl (8CB) was procured from Sigma Aldrich and molecular structure of 8CB is shown in Figure 3.1(a). Octadecylamine functionalized single walled CNT (ODA-

SWCNT) was purchased from Carbon Solutions Inc and structure is shown in Figure 3.1(b). As ODA-SWCNT is a functionalized CNT, at low concentration it gets disperse in chloroform solvent very well. Using the solution, we have prepared ODA-SWCNT nanocomposites of 8CB and the concentration of ODA-SWCNT is varied from 0.05 to 0.15wt%. In Figure 3.2, a photograph of solution of ODA-SWCNT dispersed in chloroform at 0.3 mg/ml (a) and 0.03mg/ml (b) is shown.

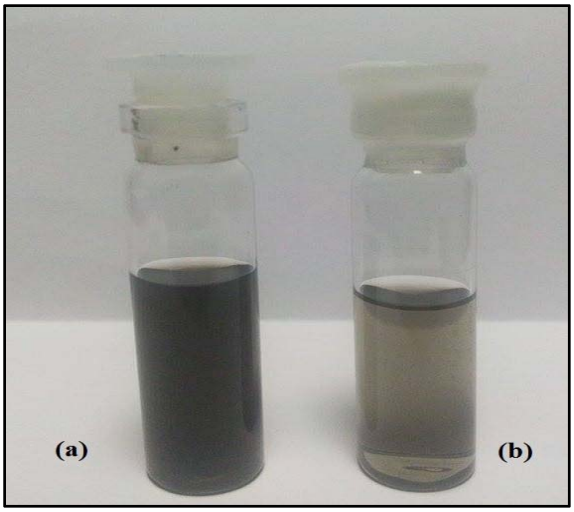

Figure 3.2: Photograph of solution of ODA-SWCNT dispersed in chloroform at (a) 0.3 mg/ml and (b) 0.03mg/ml.

The planar aligned cells are prepared using indium tin oxide (ITO) coated glass plates. The thickness of the cells is ~10 μm. The electro-optic as well as dielectric measurements are carried out at 4.1 kHz. Prior to any measurements, pure 8CB and its nanocomposite LC cells are observed in the nematic phase under a polarizing microscope. Like a pure 8CB cell, the ODA-SWCNT nanocomposite LC cells reveal a uniform texture indicating a uniform nematic director field between crossed polarizers. The dielectric constant parallel and perpendicular to the molecular long axis are denoted by $\varepsilon_{\parallel}$ and $\varepsilon_{\perp}$, respectively. For measuring the $\varepsilon_{\parallel}$, homeotropic cells are prepared by coating the ITO glass plates with a surfactant, trimethoxy (octadecyl) silane. The dielectric measurement of each sample is carried out as a function of temperature at a frequency of 4.1 kHz. The dielectric constant is also recorded as a function of voltage at a given temperature. The electro-optic response of the pure 8CB and its nanocomposites in nematic phase was recorded on application of 60Hz square signal. The rise and decay times in planar aligned cell were measured from the transmittance variation between 10% to 90% and 90% to 10% of the maximum transmittance, respectively [18].

3.2.1 Estimation of birefringence

The birefringence ($\Delta\mu$) of the LC sample is estimated using the transmitted intensity data [18]. The planar LC cell filled with sample is placed in the hot stage, which is kept between crossed polarizers. It was ensured that the rubbing direction of cell is making an angle of 45° with either of the polarizers in order to get the maximum intensity. A laser light of wavelength of 633 nm is incident on the sample and the transmitted intensity as a function of temperature is recorded using a photodiode. The transmitted intensity is given by

$$I_{tr} = I_0(1-\cos\Delta\phi)/2 \qquad (3.1)$$

where I_0 is the intensity of light incident on the LC sample and $\Delta\phi$ is the optical phase difference arising due to the LC cell. The $\Delta\phi$ is given by

$$\Delta\phi = 2\pi\Delta\mu d/\lambda \qquad (3.2)$$

where $\Delta\mu = \mu_e - \mu_o$ is the birefringence, d is the thickness of the cell and λ is the wavelength of incident light. In nematic phase, the transmitted intensity varies with the temperature due to optical phase retardation. The transmitted intensity profile of pure 8CB as a function of temperature is shown in Figure 3.3 (a). The thickness of the cell was ~ 8.5μm. The change in phase difference near the isotropic to nematic temperature was estimated by measuring the transmitted intensity as a function of applied voltage (Figure 3.3 (b). Using this method we have estimated $\Delta\mu$ of 8CB and compared with the data reported in literature.

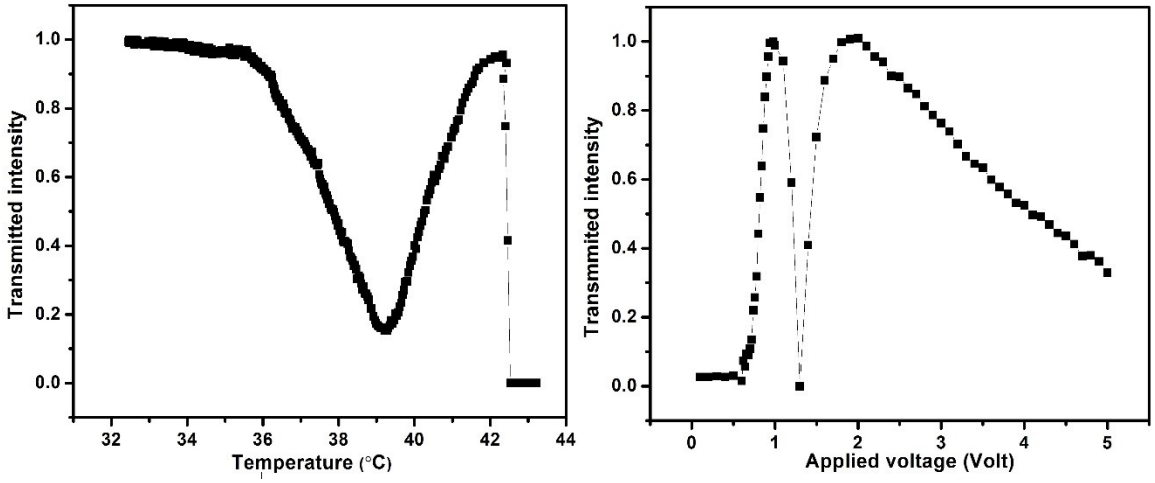

Figure 3.3: (a) The temperature variation of the transmitted intensity of 8.5 μm thick sample of 8CB and (b) transmitted intensity as a function of applied voltage.

3.3 Results and discussion

The variation of $\Delta\mu$ as a function of reduced temperature ($T-T_{NI}$) for pure 8CB and its ODA-SWCNT nanocomposites is shown in Figure 3.4. Here, T_{NI} is the temperature for nematic-isotropic phase transition and T is any given temperature. The observed value of $\Delta\mu$ for pure 8CB is in good agreement with the data reported in literature [19]. The value of $\Delta\mu$ is enhanced only by ~1% at a reduced temperature of $T-T_{NI}$ = -2°C in the highest concentration of ODA-SWCNT nanocomposite of 8CB as compared to that of pure 8CB. The value of $\Delta\mu$ enhances as the smectic phase is approached and is enhanced by ~6% at $T-T_{NI}$ = -8°C for the nanocomposites of 8CB as compared to that of pure 8CB. The value of $\Delta\mu$ of a LC material is dependent on the π- electron conjugation of the molecular core, thus the more linearly conjugated LC would exhibit a larger optical anisotropy. In an earlier work, it was suggested that increase in the effective molecular conjugation length leads to increase in birefringence [20]. In the present chapter, due to the incorporation of longer ODA-SWCNTs, the effective molecular conjugation length may increase leading to increase in $\Delta\mu$ value.

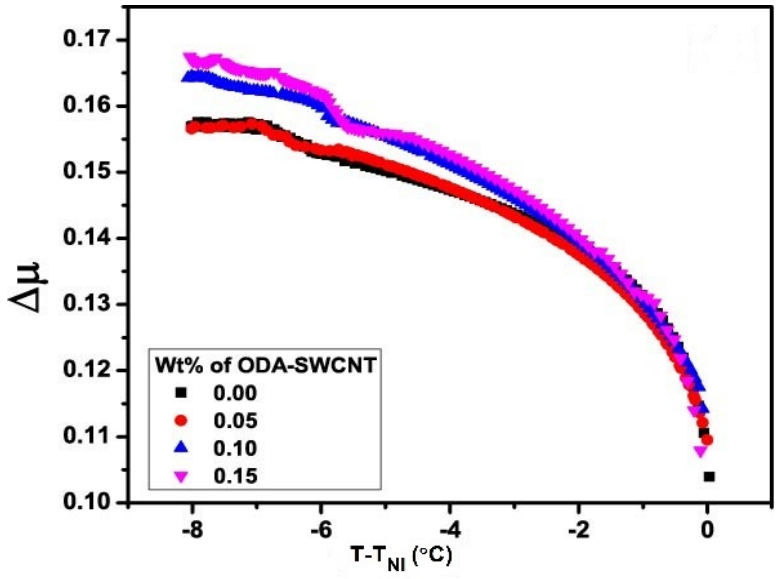

Figure 3.4: Variation of birefringence ($\Delta\mu$) as a function of reduced temperature ($T-T_{NI}$) for pure 8CB and its ODA-SWCNT nanocomposites.

3.3.1 Dielectric constant measurement

The dielectric measurements are carried out on pure 8CB as well as its ODA-SWCNT nanocomposites. The dielectric constant for pure 8CB and its ODA-SWCNT nanocomposites as a

function of temperature is shown in Figure 3.5. The $\varepsilon_{\parallel}$ and $\varepsilon_{\perp}$ components of dielectric constant are measured using planar and homeotropic cells. As the temperature decreases from isotropic state, the $\varepsilon_{\parallel}$ starts to increases whereas $\varepsilon_{\perp}$ decreases. On approaching the temperature to SmA phase, $\varepsilon_{\parallel}$ starts to decrease because the interaction of a dipole moment with the dipoles of surrounding molecules in the smectic phase is different from that of in the nematic phase. For dipoles situated in the central part of the molecules, the distance between the dipoles of molecules in different smectic layers is much greater than the distance between neighbouring dipoles in the same layer [21]. The antiparallel correlation of dipole moment with neighbours within the layers is possible in smectic phase. Hence, $\varepsilon_{\parallel}$ starts to decrease on approaching the temperature to smectic phase. The dielectric constant $\varepsilon_{\perp}$ also changes as the temperature reach to smectic phase. In some compounds, it may increases on approaching the temperature to smectic phase due to parallel correlation of dipole moments.

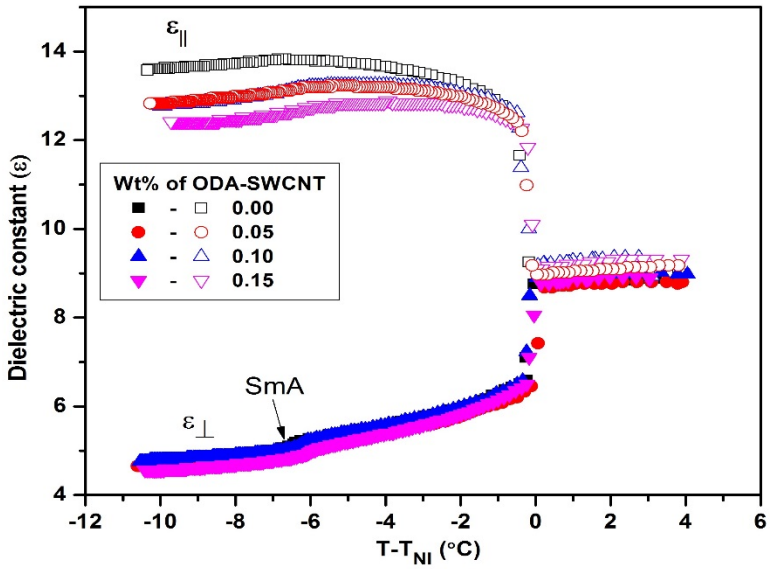

Figure 3.5: Variation of dielectric constant (ε) as a function of reduced temperature ($T-T_{NI}$) for pure 8CB and its ODA-SWCNT nanocomposites.

The value of $\varepsilon_{\parallel}$ decreases with increasing concentration of ODA-SWCNT. In case of highest concentration of ODA-SWCNT nanocomposites at $T-T_{NI} = -8°C$, the decrease in $\varepsilon_{\perp}$ is ~6% while the decrement in $\varepsilon_{\parallel}$ is ~9.5%. As a result, the dielectric anisotropy ($\Delta\varepsilon$) decreases in the nematic phase with increase in concentration of ODA-SWCNT (Figure 3.7). The values of $\Delta\varepsilon$ for pure 8CB are in good agreement with literature as shown in Figure 3.6 [22, 23].

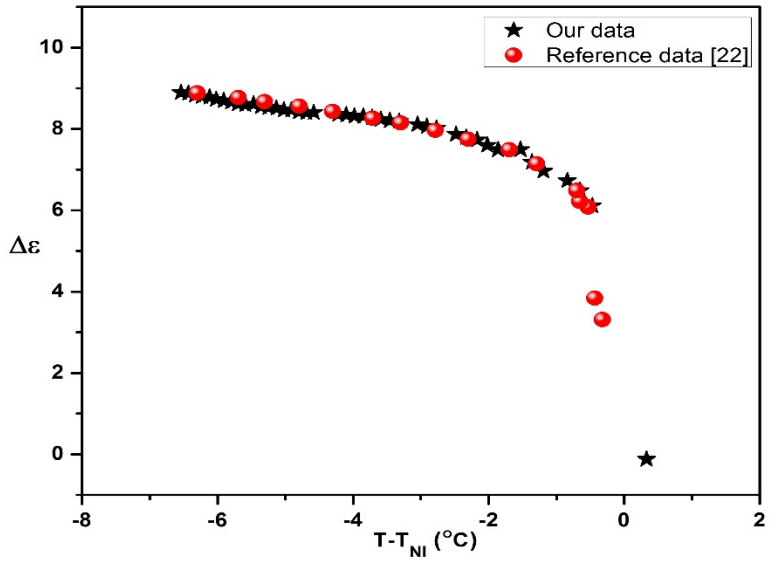

Figure 3.6: Variation of the dielectric anisotropy (Δε) as a function of reduced temperature (T-T_{NI}) for 8CB (*and o symbols correspond to Δε from our measurements and reference [22] respectively).

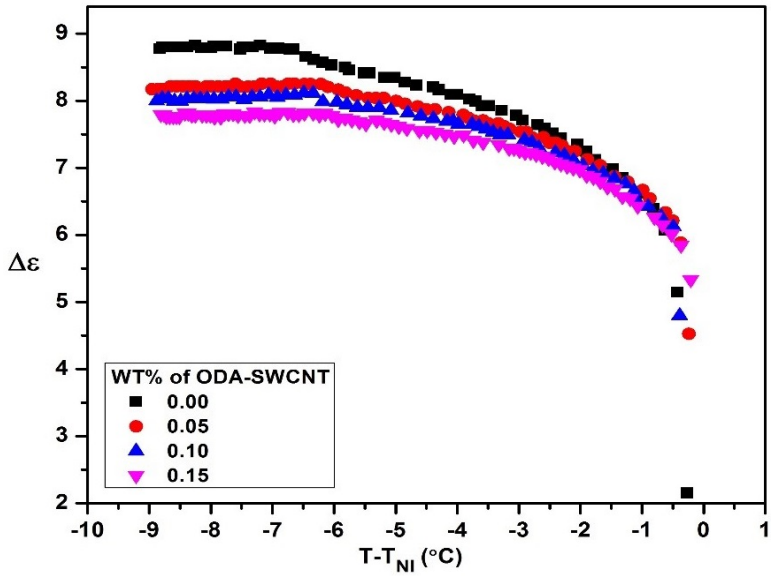

Figure 3.7: Variation of dielectric anisotropy (Δε) as a function of reduced temperature (T-T_{NI}) for pure 8CB and its ODA-SWCNT nanocomposites.

In an azoxy benzene compound [24], value of Δε decreased with decreasing temperature which was suggested due to the occurrence of smectic phase at lower temperatures. It was suggested that as the distance between the molecules in smectic planes is much smaller than the distance between different planes, an increased antiparallel correlation between the components of the dipole moments along the molecular axis can be expected. Consequently, the effective dipole

moment in this direction is reduced leading to a decrease of $\varepsilon_{\parallel}$. Similarly, due to presmectic ordering in the nanocomposites of 8CB, the antiparallel correlation of the dipoles parallel to the nematic director increases and as a result, the effective dipole moment in the nematic phase reduces leading to decrease of $\varepsilon_{\parallel}$ [24, 25].

3.3.2 Order parameter

The order parameter (S) is estimated as a function of temperature from the value of $\Delta\varepsilon$. The temperature variation of S in nematic phase can be fitted to Haller's extrapolation formula [26], viz.

$$\Delta\varepsilon = \Delta\varepsilon_0 (1 - \frac{T}{T*})^{\beta} \qquad (3.3)$$

and

$$S = \frac{\Delta\varepsilon}{\Delta\varepsilon_0} \qquad (3.4)$$

where T* corresponds to the clearing temperature at which S smoothly reduces to zero (if it did not have a discontinuous jump at clearing temperature), $\Delta\varepsilon_0$ is the dielectric constant of LC molecules in perfectly aligned state and β is a constant. The temperature variation of $\Delta\varepsilon$ fitted using the Haller's extrapolation method for pure 8CB is shown in Figure 3.8.

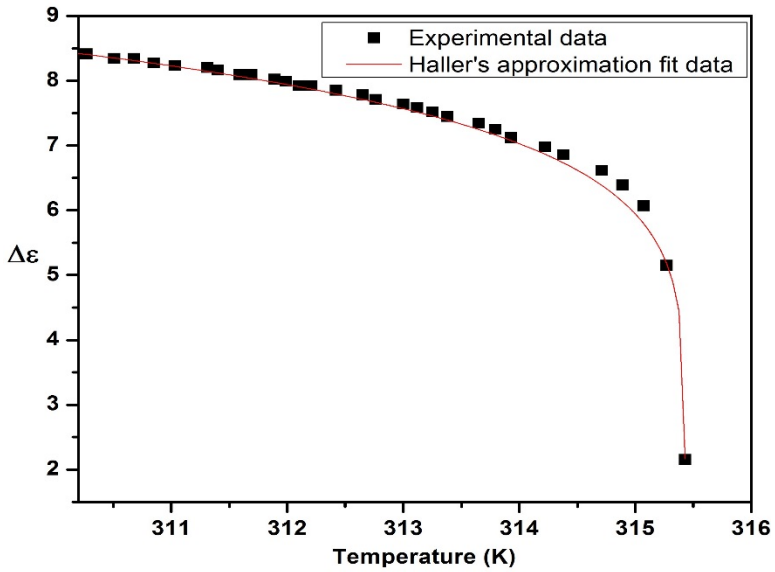

Figure 3.8: Temperature variation of $\Delta\varepsilon$ fitted using the Haller's extrapolation method for pure 8CB.

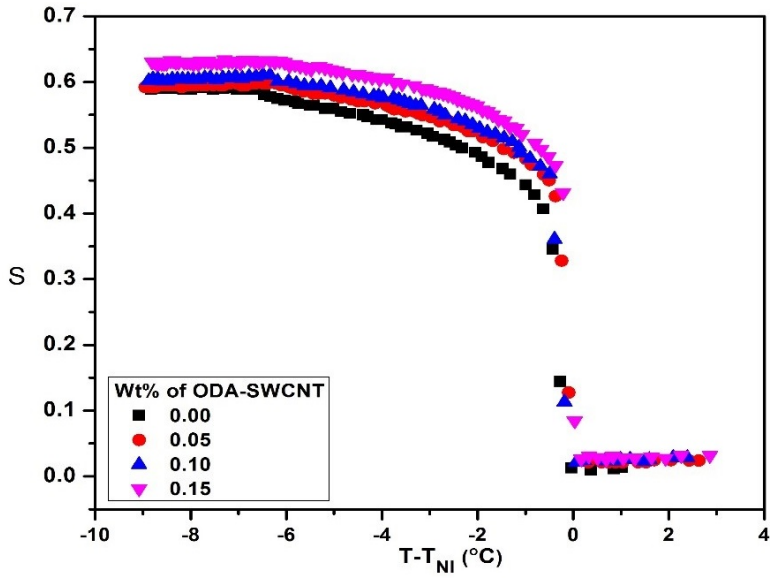

Figure 3.9: Order parameter (*S*) as a function of reduced temperature (T-T_{NI}) for pure 8CB and its ODA-SWCNT nanocomposites.

The variation of *S* for pure 8CB and its nanocomposites is shown in Figure 3.9. The value of *S* at any given temperature increases with increasing concentration of ODA-SWCNT. This indicates the orientational order increases due to the incorporation of ODA-SWCNTs. The *S* is increased by 5 % in highest concentration of ODA-SWCNT as compared to pure 8CB.

3.3.3 Elastic constant measurement

In planar geometry, the LC material is sandwiched between two parallel plates and the easy axis of the anchoring of the top and bottom alignment layers is parallel to the plates. In the absence of fields, the LC director is uniformly aligned parallel to substrate. When an applied voltage is above the threshold voltage (V_{th}), the LC director starts to move away from plane of substrate and parallel to the applied electric field. Due to the anchoring at the surface of the plates, LC director in the distorted state is not uniform. Elastic constant of such distorted state corresponds to splay elastic constant (K_{11}). In planar aligned cell, the V_{th} is related to $\Delta\varepsilon$ and K_{11} as

$$V_{th} = \pi\sqrt{\frac{K_{11}}{\varepsilon_0 \Delta\varepsilon}} \qquad (3.5)$$

The K_{11} of a positive dielectric anisotropy LC in a planar aligned cell is determined using the Equation 3.5. The K_{11} value as a function of reduced temperature for pure 8CB and its ODA-SWCNT nanocomposites is shown in Figure 3.10 (a). The estimated value of K_{11} for pure 8CB

compares well with that of literature as shown in Figure 3.10 (b) [22, 23]. As the concentration of ODA-SWCNT increases, the elastic constant at any given temperature increases and the effect is more pronounced on approaching towards SmA (i.e., $T\text{-}T_{NI}$ = -5 to -6.5 ^{0}C).

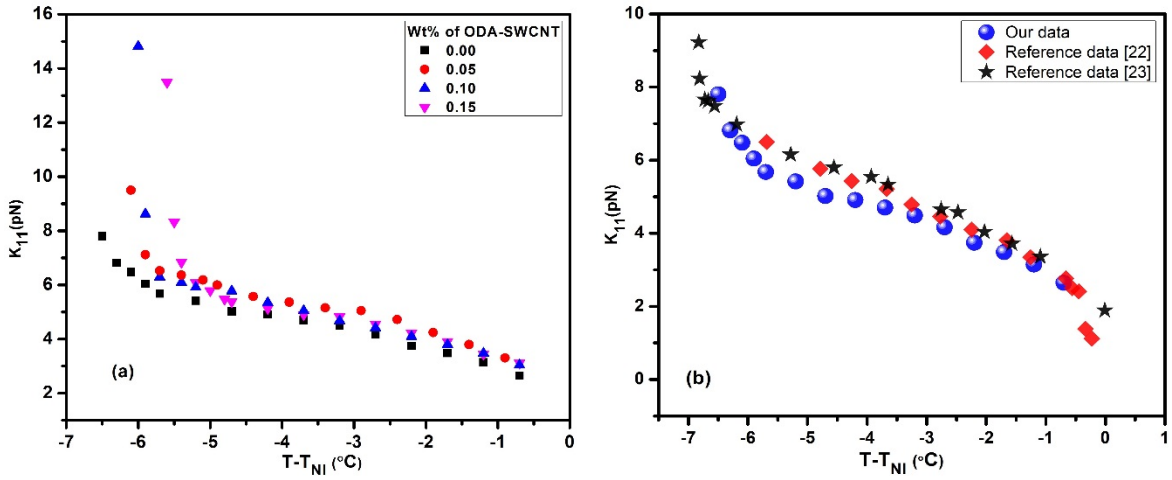

Figure 3.10: (a) Splay elastic constant (K_{11}) as a function of reduced temperature ($T\text{-}T_{NI}$) for pure 8CB and its ODA-SWCNT nanocomposites and (b) estimated K_{11} for pure 8CB and reference [22, 23].

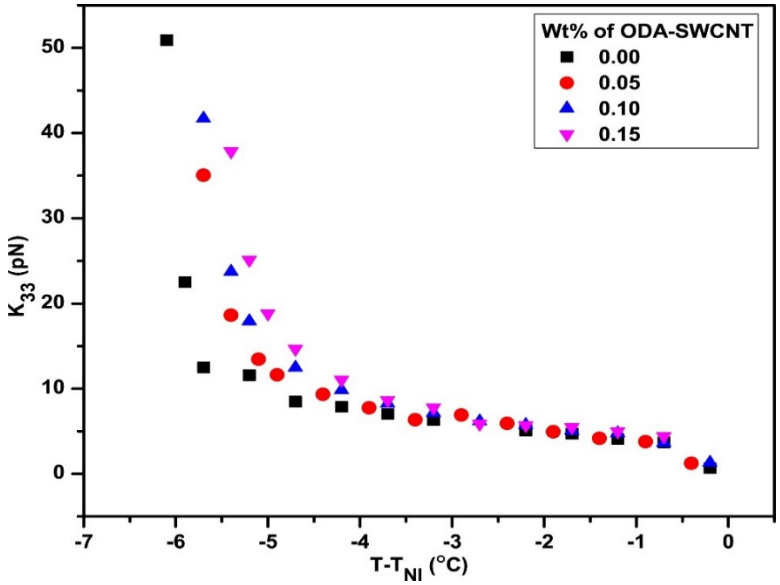

Figure 3.11: Variation of bend elastic constant (K_{33}) as a function of reduced temperature ($T\text{-}T_{NI}$) for pure 8CB and its ODA-SWCNT nanocomposites.

The bend elastic constant (K_{33}) is estimated from the cell capacitance data at voltages above the threshold voltage using the *C-V* curve method [22, 27-29]. The capacitance at any particular position in the cell is dependent on the applied voltage, the dielectric anisotropy and elastic constant anisotropy.

The temperature variation of K_{33} of 8CB and its ODA-SWCNT nanocomposites is shown in Figure 3.11. The value of K_{33} increases as the concentration of ODA-SWCNT increases at any given reduced temperature. As the smectic phase is approached, the correlation length ξ increases typically from a few hundred Å (at a few degrees above the N-Sm transition temperature) to a few thousand Å (at a few tenths of a degree above the N-Sm transition temperature) [2, 20, 30]. Coherence length ξ is a measure of the length over which order parameter fluctuations are correlated. The relatively long range pseudo layer structure within the fluctuating smectic droplets inhibit a bend or twist distortion, as these deformations involve compression or dilation of pseudolayers. This leads to an increase of K_{33} and twist elastic constant (K_{22}) and ξ [2, 30]. Hence, we propose that with incorporation of ODA-SWCNT into the bulk of 8CB the pseudolayer structure within the comparatively bigger droplets might lead to a further increase in the value of ξ and hence lead to increase in the value of elastic constants as the smectic phase is approached. From both plots of K_{33} and K_{11}, it can be clearly inferred that the temperature range over which smectic phase is observed increases with increasing concentration of ODA-SWCNT.

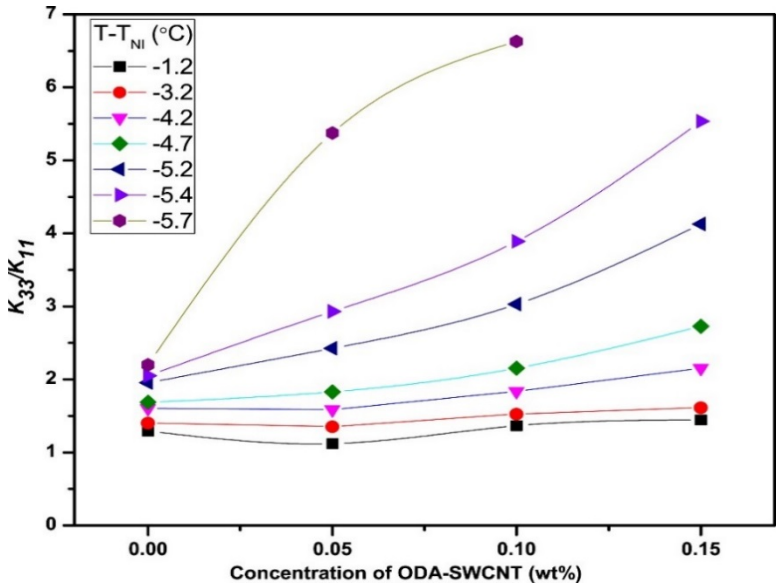

Figure 3.12: Elastic constant ratio (K_{33}/K_{11}) as a function of concentration of ODA-SWCNT in the nanocomposites of 8CB at various temperatures.

The ratio of elastic constants (K_{33}/K_{11}) as a function of ODA-SWCNT in nanocomposites of 8CB is shown in Figure 3.12. The variation of K_{33}/K_{11} as a function of ODA-SWCNT concentration in 8CB at higher temperature is linear and invariant with respect to concentration.

However, at reduced temperatures of 4°C and above, the variation of K_{33}/K_{11} as a function of ODA-SWCNT concentration deviates more and more from linearity.

Meer *et.al* [30] had developed a simple model for estimating the stiffness constants of NLC based on distributed harmonic forces between the molecules. Considering molecular centres of neighbours distributed at random around the excluded volume due to the central molecule, the ratio of K_{33}/K_{11} is predicted to vary as $(L/W)^2$. For the molecules with short alkyl chains, the ratio of K_{33}/K_{11} is indeed found to increase with L/W with introduction of relatively rigid end or side groups. However, within a homologous series, ratio of K_{33}/K_{11} decreases with increase in the length of alkyl chain. With the introduction of ODA-SWCNT the former effect holds good which leads to an increase in ratio of K_{33}/K_{11}.

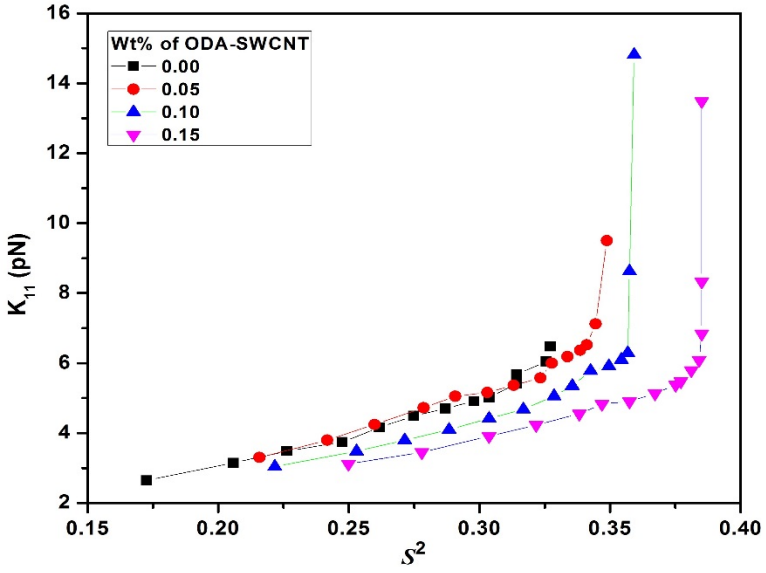

Figure 3.13: Splay elastic constant (K_{11}) as a function of square of order parameter (S^2) in the nematic phase for pure 8CB and its ODA-SWCNT nanocomposites.

According to mean filed theory, $K_{ii} \propto S^2$ at high temperature [31]. The variation of K_{11} and K_{33} elastic constants as function of square of estimated order parameter (S^2) for pure 8CB as well as its ODA-SWCNT nanocomposites are shown in Figure 3.13 and 3.14. K_{11} and K_{33} are proportional to S^2 at lower values of order parameter (i.e., at high temperature) and start diverging as the sample approaches smectic phase. The divergence becomes pronounced with increase in concentration of ODA-SWCNT, which is due to an increase in the pseudo layer structure at low temperatures.

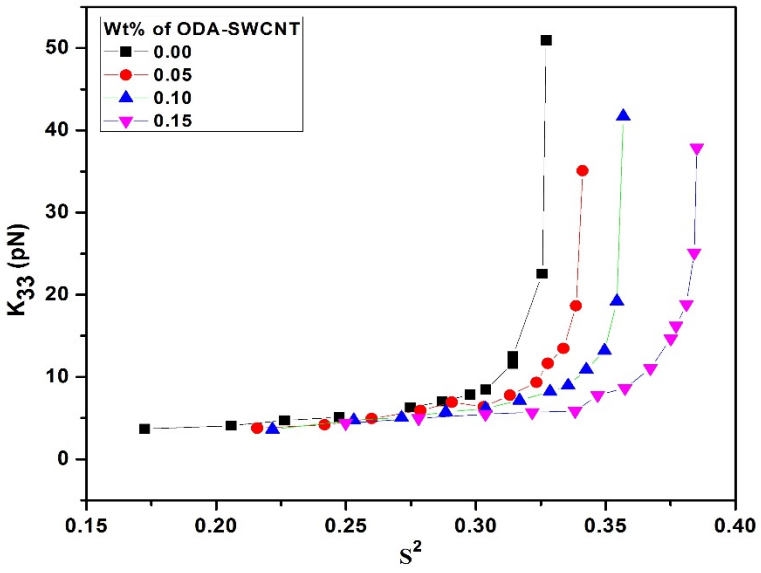

Figure 3.14: Bend elastic constant (K_{33}) as a function of square of order parameter (S^2) in the nematic phase for pure 8CB and its ODA-SWCNT nanocomposites.

3.3.4 Electro-optic response time

The variation of V_{th} as a function of (T-T_{NI}) in the nematic phase for pure 8CB as well as for its nanocomposites is shown in Figure 3.15. The value of V_{th} at any given temperature increases with increasing concentration of the dopant ODA-SWCNT due to increase of K_{11}.

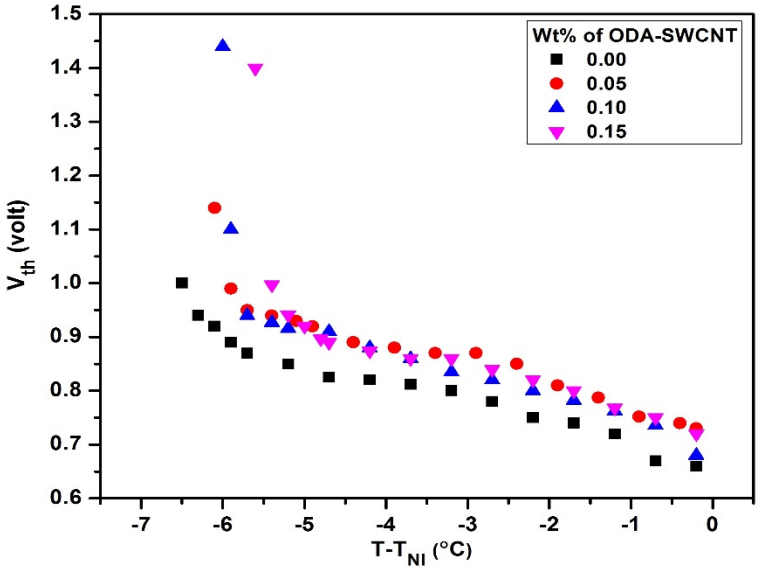

Figure 3.15: Threshold voltage (V_{th}) as a function of reduced temperature (T-T_{NI}) for pure 8CB and its ODA-SWCNT nanocomposites.

The electro-optic switching of 8CB in the nematic phase on application of modulated 60Hz square wave (1 kHz carrier frequency) is recorded as a function of voltage. These measurements were carried out at a reduced temperature of $T\text{-}T_{NI}$ = -2°C and -3°C at which the ratio of K_{33}/K_{11} are almost similar for all concentrations indicating no smectic like domains at these temperatures. The rise time and decay time as function of applied voltage for pure 8CB and its ODA-SWCNT nanocomposites is shown in Figure 3.16. For a given sample, the rise time as a function of applied voltage decreases whereas that of the decay time increases.

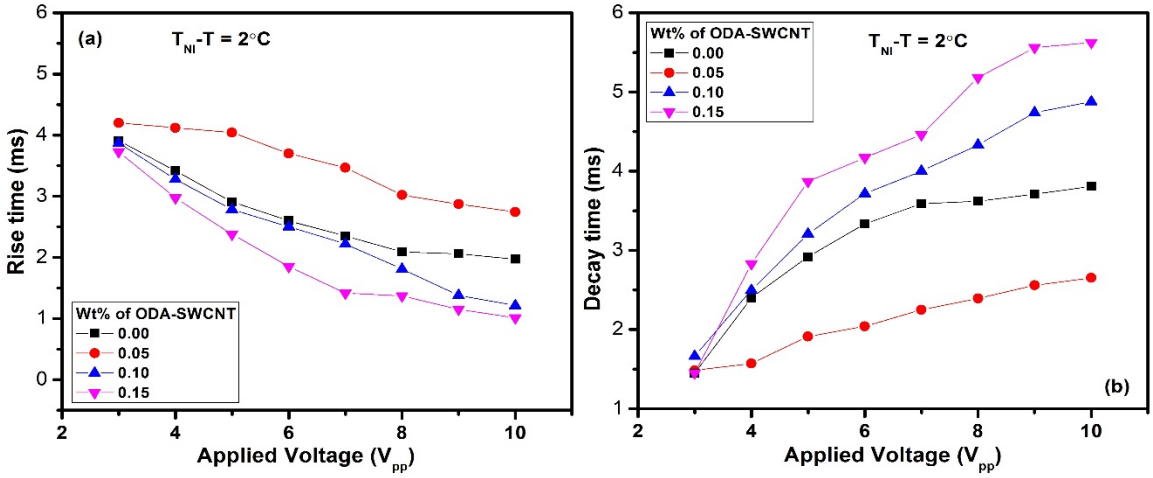

Figure 3.16: (a) Rise time and (b) decay time as a function of applied voltage peak-to-peak (V_{PP}) in the nematic phase at a reduced temperature $T\text{-}T_{NI}$= -2^0C for 8CB as well as its ODA-SWCNT nanocomposites.

At a particular value of applied voltage, the rise time increases for 0.05wt% of ODA-SWCNT nanocomposites of 8CB compared to that of pure 8CB. However, with further increase in the concentration of ODA-SWCNT at any given applied voltage, the rise time decreases (Figure 3.16 (a)). Whereas, at any particular value of applied voltage, the decay time for 0.05wt% of ODA-SWCNT nanocomposite of 8CB decreases compared to that of pure 8CB (Figure 3.16(b)). On further increase in concentration of ODA-SWCNT, the decay time increases. These results indicate that at lower concentration ODA-SWCNT (0.05 wt%), the nanotubes prefer to align in the vicinity of the aligning PI on the substrate, as already reported in our earlier work [15]. However, as the concentration increases, the ODA-SWCNT is dispersed into the bulk of the nematic medium leading to a faster switching on application of external electric field. On removal of external field, the ODA-SWCNT nanocomposite with higher concentrations take longer time compared to the pure LC to come back to the original state. In an earlier work, it is reported that the LC sample

with stronger anchoring strength at the polymer/LC interface took less time to return to the original state upon removal of the field [32].

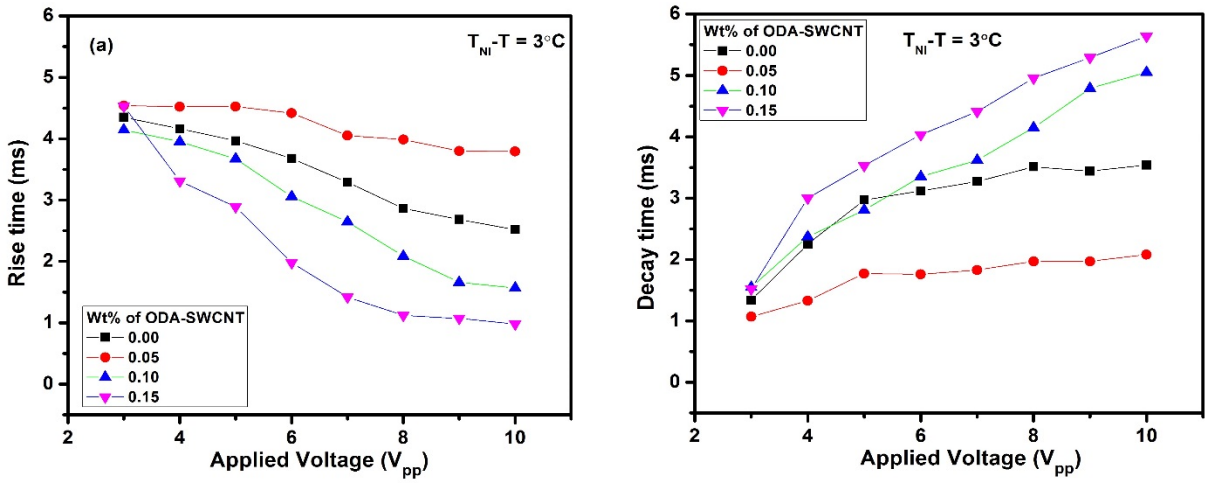

Figure 3.17: Rise time (a) and (b) decay time as a function of applied voltage peak-to-peak (V_{PP}) in the nematic phase at a reduced temperature $T-T_{NI}$= -3°C for 8CB as well as its ODA-SWCNT nanocomposites.

We have also measured the response time at a reduced temperature of $T-T_{NI}$ = -3°C. As the temperature decreases from isotropic state, response time increases due to increase in the viscosity. It can be seen from Figure 3.17 that the rise time and decay time maintain the same trend as it was measured at $T-T_{NI}$ = -2°C. On initial addition of ODA-SWCNT in the LC, the anchoring strength at the PI and LC-CNT interface increases due to the π-π electron stacking between ODA-SWCNT, LC and the aligning layer [15, 33]. As the concentration of ODA-SWCNT increases, the nanotubes disperse in the bulk LC medium where the LC molecules around the ODA-SWCNT form larger domains. On application of external electric field, these domains reorient with the field, and on switching off the field, it takes longer time for the system to relax. Optical response time is linearly proportional to the director reorientation time and is weakly dependent on the initial applied voltage. The slower optical decay time is believed to originate from slightly weaker restoring elastic torque [32].

Based on our studeis, we propose a model as shown in Figure 3.17. For the very low concentration of the ODA-SWCNT (≤ 0.05 wt%) in 8CB, more number of the ODA-SWCNTs are anchored at the alignment layer (Figure 3.18 (a)). Such anchoring of the ODA-SWCNT enhances the rise time of electro-optic response on application of electric field (Figure 3.18(b)). With the increase in

concentration of ODA-SWCNT (≥ 0.05 wt%), in addition to the alignment layer, the ODA-SWCNTs is distributed in the bulk LC medium (Figure 3.18(c)). Such distribution of the ODA-SWCNTs brings down the rise time of the electro-optic response (Figure 3.18(d)).

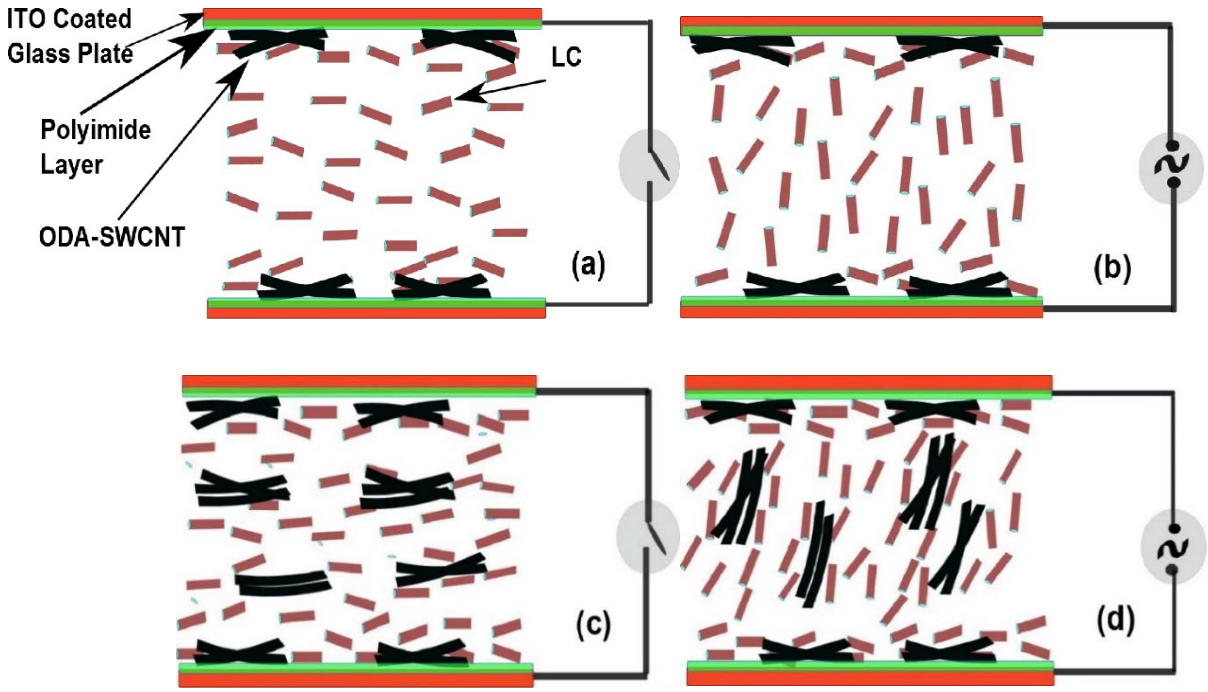

Figure 3.18: A schematic model representing the orientation of ODA-SWCNT nanocomposites of LC in the planar aligned LC cell: at lower concentration of ODA-SWCNT (≤ 0.05 wt%) (a) without and (b) with electric field, and at higher concentration of ODA-SWCNT (c) without and (d) with electric field.

3.4 Conclusions

The electro-optic and dielectric properties of pure 8CB and its ODA-SWCNT nanocomposites are investigated. The electro-optic threshold voltage in the nematic phase of ODA-SWCNT nanocomposite of 8CB is enhanced as compared to that of pure 8CB. The dielectric anisotropy as a function of reduced temperature decreases with increase in concentration of ODA-SWCNT. The ratio of bend to splay elastic constants (K_{33}/K_{11}) of ODA-SWCNT nanocomposite of 8CB is enhanced considerably as compared to that of pure LC near to the nematic to smectic transition temperature. The temperature range of smectic phase increases with increase in concentration of ODA-SWCNT. The electro-optic response rise time increased at low concentration of ODA-SWCNT (≤0.05 wt%) indicating the presence of ODA-SWCNT at the alignment layer. At higher concentrations (>0.05 wt % and ≤ 0.15 wt%) of ODA-SWCNT the rise time decreases due to formation of the large size nematic domains formed around the ODA-SWCNT distributed in the

nematic medium. At the lower concentration of ODA-SWCNTs (0.05 wt%), the anchoring of the nanotubes at the LC-electrode interface is favoured. At higher concentration of the ODA-SWCNTs, in addition to the anchoring at the interface, the nanotubes which are dispersed in the LC medium increases the orientational ordering. Our preliminary study suggests that the CNT in the alignment layer also affects the optical response time of LC as well as other physical parameters. We have observed a significant change in the physical properties and response time of NLC using a mixture of PI and CNT as an alignment layer, which is discussed in next chapter.

References:

1. M. J. Bradshaw, E. P. Raynes, I. Fedak, A. J. Leadbetter, J Phys France. 45, 157, **1984**.
2. P. G. De Gennes, J. Prost. *The Physics of Liquid Crystals*, Clarendon Press; Oxford. **1993**.
3. S. Chandrasekhar, *Liquid Crystals*, Cambridge University Press; Cambridge. **1992**.
4. S. Aya, H. Obara, D. Pochiecha, F. Araoka, K. Okano, K. Ishikawa, E. Gorecka, T. Yamashita, H. Takazoe, Adv. Mater. 26, 1918, **2014**.
5. R. Balachandran, V. P. Panov, J. K. Vij, A. Kocot, M. G. Tamba, A. Kohlmeier, G. H. Mehl, Liq. Cryst. 40, 681, **2013.**
6. S. Kaur, J. Addis, C. Greco, A. Ferrarini, V. Gortz, J. W. Goodby, H. F. Gleeson, Phys. Rev. E. 86, 041703, **2012**.
7. A. Chandran, J. Prakash, K. K. Naik, A. K. Srivastava, R. Dabrowski, M. Czerwinski, A. M. Biradar, J. Mater. Chem. C. 2, 1844, **2014**.
8. U. B. Singh, R. Dhar, R. Dabrowski, M. B. Pandey, Liq. Cryst. 40, 774, **2013**.
9. H. K. Chung, H. G. Park, Y. S. Ha, J. M. Han, J. W. Lee, D. S. Seo, Liq. Cryst. 40, 632, **2013**.
10. P. Goel, P. L. Upadhyay, A. M. Biradar, Liq. Cryst. 40, 45, **2013**.
11. M. D. Lynch, D. L. Patrick, Nanoletters. 2, 1197, **2002**.
12. I. Dierking, G, Scalia, P. Morales, J. Appl. Phys. 97, 044309, **2005**.
13. H. Qi, T. Hegmann, J. Mater. Chem. 18, 3288, **2008**.
14. R. Dhar, A. S. Pandey, M. B. Pandey, S. Kumar, R. Dabrowski, Appl. Phys. Express. 1, 12501, **2008**.
15. V. Manjuladevi, R. K. Gupta, S. Kumar, J. Mol. Liq. 171, 60, **2012**.
16. R. Basu, Appl. Phys. Lett. 103, 241906, **2013**.
17. Y. J. Lim, S. S. Bhattacharya, W. Tie, H. R. Park, Y. H. Lee, S. H. Lee, Liq. Cryst. 40, 1202, **2013**.

18. H. Lee, S. Yang, J. H. Lee, Y. S. Park, Appl. Phys. Lett. 104, 191601, **2014**.
19. H. Gruler, T. J. Scheffer, G. Z. Meier, Z. Naturforsch. 27, 966, **1972.**
20. D. V. Sai, P. Satyanarayana, V. S. S. Sastry, J. Herman, P. Kula, R. Dabrowski, S. Dhara, Liq. Cryst. 41, 591, **2014.**
21. L. Cheung, R. B. Meyer, H. Gruler. Phys. Rev. Lett. 31, 349, **1973**.
22. S. Das gupta, P. Chattopadhyay, S. K. Roy, Phys. Rev. E 63, 041703, **2001**.
23. S. W. Morris, P. P. Muhoray, D. A. Balzarini, Mol. Cryst. Liq. Cryst. 139, 263, **1986**.
24. W. H. De Jeu, T. W. Lathouwers, P. Bordewijk, Phys. Rev. Lett. 32, 40, **1974**.
25. P. P. Karat, N. V. Madhusudana, Mol. Cryst. Liq. Cryst. 36, 51, **1976**.
26. I. Haller, Prog. Solid State Chem. 10, 103, **1975**.
27. A. Zawadzki, H. G. Walton, Mol. Cryst. Liq. Cryst. 569,10, **2012**.
28. A. Chakraborty, M. K. Das, B. Das, A. Lehmann, C. Tschierske. Soft Matter. 9, 4273, **2013**.
29. T. Uchida, Y. Takahashi, Mol Cryst Liq. Cryst. 72, 133, **1981**.
30. B. W. Van der Meer, F. Postma, A. J. Dekker, W. H. De Jeu, Mol. Phys. 45, 1227, **1982**.
31. W. Maier and A. Saupe, Z. Naturforsch., A 14, 882, **1959.**
32. W. Yang, T. Lan, S. Xia, L. Ma, Y. Wang, Liq. Cryst. 41, 202, **2014**.
33. S. Y. Lu, L. C. Chien, Opt. Express. 16, 12777, **2008**.

Chapter 4

Fast response in twisted nematic liquid crystal cells: Effect of functionalized carbon nanotubes

4.1 Introduction

In chapter 3, we have presented the results of our investigation on effect of octadecylamine functionalized SWCNTs (ODA-SWCNT) on elastic constants and optical response time of a mesogen exhibiting both nematic as well as smectic phase. We observed that on doping ODA-SWCNT in LC material the nematic phase range decreases with increasing concentration of ODA-SWCNT and the dielectric anisotropy decreases with an increase in the concentration of ODA-SWCNT. The rise time decreases and decay time in planar aligned cell increases in the sample with highest concentration of ODA-SWCNT. In this chapter, we are presenting the results on nanocomposites of NLC in twisted nematic geometry. The study of nanocomposites of liquid crystals (LCs) and nanomaterials is of great importance from both fundamental and application point of view [1, 2]. The nematic phase exhibited by LC material is widely employed in display industry due to its low viscosity and easy reorientation of LC molecules on application of external field. The orientation of molecules in nematic liquid crystal (NLC) can be manipulated on application of external field because of their long range orientational order. Doping nanomaterials can modify the physical properties of the host LC [3-6]. The carbon nanotube (CNT) is proved to be one of the best dopants in the case of calamitic LC host due to its structural similarity, though with a larger aspect ratio, and unique electronic properties [7]. The inclusion of CNT in NLC matrix improves the electro-optic switching characteristics and physical properties of NLC such as dielectric anisotropy, threshold voltage (V_{th}), elastic constant, memory effect and response time of NLC in twisted as well as planar alignment modes [8-18].

The lower value of V_{th} and faster response time is desirable for the better performance of LC based devices. The slow response time of liquid crystal display devices cause some defects such as color break and high power consumption which may degrade the performance of display device [19-20]. Several approaches have been made to shorten the response time of NLC by incorporating appropriate nanomaterial in NLC matrix [17, 21]. It has been found that the incorporation of CNTs in twisted nematic (TN) LC can significantly modify the elastic constants and rotational viscosity which leads to reduction in the response time of the NLC composite [18,23]. Recently, the fast electro-optic switching in a graphene mixed NLC hybrid cells has been reported. Based on their observations they suggest that the presence of graphene in NLC has reduced the rotational viscosity and conductivity of pure NLC by trapping the free ions in LC medium [23].

The orientation of NLC director close to the substrate surface is influenced by surface alignment. The strong anchoring of NLC at the alignment layer also affects the orientation of NLC molecules in bulk medium. The alignment layer plays key role in NLC devices to determine the value of V_{th} and response time [24]. Lee *et al*. [25] have observed the effect of mixture of multi-walled CNTs (MWCNTs) and Polyimide (PI) on relaxation time and splay elastic constant of a NLC in planar alignment mode. They observed that the NLC enclosed in a cell prepared with mixture of MWCNT and PI in planar mode shows faster relaxation time and larger splay elastic constant compared to the cell prepared with pure PI. The effect of MWCNT in both NLC host and PI alignment layer on the electro-optic properties of the NLC system has also been reported. Doping MWCNT in NLC as well as PI alignment layer reduces the response time as well as V_{th} compared to that of pure NLC [26]. The study on mixture of LC and CNT in different alignment modes have been reported by many research groups [27-29]. The pristine CNTs aggregate and form bundles because of strong van der Waals force due to which they do not disperse easily in many organic solvents. The solubility in organic solvents enhances on organic functionalization of CNTs [7, 30, 31] which are also comparatively shorter length ~100-300nm.

In this chapter, we describe the effect of ODA-SWCNT on the response characteristics, i.e., rise time and fall time of a NLC in TN mode. On increasing the concentration of ODA-SWCNT, faster response time was observed compared to that pure NLC. The optical response time of a NLC reduces due to incorporation of CNTs in the LC host. Such reduction is believed to be due to increase in elastic constant of the nanotubes doped LC system. It is very interesting to

study the effect of ODA-SWCNT in the PI alignment layer on the response time of NLC. Our investigation on TN cells prepared using mixture of ODA-SWCNT and PI alignment layer indicates that the increase in threshold electric field (E_{th}) might be due to strong anchoring between LC and ODA-SWCNT. We have observed a reduction in optical response time for the TN cell prepared with PI-ODA-SWCNT mixture compared to that of pure PI alignment layer.

4.2 Materials and methods

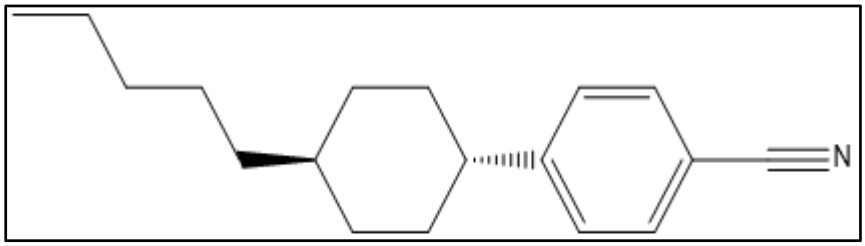

Figure 4.1: Molecular structure of 5PCH (4-trans-pentylcyclohexylcyanobenzene).

The nematic liquid crystal, 5PCH (4-trans-pentylcyclohexylcyanobenzene) and the ODA-SWCNT were procured from Sigma-Aldrich and Carbon Solutions Inc. USA, respectively. We prepared the nanocomposites of ODA-SWCNT and 5PCH at 0.025, 0.05 and 0.1 wt% of ODA-SWCNT in 5PCH. Here onwards we refer to the pure 5PCH as sample A and nanocomposites of 5PCH with 0.025, 0.05 and 0.1 wt% of ODA-SWCNT as samples B, C and D, respectively. The TN cells were fabricated using indium-tin-oxide (ITO) glass plates treated with PI. The thickness of TN cells was around 8 μm. The measurement of dielectric constant of each sample was carried out as a function of applied voltage at a frequency of 4.1 kHz. The study on electro-optic properties of 5PCH and its ODA-SWCNT nanocomposites was carried out in wide temperature range of nematic phase as a function of applied voltage. The alignment of NLC was checked using polarizing optical microscope (POM) by placing the TN cell between crossed polarizers. The values of V_{th} were estimated from the capacitance versus voltage (C-V) plot as well as voltage-dependent transmittance curves. Response time measurement was carried out by applying a signal of amplitude modulated square wave of frequency of 60 Hz (carrier frequency of 1 kHz) across the cell and the transmitted light intensity as a function of applied voltage was detected using a photo diode [9,32]. The decay and rise times in the normally white TN mode cells were measured from the transmittance variation from 10 to 90% and 90 to 10% of the maximum transmittance, respectively [32].

4.3 Results and discussion

4.3.1 Polarizing optical microscopy (POM)

The optical textures of the TN cells filled with 5PCH and its ODA-SWCNT nanocomposites are observed under a POM and are shown in Figure 4.2. All the samples show a homogeneous bright state, and no indication of agglomeration or phase separation due to the incorporated ODA-SWCNTs is seen in any of the nanocomposites.

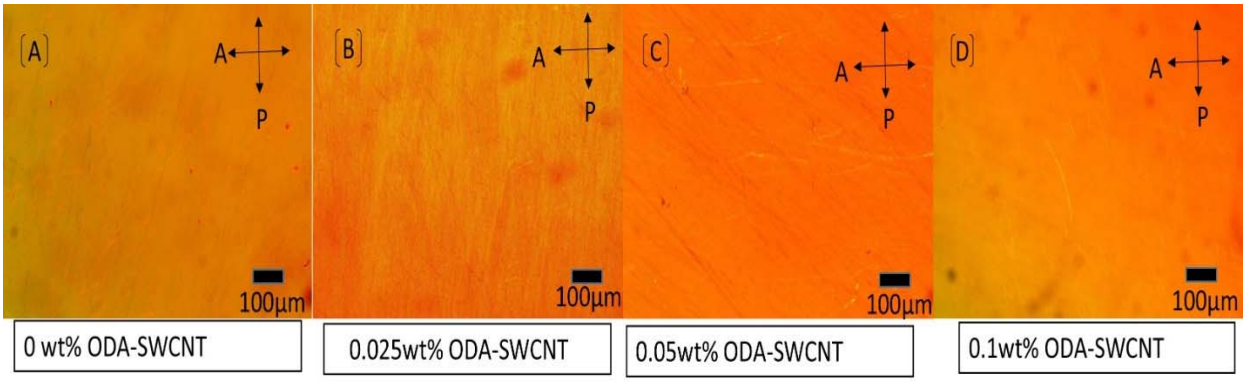

Figure 4.2: Optical textures of pure 5PCH and its ODA-SWCNT nanocomposites in TN cells as observed between the cross polarizers of a polarizing optical microscope.

The transmitted intensity curves for pure 5PCH and its ODA-SWCNT nanocomposites in normally white TN mode as a function of applied voltage is shown in Figure 4.3. on application of external electric field ($E > E_{th}$), the NLC molecules, on average, tend to orient along the direction of applied field except for the LC molecules those which are very near to the substrate. When an electric field above E_{th} is applied to the LC cells, molecules switch from twisted nematic state to homeotropic state due to torque exerted by the electric field. The effective switching amplitude of TN LC molecules can be obtained by subtracting 10 % from 90 % threshold voltage in voltage dependent transmittance curves [4]. It can be seen from Figure 4.3 that the switching amplitude for ODA-SWCNT nanocomposites of 5PCH decreases with increasing concentration of ODA-SWCNT compared to that of pure 5PCH. Such reduction in the switching amplitude in TN cell is consistent with the interpretation of response time measurements. The study in TN mode of LC cell is useful because in this mode, the response time can easily be determined due to single transition from bright to dark state on application of applied external field whereas in planar mode multiple intensity curve are observed due to phase retardation [34].

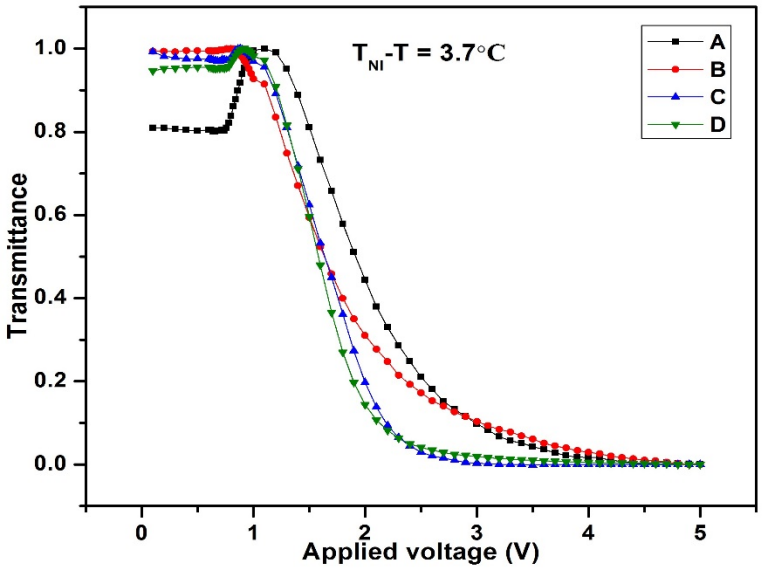

Figure 4.3: Transmitted intensity as a function of applied voltage for pure 5PCH and its ODA-SWCNT nanocomposites at a reduced temperature (T_{NI}-T) of 3.7°C.

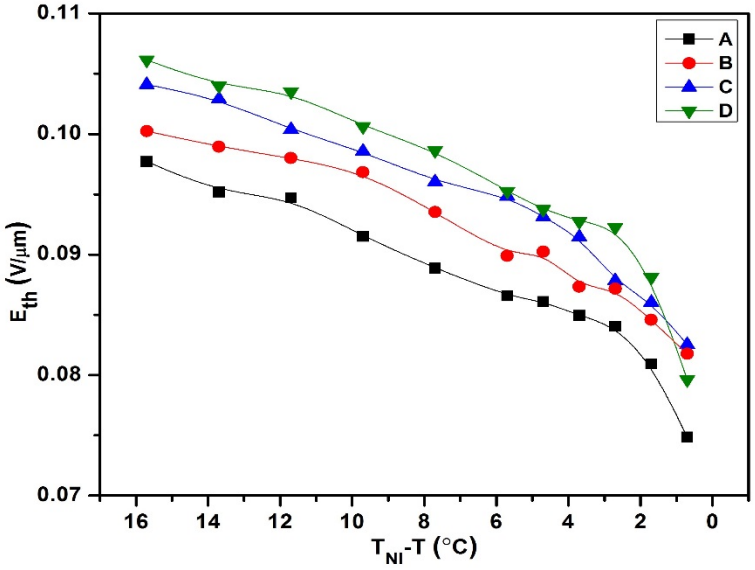

Figure 4.4: Threshold electric field (E_{th}) as a function of reduced temperature (T_{NI}-T) for pure 5PCH and its ODA-SWCNT nanocomposites.

The variation of E_{th} for 5PCH as well as its ODA-SWCNT nanocomposites as a function of reduced temperature (T_{NI}-T) is displayed in Figure 4.4. We observed that E_{th} value increases with increase in the concentration of ODA-SWCNT. The E_{th} value increased by ~9% in the nanocomposite with the highest concentration of ODA-SWCNT compared to that of pure 5PCH.

The increase in the E_{th} might be due to the increase in the elastic constant of 5PCH after doping with ODA-SWCNT.

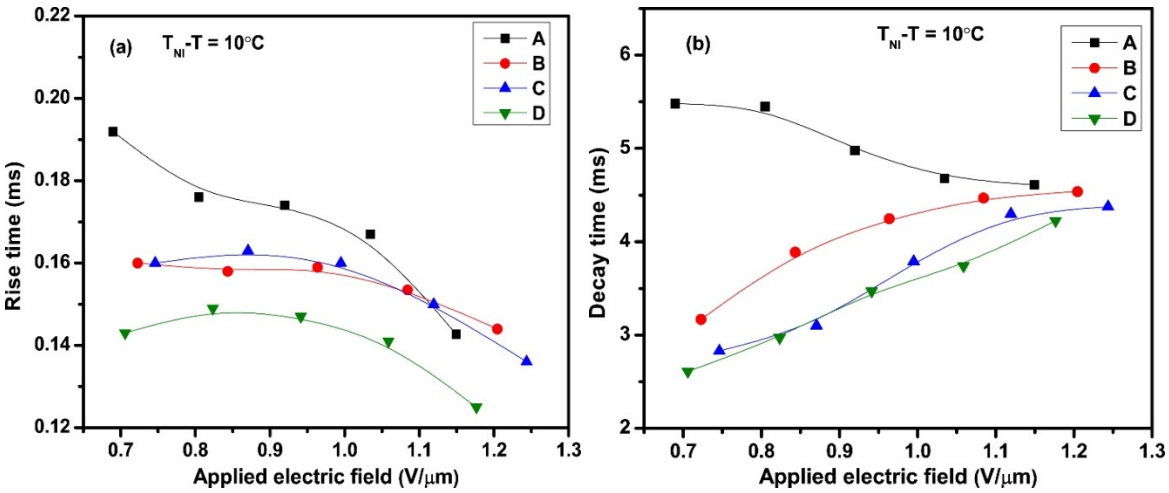

Figure 4.5: (a) Rise time and (b) decay time of the TN cells as a function of applied electric field for pure 5PCH and its ODA-SWCNT nanocomposites.

The rise time and decay time as a function of applied electric field for pure 5PCH and its ODA-SWCNT nanocomposites at T_{NI}-T = 10° C are shown in Figure 4.5(a) and 4.5(b) respectively. The decay time decreases for ODA-SWCNT nanocomposites of 5PCH with increase in concentration of ODA-SWCNT compared to that of pure 5PCH. The rise time of ODA-SWCNT nanocomposites of 5PCH decreases with increase in the concentration of ODA-SWCNT compared to that of pure 5PCH. With addition of CNT in NLC, the rotational viscosity decreases and thereby affects the rise time of LC [17]. This result is consistent with our previous findings; i.e., the rise time decreases on increasing the concentration of ODA-SWCNT in nematic phase of LC [28]. The reduction in total response time for samples B, C and D is ~ 41, 47 and 51% with respect to sample A at an applied electric field ~ 0.7 V/μm. In chapter 3, the effect of CNT on the response time of LC is discussed. The rise time of the CNT doped LC was reduced compared to that pure LC, and it was suggested that due to strong van der Waals interaction between LC molecules and CNT leads to an increase in the elastic constant as well as the order parameter [32, 25]. The strong anchoring between NLC and CNT increases the elastic energy of NLC due to increase in the elastic constant [22, 23, 26] thereby leading to a reduction in the rise time [25]. The fast response time in case of ODA-SWCNT nanocomposites of 5PCH can be attributed to the decrease in the rotational viscosity and increase in anchoring energy [34]. We have also observed that the T_{NI} of the

nanocomposite of 5PCH with highest concentration of ODA-SWCNT (sample D) was 1.8° lower than the T_{NI} observed for pure 5PCH.

4.4 Effect of ODA-SWCNT in alignment layer on electro-optic response of NLC

The effect of incorporation of ODA-SWCNT in the PI alignment layer on the electro-optic switching characteristics and response time of pure 5PCH in TN mode has been investigated. The reliable and stable alignment layer of ODA-SWCNT mixed with PI not only provides transparent conducting alignment layer but also improves the switching of NLC confined in TN mode LC cells. In order to investigate the effect of alignment layer on the electro-optic response characteristics, small amounts of ODA-SWCNT were mixed with PI. The three different mixtures of ODA-SWCNT and PI were prepared by dispersing 0.16, 0.33 and 0.66 μg of ODA-SWCNT in 1 ml PI solution. For convenience, we refer the pure PI alignment layer as AL1 and three mixtures of PI and ODA-SWCNT used as alignment layers are named as AL2, AL3 and AL4 as per increasing concentration of ODA-SWCNT. The ITO substrates were treated with these mixtures of PI and ODA-SWCNT. We have prepared TN cells of thickness of around 8 μm. The measurements of E_{th} and the dielectric constant of each sample were carried out as a function of applied voltage at a frequency of 4.1 kHz. The decay and rise times were measured by applying a signal of amplitude modulated square wave of frequency of 60 Hz (carrier frequency of 1 KHz) across the cell. The atomic force microscope (NTMDT, SolverPro P47) images of different alignment layers deposited on ITO substrates were obtained in contact mode using silicon tips of spring constant 0.2 N/m. The horizontal and vertical dimensions of the AFM was calibrated using test gratings (TGZ - series, NTMDT).

Electro-optic switching characteristics

The voltage dependent transmittance for pure 5PCH in TN mode fabricated with mixtures of ODA-SWCNT and PI is shown in Figure 4.6. The E_{th} value of 5PCH enclosed in TN cells prepared with mixtures of ODA-SWCNT and PI mixture is found to be higher compared to that of pure PI at any given temperature as shown in Figure 4.7. With increase in the concentration of ODA-SWCNT in the PI alignment layer, the value of E_{th} increases. The increase in E_{th} also suggests that the surface anchoring effect of the sample prepared with ODA-SWCNT and PI mixture is stronger than that of pure PI alignment layer which leads to increase in effective elastic constant (K) of LC. The

increased value of elastic constant suggests that the order parameter (S) of LC is improved because elastic constants are related to order parameter as $K_{ii} \propto S^2$.

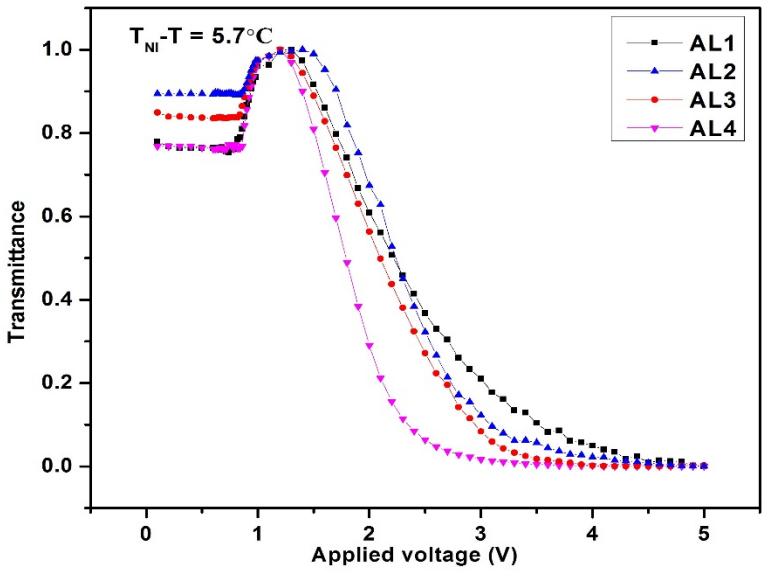

Figure 4.6: Transmittance as a function of applied voltage for pure 5PCH in TN cell fabricated using mixtures of PI and ODA-SWCNT as alignment layers.

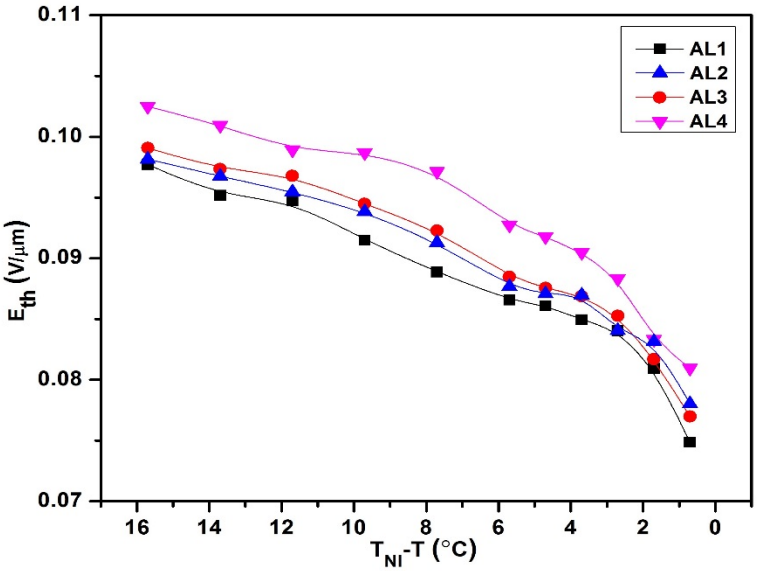

Figure 4.7: Threshold electric field (E_{th}) as a function of reduced temperature (T_{NI}-T) for pure 5PCH in TN cell fabricated using mixtures of PI and ODA-SWCNT as an alignment layer.

The variation of dielectric constant (ε) of 5PCH as a function of applied voltage in TN mode cells prepared with mixture of PI and ODA-SWCNT as well as pure PI alignment layers is shown in Figure 4.8. With addition of ODA-SWCNT in PI alignment layer, the value of ε of 5PCH in TN mode at any given applied voltage is slightly decreased. However the slight enhancement

of E_{th} of 5PCH observed in cells prepared using alignment layers AL2, AL3 and AL4 compared to the cell prepared using AL1 indicates that the elastic constant in the former case is enhanced.

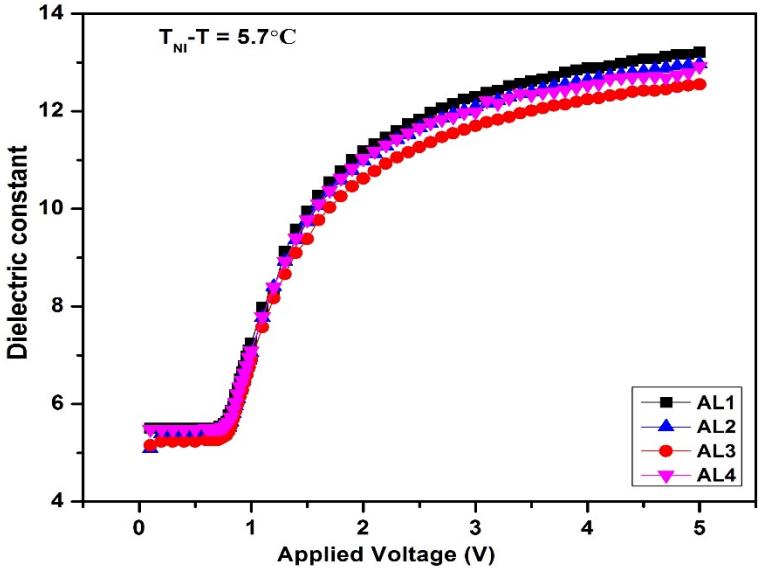

Figure 4.8: Dielectric constant as a function of applied voltage for pure 5PCH in TN cell fabricated using mixtures of PI and ODA-SWCNT as alignment layers.

The measured oscillograms of normally white TN mode cells prepared using various alignment layers at an applied voltage of 10 V is shown in Figure 4.9. It can be clearly seen that the NLC enclosed in the TN cell fabricated using PI alignment layer containing ODA-SWCNT responds faster compared to the one prepared using pure PI.

The rise and decay times for pure 5PCH in TN mode cells as a function of applied electric field with the sample prepared with mixed PI-ODA-SWCNT and pure PI alignment layer are shown in Figure 4.10 (a) and (b) respectively. The introduction of ODA-SWCNT into PI alignment layer results in a remarkable improvement in optical response time of 5PCH compared to the response time observed in ODA-SWCNT nanocomposites of 5PCH. The decay time in the TN cells prepared with mixture of PI and ODA-SWCNT is reduced by more than 65% compared to TN cells prepared with pure PI alignment layer. The alignment of LC devices rely on the surface anchoring energy and ability of alignment layer to induce a tilt in LC molecules near the surface of substrate, known as the pre-tilt angle [29]. The pre-tilt angle is responsible for the uniform texture of LC cells. As the measurements have been carried out at voltage $V > V_{th}$, the observed improvement in response time in this case can be attributed mainly to the effect of surface anchoring [31].

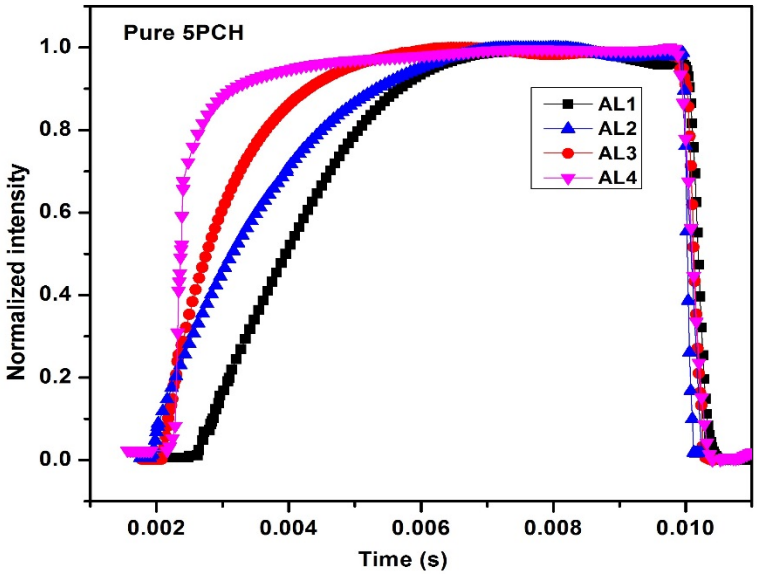

Figure 4.9: Measured oscillograms for 5PCH in TN cells prepared with pure PI and mixtures of PI and ODA-SWCNT as alignment layers at an applied voltage of 10V.

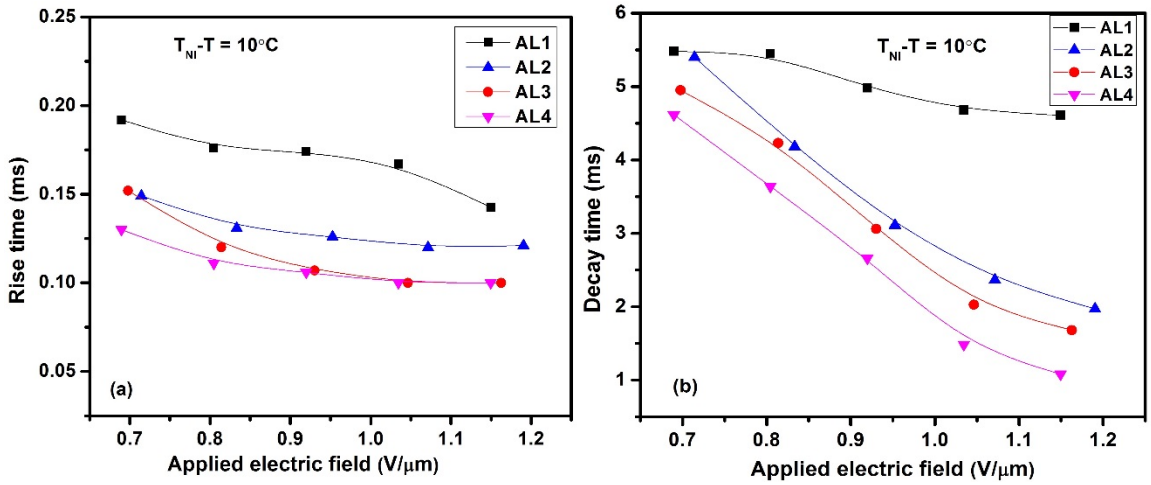

Figure 4.10: (a) Rise time and (b) decay time as a function of applied electric field for pure 5PCH in TN cell fabricated using mixtures of PI and ODA-SWCNT as alignment layer.

The rise time (τ_r) and decay time (τ_0) is related to the voltage switching ratio and anchoring energy through the following equations [34]:

$$\tau_r = \frac{\tau_0}{(V/V_{th})^2 - 1} \tag{4.1}$$

and

$$\tau_0 = \frac{\gamma}{K\pi^2}\left(d^2 + \frac{4dK}{W} + \frac{4K^2}{W^2}\right) \tag{4.2}$$

where W, K and γ represents the anchoring strength coefficient, effective elastic constant and rotational viscosity of the NLC matrix, respectively. Here d is the thickness of LC cell. The rise time not only depends on the anchoring energy but also on voltage switching ratio (V/V_{th}).
The effective elastic constant (K) is given

$$K = K_{11} - \frac{(2K_{22} - K_{33})}{4}$$

Where K_{11}, K_{22} and K_{33} are splay, twist and bend elastic constants of NLC, respectively [35].
We have observed that the rise time in the TN cells prepared with mixture of PI and ODA-SWCNT is reduced by more than 30% compared to TN cells prepared with pure PI alignment layer. The presence of ODA-SWCNT at surface of substrate leads to enhancement in the K value due to strong interaction between LC and ODA-SWCNT, which is reflected as increase in the value of E_{th}. The decay time of NLC depends on the surface anchoring on the substrates and thickness d of LC cell. After mixing the ODA-SWCNT in PI, the total response time has been reduced by 56%, 62% and 75% for the samples prepared using AL2, AL3 and AL4, respectively compared to the one prepared using AL1. In case of large surface anchoring, the optical response time is related to thickness of LC cell as $\tau_0 \propto d^2$. In this study, we have used LC cells of similar thickness, so change in the response time is considered due to change in the surface anchoring on the substrates after dispersing the ODA-SWCNT in PI alignment layer. The anchoring strength at the alignment layer and NLC interface is enhanced due to of π–π stacking interaction between NLC, ODA-SWCNT and PI leading to observed decrease in the optical response time [28].

We have observed the decay time of 5PCH is reduced in TN cells prepared using PI alignment layer containing ODA-SWCNT as well as ODA-SWCNT nanocomposites of 5PCH and the value of decay time decreases with increase in concentration of ODA-SWCNT in both the cases. In the latter case as we have used same PI alignment layer hence the reduction in rotational viscosity of the medium due to introduction of ODA-SWCNT in 5PCH might be responsible for the observed reduction in response time. While in the cells prepared using alignment layers on incorporation of ODA-SWCNT in the PI, surface anchoring might be responsible for the observed fast switching.

4.5 AFM characterization of alignment layer of polyimide and mixture of polyimide and ODA-SWCNT

In order to understand the role of surface morphology on the switching behavior of the TN cells prepared using various alignment layers we have characterized the substrates treated with various alignment layers using the AFM technique. The surface morphology and roughness of the PI and ODA-SWCNT mixed PI alignment layers are studied using AFM images. The AFM images of different alignment layers were obtained in contact mode using silicon tips of spring constant 0.2 N/m. The AFM images of the surface of the samples AL1, AL2, AL3 and AL4 are shown in Figure 4.11.

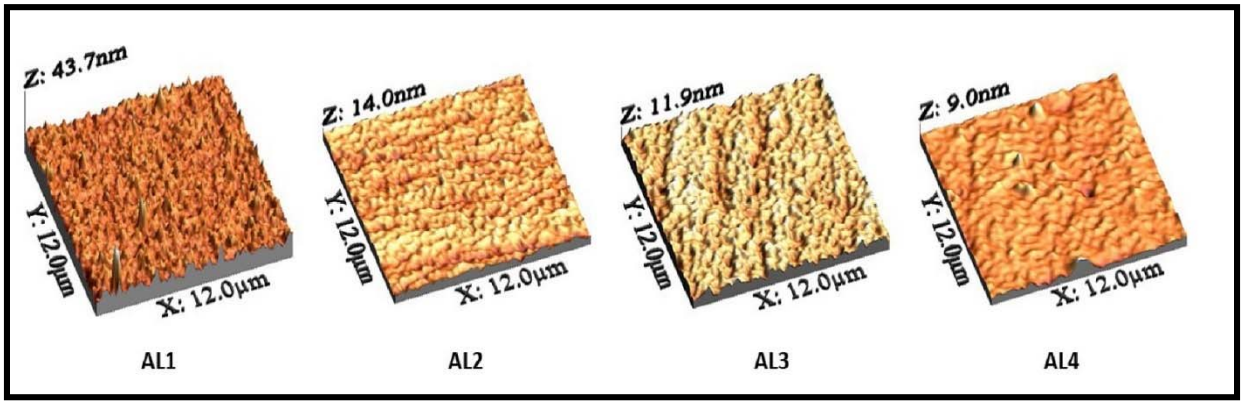

Figure 4.11: AFM images of ITO substrates treated with pure PI and mixtures of ODA-SWCNT and PI.

The average and root mean square (RMS) roughness of the samples are estimated and shown in Figure 4.12. The surface of the pure PI alignment layer exhibits the highest roughness. The roughness of the alignment layer decreases with increasing concentration of incorporated ODA-SWCNT in PI. Due to decrease in surface roughness, the interaction of the alignment layer with that of the LC molecules and ODA-SWCNT increases leading to an enhancement in surface anchoring. Such improvement in surface anchoring might be a key factor responsible for the fast response of the LC cells fabricated using ODA-SWCNT mixed PI alignment layer.

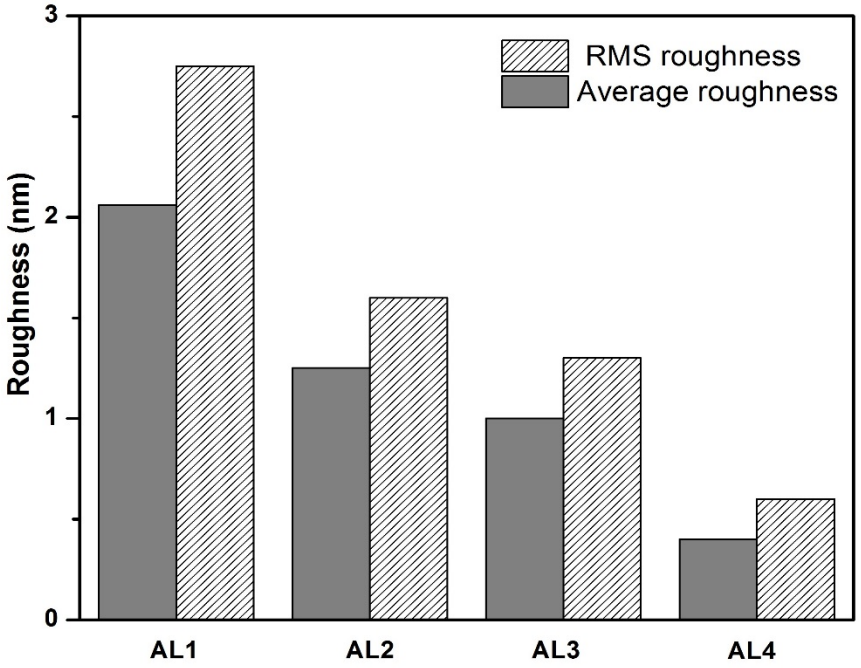

Figure 4.12: Roughness of ITO coated glass plates treated with pure PI and its mixture with different concentration of ODA-SWCNT.

4.6 Conclusions

The effect of dopant ODA-SWCNT on the electro-optic switching characteristics as well as optical response time of 5PCH in TN mode was investigated. The optical response time of ODA-SWCNT nanocomposites of 5PCH was reduced compared to that of pure 5PCH, whereas an enhancement in the value of threshold electric field was observed. A fast response time is observed with increase in concentration of ODA-SWCNT in NLC host. The optical response of pure 5PCH in TN cells prepared using mixtures of PI and ODA-SWCNT as alignment layer is also investigated. The optical response time of 5PCH in a TN cell fabricated with a mixture of PI and ODA-SWCNT reduced by ~ 75 % compared to the one prepared using pure PI alignment layer. The presence of ODA-SWCNT in the alignment layer enhances the surface anchoring of the NLC molecules leading to increase in elastic constant and reduction in the rotational viscosity of the NLC, which leads to a reduction in the optical response time of NLC. The surface roughness of ODA-SWCNT incorporated PI alignment layer treated substrate was reduced compared to that of pure PI treated substrate. The π-π interaction between the ODA-SWCNT, NLC and the PI alignment layer leads to enhanced surface anchoring of the NLC molecules at the substrate. This strong surface anchoring gives rise to increase in elastic constant which gets reflected as a reduction in the optical

response time of NLC. In this chapter, we have presented the results of our investigation on the effect of doping ODA-SWCNT on pure NLC in TN geometry. It is interesting to study the effect of CNT in PI alignment layer in the planar geometry also. In next chapter, we have demonstrated the results of LC wherein LC cells were treated with mixture of PI and CNT.

References:

1. L. Quan, *Nanoscience with liquid crystal: from self-organized nanostructure to applications,* Springer, **2014**.
2. V. Manjuladevi, R. K. Gupta, *Effect of nanomaterials on physical properties of liquid crystal,* NOVA Science Publishers, 69-90, **2015**.
3. S. Y. Lu, L. C. Chien, Opt. Express. 16, 12777, **2008**.
4. W. K. Lee, Y. S. Choi, Y. G. Kang, J. Sung, D. S. Seo, C. Park, Adv. Funct. Mater. 21, 3843, **2011**.
5. A. Kumar, M. Biradar, Phys. Rev. E. 83, 041708, **2011**.
6. I. Dierking, G. Scalia, P. Morales, J. Appl. Phys. 97, 044309, **2005**.
7. V. Manjuladevi, R. K. Gupta, S. Kumar, J. Mol. Liq. 171, 60, **2012**.
8. W. Lee, C. Y. Wang, Y. C. Shih, Appl. Phys. Lett. 85, 513, **2004**.
9. S. Gauza, X. Zhu, W. Piecek, R. Dabrowski, S. T. Wu, J. Disp. Tech. 3, 250, **2007**.
10. M. D. Lynch, D. L. Patrick, Nano Lett. 2, 1197, **2002**.
11. J. Kumar, R. K. Gupta, V. Manjuladevi, AIP Conf. Proc. 1536, 693, **2013**.
12. H. Qi, T. Hegmann, J. Mater. Chem. 18, 3288, **2008**.
13. R. Dhar, A. S. Pandey, M. B. Pandey, S. Kumar, R. Dabrowski, Appl. Phys. Express. 1, 121501, **2008**.
14. F. Haraguchi, K. I. Inoue, N. Toshima, S. Kobayashi, K. Takatoh, Jpn J. Appl. Phys. Part 2, 46, **2007**.
15. M. Middha, R. Kumar, K. K. Raina, Liq. Cryst. 42, 7, **2015**
16. R. Basu, G. Iannacchione, Phys. Rev. E, 81, 051705, **2010**.
17. H. Y. Chen, W. Lee, N. A. Clark. Appl. Phys. Lett. 90, 033510, **2007**.
18. C. Y. Huang, C. Y. Hu, H. C. Pan, K. Y. Lo, Jpn. J. Appl. Phys. 44, 8077, **2005**.
19. Z. Luo, F. Peng, H. Chen, M. Hu, J. Li, Z. An, S. T. Wu, Opt. Mater Exp. 5, 603, **2015**.
20. Z. Luo, S. T. Wu, J. Disp. Tech. 10, 367, **2014**.

21. I. S Baik, S. Y. Jeon, S. H. Lee, K. A. Park, S. H. Jeong, K. H. An, Y. H. Lee, Appl. Phys. Lett. 87, 263110, **2005**.
22. C. Y. Huang, H. C. Pan, C. T. Hsieh, Jpn. J. Appl. Phys. 45, 6392, **2006**.
23. R. Basu, A. Garvey, D. Kinnamon, J. Appl. Phys. 117, 074301, **2015**.
24. X. Nie, R. Lu, H. Xianyu et al. J. Appl, Phys. 101, 103110, **2007**.
25. H. Lee, S. Yang, J. H. Lee, Y. S. Park, Appl. Phys. Lett. 104, 191601, **2014**.
26. K. J. Lee, H. G. Park, H. C. Jeong, D. H. Kim, D. S. Seo, J. W. Lee, B. M. Moon, Liq Cryst. 41, 25, **2014**.
27. S. Y. Jeon, S. H. Shin, S. J. Jeong, S. H. Lee, S. H. Jeong, Y. H. Lee, H. C. Choi, K. J. Kim, Appl. Phys. Lett. 90, 121901, **2007**.
28. J. Kumar, V. Manjuladevi, R. K. Gupta, S. Kumar, Liq Cryst. 42, 3, **2015**.
29. E. Luder. *Liquid crystal displays: addressing schemes and electro-optical effects*. Wiley, Chichester, **2001**.
30. J. Chen, M. A. Hamon, H. Hu, Science. 282, 95, **1998**.
31. S. Niyogi, M. A. Hamon, H. Hu, Science. 35, 1105, **2002**.
32. K. Tarumi, U. Frinkenzeller, B. Schuler, Jpn J. Appl. Phys. 31, 2829, **1992**.
33. N. Podoliak, O. Buchnev, M. Herrington, RSC Adv. 4, 46068, **2014**.
34. J. L. Erickson. Trans. Soc. Rheol. 5, 23, **1961**.
35. F. M. Leslie. Arch Ration Mech Anal. 28, 265, **1968**.

Chapter 5

Effect of ODA-SWCNT in alignment layer on the physical properties and optical response time of nematic liquid crystal

5.1 Introduction

In previous chapter, we have described the effect of doping octadecylamine functionalized carbon nanotubes (CNTs) in alignment layer on the response time of the 4-trans-pentylcyclohexylcyanobenzene (5PCH) nematic liquid crystal (NLC) in twisted nematic geometry. Different alignment geometries such as vertical, planar, in-plane and hybrid alignment can be obtained from specific treatment of the surface of substrate [1]. Each of them has its own merit and demerit from application point of view. The alignment layer affects the initial orientation of the LC molecules at the substrate as well as in the bulk. Most of the LC display devices typically contain a polyimide (PI) transparent alignment layer to control the orientation and to get stable and uniform layer of LC molecules. The properties of LC can be altered through addition of nanomaterials such as nanoparticles and carbon nanotubes in PI.

In the last two decades, several efforts have been invested to improve the performance of LC device. Besides the mixture of LC and nanomaterials, the effect of nanomaterial as an alignment layer on the physical parameters such as dielectric anisotropy and elastic constant as well as response time of LCs have been studied [2-9]. The inherent conductivity and self-alignment properties of CNTs make them alternative as an alignment layer [10-11]. Due to their one dimensional nano structure, CNTs can be used for aligning the LC molecules. Russell *et al*. [10] showed that the CNT bundles deposited on glass could align the LC molecules. Lee *et al*. [12] reported that Multi-walled CNTs (MWCNT) in the polyimide used as an alignment layer results in better uniform LC alignment, which help to improve response time of LC sample. The physical

reason of getting fast response time might be enhancement in strength of surface anchoring due to strong interaction between CNTs and LC.

Lee *et al*. [13] have reported that the mixtures of MWCNT and PI as an alignment layer in planar cell results in fast relaxation time and enhancement of the splay elastic constant. Recently, we have also reported that functionalized SWCNT in PI aligning layer of twisted nematic (TN) cells, improve the electro-optic switching of NLC [14]. The atomic force microscopy (AFM) study of the pure PI and CNT-PI mixture coated surfaces reveals that the roughness of the functionalized CNT-PI deposited surface is less than that of pure PI deposited sample.

In this chapter, we are presenting our studies on the effect of functionalized SWCNT as an alignment layer on the dielectric permittivity as well as optical response time of NLC in planar aligned LC cells. It is also interesting to see the effect of only functionalized SWCNT as an alignment layer on the optical response time of NLC material. The development of SWCNTs based application requires uniform deposition of CNTs on the substrate. The functionalized SWCNTs are deposited on indium tin oxide (ITO) coated glass plates using spin coating unit and Langmuir Blodgett technique and their effect on the dielectric permittivity and the electro-optic switching of NLC material is observed. The results are compared with that of LC cell treated with pure PI, which is mechanically rubbed.

5.2 Materials and methods

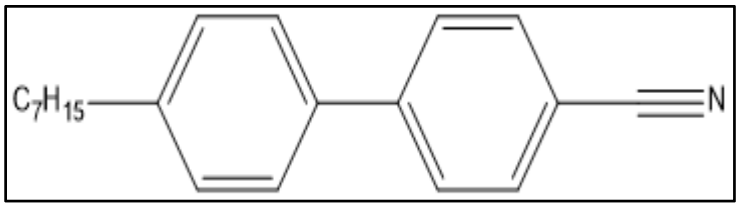

Figure 5.1: Chemical structure of 4-heptyl-4′-cyanobiphenyl (7CB).

The 4-heptyl-4′-cyanobiphenyl (7CB) was procured from sigma Aldrich. The octadecylamine functionalized SWCNTs (ODA-SWCNT) was purchased from Carbon solutions Inc. USA. The homogeneous and stable dispersions of ODA-SWCNT in PI were prepared. The ODA-SWCNT was dissolved in chloroform solvent and it was sonicated for 6 to 7 hours. After ensuring the complete dispersion, the solution of ODA-SWCNT and chloroform was added into 1 ml polyimide (PI). The NLC, 7CB exhibits positive dielectric anisotropy ($\Delta\varepsilon > 0$), hence planar cells were used for investigations. The planar LC cells were prepared using ITO coated glass plates with pure PI

and mixture of ODA-SWCNT and PI with different concentration (0.16, 0.33 and 0.66 µg/ml PI). The pure PI and ODA-SWCNT+PI mixed alignment layer used are referred as AL1, AL2, AL3 and AL4, respectively.

We have also prepared two planar LC cells using only ODA-SWCNT by spin coating and LB technique. A solution of concentration 0.03mg/ ml of ODA-SWCNT is prepared in high performance liquid chromatography (HPLC) grade chloroform. The Langmuir monolayer (LM) of ODA-SWCNT is formed by spreading 700 µl of the solution onto ion-free water subphase. LB films of ODA-SWCNT is deposited onto ITO substrates at target surface pressure (π_t) = 8mN/m after running three isocycles. The concentration 0.03mg/ ml of ODA-SWCNT into chloroform is taken for the fabrication of LC cell using spin coating technique. Both of these cells are prepared without rubbing of the substrate. Thickness of the LC cells is maintained ~ 9 µm. The alignment of the LC molecules is observed using a polarizing optical microscope (POM). The dielectric anisotropy ($\Delta\varepsilon$), threshold voltage (V_{th}), splay (K_{11}) and bend (K_{33}) elastic constants as functions of applied voltage and temperature are measured. We have measured V_{th}, and dielectric constant as a function of temperature at a frequency of 4.1kHz. Response time measurement is carried out by applying a modulated signal of square wave of frequency of 60 Hz (1 kHz carrier frequency) across the cell. The rotational viscosity is also estimated using the values of K_{11} and decay time at different temperatures.

5.3 Results and discussion

The interaction between NLC and material used as alignment layer determine the strength of surface anchoring. The alignment layer plays an important role in optical response time and ordering of molecules in the bulk LC medium.

5.3.1 Polarizing optical microscopy

The alignment of LC molecules in planar cells treated with pure PI and mixture of ODA-SWCNT and PI is observed using the POM. We obtained homogenous alignment in all LC cells as shown in the Figure 5.2. The homogenous alignment is confirmed from bright and dark state after rotating the rubbing direction of cell by 45° and 0° with respect to polarization axis of anyone of the crossed polarizers. The images A, C, E and G in Figure 5.2 are observed by keeping the LC cells making 45° of rubbing direction with respect to transmission axis of polarizer. The images B, D, F and H show the dark state appear at 0° rotation of the sample director with respect to one of the crossed

polarizers, which confirms the uniform planar alignment of LC sample. The texture study reveals that the presence of ODA-SWCNT in the PI favors the planar alignment. All LC cells are rubbed with soft cloth after the deposition of alignment layer using spin coating unit. The rubbing process induces topographical surface grooves, which facilitates the LC molecules to be oriented along the rubbing direction [15]. The LC molecules align along the rubbing direction in order to minimize the surface energy [16]. The rubbing process also helps to remove the aggregation or large bundles of CNTs as well as to improve the alignment of LC material.

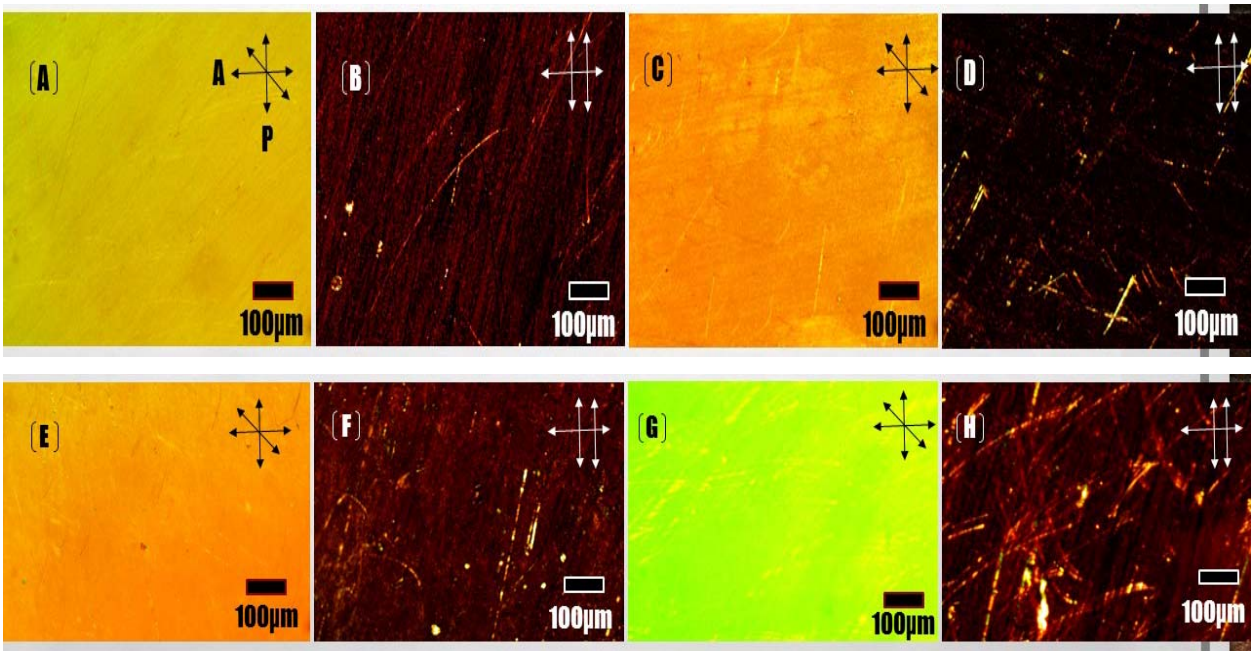

Figure: 5.2: POM images of 7CB confined in LC cells prepared with pure PI (A) and (B), mixture of PI and ODA-SWCNT with 0.16 µg/ml concentration (C) and (D), 0.33 µg/ml concentration (E) and (F) 0.66 µg/ml concentration (G) and (H). Rubbing direction is at 45° to the polarizer in Figure 5.2(A), (C), (E) and (G) while those are parallel to the polarizer shown in Figure 5.2 (B), (D), (F) and (H).

5.3.2 Dielectric constant measurement

The variation of parallel ($\varepsilon_{\parallel}$) and perpendicular ($\varepsilon_{\perp}$) component of dielectric permittivity as a function of reduced temperature (T_{NI}-T) is shown in Figure 5.3. The value of $\varepsilon_{\perp}$ for AL2, AL3 and AL4 is almost similar to that of AL1, whereas $\varepsilon_{\parallel}$ increases with increasing concentration of ODA-SWCNT into PI. The $\varepsilon_{\parallel}$ is measured at 5 volt using same LC cell which is used for the

measurement of $\varepsilon_{\perp}$. The slight increase in $\varepsilon_{\parallel}$ is attributed to presence of the ODA-SWCNT in PI alignment layer.

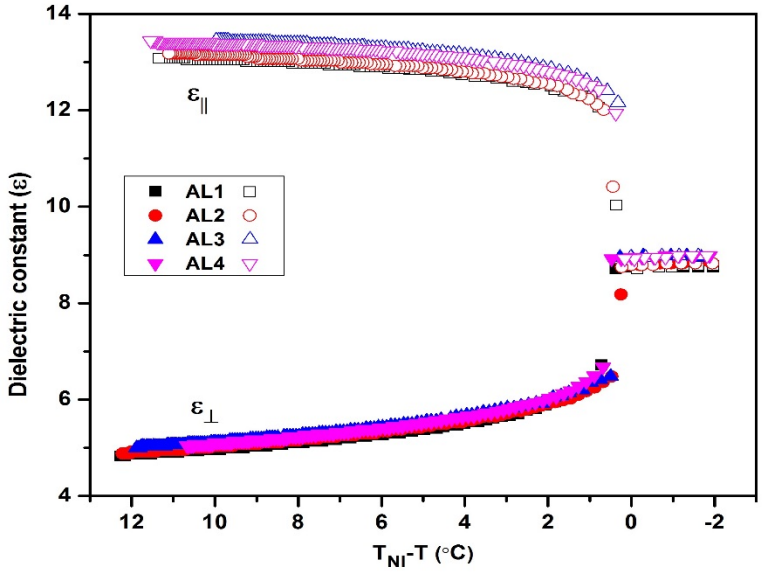

Figure 5.3: Dielectric constant ($\varepsilon_{\perp}$, $\varepsilon_{\parallel}$) as a function of reduced temperature (T_{NI}-T) for pure7CB in planar cell fabricated using pure PI as well as mixtures of PI and ODA-SWCNT as the alignment layer.

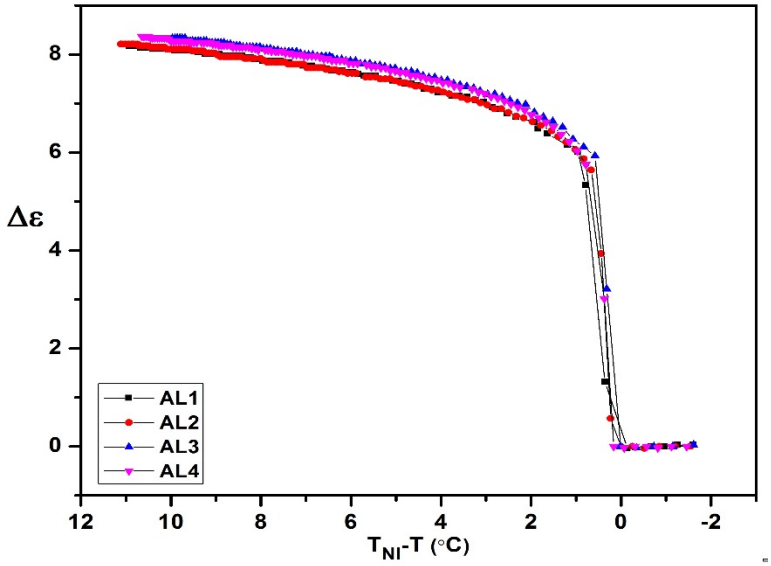

Figure 5.4: Dielectric anisotropy as a function of reduced temperature (T_{NI}-T) for pure 7CB in planar cell fabricated using pure PI as well as mixtures of PI and ODA-SWCNT as the alignment layer.

The dielectric anisotropy (Δε) is estimated using the measured value of $\varepsilon_{\parallel}$ and $\varepsilon_{\perp}$ for all LC cells and it is shown in Figure 5.4. The dielectric anisotropy depends on the interaction strength of

the LC with an applied electric field, and is therefore an important parameter which can influence the V_{th}. The value of Δε is found to be higher for AL2, AL3 and AL4 cells in comparison to that of AL1. For AL4 sample, which contain highest concentration of ODA-SWCNT in PI alignment layer, the Δε is increased by ~3 % as compared to that in pure PI alignment layer. The enhanced Δε suggests that the order parameter is improved in the LC cells which are treated with mixture of PI and ODA-SWCNT.

5.3.3 Elastic constant measurement

The variation of V_{th} for 7CB enclosed in planar cells prepared with the alignment layer composed of ODA-SWCNT and PI mixture is shown in Figure 5.5 (a). At low concentration of ODA-SWCNT into PI, the V_{th} value is found to be similar to that in pure PI at any given temperature. The V_{th} value increases with increasing concentration of ODA-SWCNT in PI. In case of AL4, which is the highest concentration of ODA-SWCNT in PI alignment layer, the V_{th} value is increased by ~5% as compared to pure PI treated LC cell. After the addition of ODA-SWCNT into PI, the additional effective interaction between 7CB and ODA-SWCNT is pronounced. This can lead to increase in strong surface anchoring and hence, an enhancement of V_{th} value is observed.

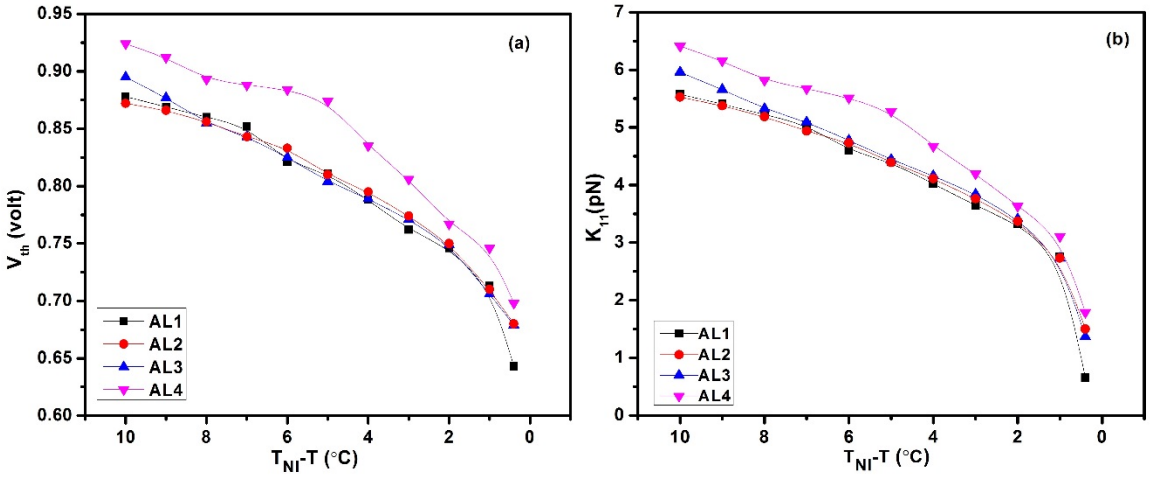

Figure 5.5: (a) Threshold voltage (V_{th}) and (b) splay elastic constant (K_{11}) as a function of reduced temperature (T_{NI}-T) for pure 7CB in planar cell fabricated using pure PI as well as mixtures of PI and ODA-SWCNT.

The splay elastic constant K_{11}, is an important parameter which can govern the switching of nematic LC in display devices. K_{11} is determined from the Freedericksz transition. K_{11} value is estimated using value of V_{th} and Δε. The variation of K_{11} as a function of T_{NI}-T is shown in Figure

5.5 (b). At low concentration of ODA-SWCNT into PI, the K_{11} value is almost similar to that measured for pure PI treated cell at given temperature. Whereas, in case of AL4, the K_{11} is increased by ~11% as compared to that in AL1. The increased value of K_{11} can be attributed to the increase of attractive interaction between ODA-SWCNT and 7CB director field on the surface of the substrate.

The variation of K_{33} as a function of reduced temperature is shown in Figure 5.6. The K_{33} value in nematic phase increases as the temperature decreases and it varies from 2 to 15 pN from T_{NI}-T=0°C to T_{NI}-T=10°C. The low concentration of ODA-SWCNT in PI alignment layer has no significant effect on the K_{33}, however in case of AL4, it is increased by ~30 % as compared to AL1. The increase in the K_{33} value suggests that presence of high concentration of ODA-SWCNT in PI leads to strong interaction with 7CB on surface of the substrate, which can alter the bend deformation. It also suggests that the order parameter (S) of LC is improved because according to the mean-field theory, elastic constants are related to order parameter as $K_{ii} \propto S^2$ [17].

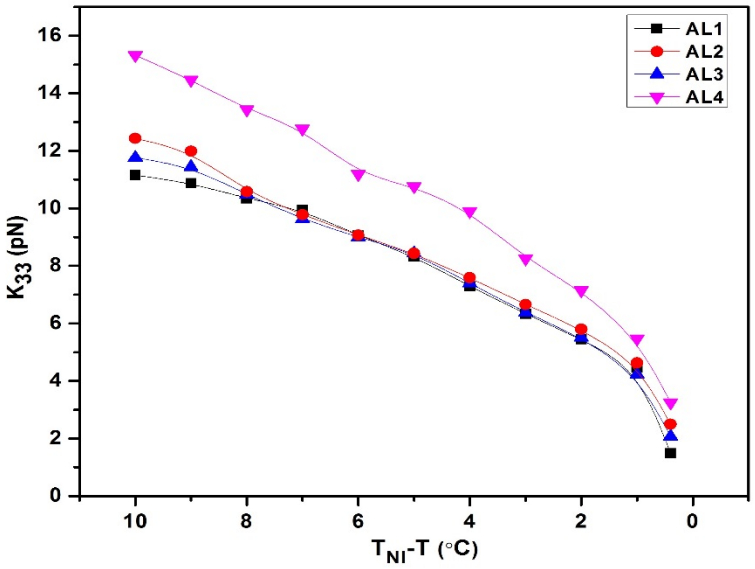

Figure 5.6: Bend elastic constant (K_{33}) as a function of reduced temperature (T_{NI}-T) for pure 7CB in planar cell fabricated using pure PI as well as mixtures of PI and ODA-SWCNT.

5.3.4 Optical response time

The optical response time (rise time and decay time) is measured at different temperatures. The rise time and decay time as a function of applied voltage at the temperature T_{NI}-T=2°C is shown

in Figure 5.7(a) and (b), respectively. We observed that the rise time and decay time decreases with increasing the temperature, which might be due to decrease in the viscosity of the LC medium.

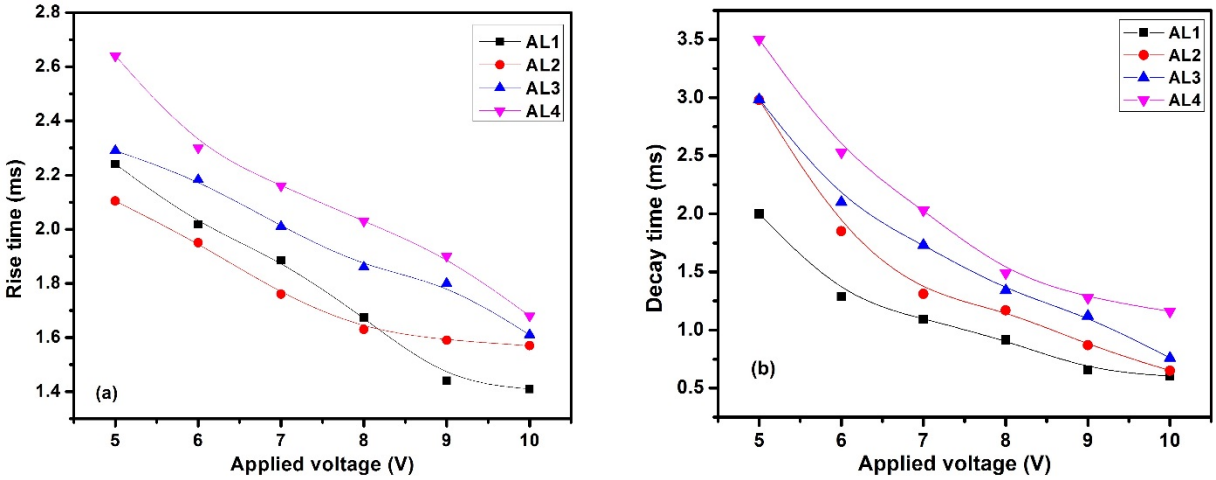

Figure 5.7: (a) Rise time and (b) decay time as a function of applied voltage for pure 7CB in planar cell fabricated using pure PI as well as mixtures of PI and ODA-SWCNT as an alignment layer.

At a given temperature, the rise time and decay time increases in the cell treated with the mixture of PI and ODA-SWCNT as compared to that measured in cell prepared with pure PI. However, in twisted nematic geometry, the response time of NLC decreases in the cell treated with mixture of PI and ODA-SWCNT, which was discussed in the previous chapter. The interaction between CNT and the LC molecules are probably related to the increase of the LC order parameter. In addition to alignment layer, the geometry of the cell also plays a role in the optical response time. The rise time of 7CB increases about 12 % in a cell coated with highest concentration of the ODA-SWCNT into PI as compared to that observed in a cell coated with pure PI. The response time is related to the elastic constant of the samples. The strong π-π electron interaction between 7CB and ODA-SWCNTs might be responsible for the increase in the rise time.

In this chapter, we are also presenting the result of our investigation on the electro-optic switching of pure 7CB using only ODA-SWCNT as an alignment layer. An alignment layer is vital for the fabrication of high-quality liquid crystal displays (LCDs). The commercially available alignment layer for LCDs is a PI film that is mechanically rubbed to form some unidirectional grooves on the surface of substrate. LC molecules follow the grooves and are aligned along it. The unidirectionally aligned CNT film naturally form groove structure with nanometer width hence, can act like an alignment layer.

The ODA-SWCNT is deposited onto ITO glass plates using spin coating and Langmuir Blodgett (LB) techniques [18]. It was observed that using spin coating, a transparent conductive alignment layer of mixtures of CNTs and thermoplastic polymer poly (methyl methacrylate) (PMMA) can be obtained, which may replace ITO [19]. While preparing the LC cells, the rubbing of the substrate also play important role. Lee *et al*. [20] have reported that the order parameter of LC confined between the unrubbed CNT web treated cell was lower than that of LC confined between the rubbed PI surface. However, order parameter of LC enclosed between rubbed CNT web is close to that of the rubbed PI sample. Due to the good transparency of the CNT film, we anticipated that it will perform well in aligning the LC molecules when introducing it into an LC cell, replacing the conventional PI aligning layer.

5.4 Polarizing optical microscopy

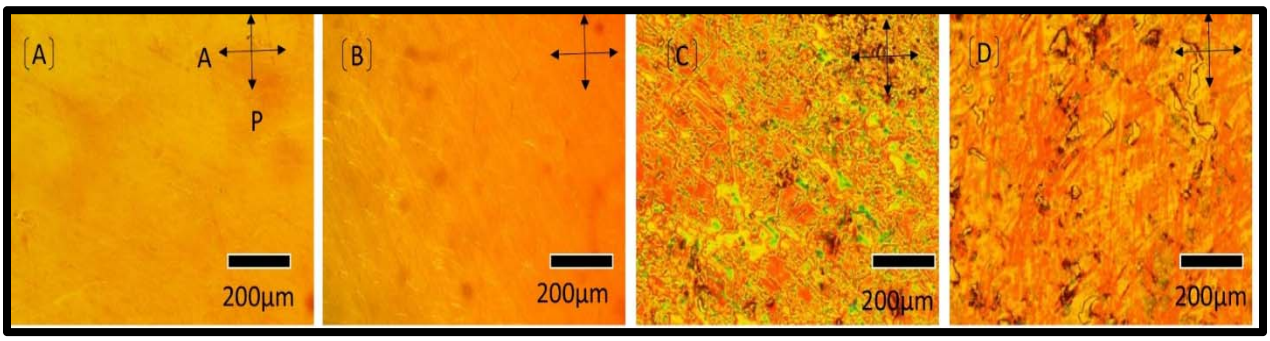

Figure 5.8: POM images of 7CB in LC cells treated with alignment layer polyimide (A) mixture of polyimide and ODA-SWCNT using spin coating (B) ODA-SWCNT using LB technique (C) ODA-SWCNT using spin coating technique (D).

The optical textures of 7CB which is confined in LC cells treated with (A) pure PI (rubbed), (B) mixture of PI and ODA-SWCNT (rubbed), (C) ODA-SWCNT deposited using LB and (D) ODA-SWCNT deposited using spin coating technique are shown in Figure 5.8.

All the images shown in Figure 5.8 are captured by placing cells between crossed polarizers of POM. The LC cells treated with pure PI and mixture of PI and ODA-SWCNT, and rubbed show the bright and dark state on rotating the rubbing direction at 45° and 0° with respect to polarization axis of one of the crossed polarizers. It is worth noting that these cells are rubbed unidirectional after depositing the alignment layer. The cells prepared using only ODA-SWCNT as an alignment layer by both spin coating and LB techniques show only bright state between crossed polarizers. Fu *et al*. [21] have reported that the SWCNT film deposited on the glass plates can provide uniform

aligning for LC molecules as successfully as PI. Thus, the alignment of the 7CB between the rubbed substrates prepared using the mixtures of PI and ODA-SWCNT was comparable to the one between the rubbed PI alignment layer.

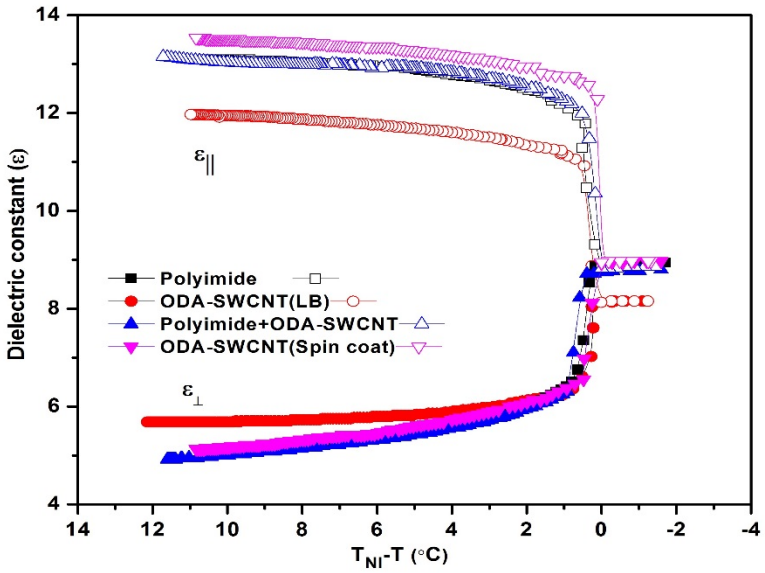

Figure 5.9: Dielectric constant as a function of reduced temperature (T_{NI}-T) for pure 7CB in planar cell fabricated using pure PI, mixture of PI and ODA-SWCNT and only ODA-SWCNT deposited by spin coating as well as LB techniques.

The variation of the dielectric constant of the 7CB as a function of reduced temperature is shown in Figure 5.9. The value of $\varepsilon_{\perp}$ is measured by applying the voltage below V_{th} value and $\varepsilon_{\parallel}$ is measured at 5 volt for all samples. The value of measured $\varepsilon_{\perp}$ in the cell treated with only ODA-SWCNT alignment layer and mixtures of PI and ODA-SWCNT were found to be similar to that measured in cell treated with pure PI, whereas the $\varepsilon_{\parallel}$ value for the sample treated with only ODA-SWCNT deposited using spin coating technique is enhanced by 2 %. In the cell treated with ODA-SWCNT using LB technique, the value of $\varepsilon_{\parallel}$ is reduced by ~8% as compared to the cell treated with pure PI alignment layer. This reduction in the $\varepsilon_{\parallel}$ value can be attributed to decrease in the splay elastic constant.

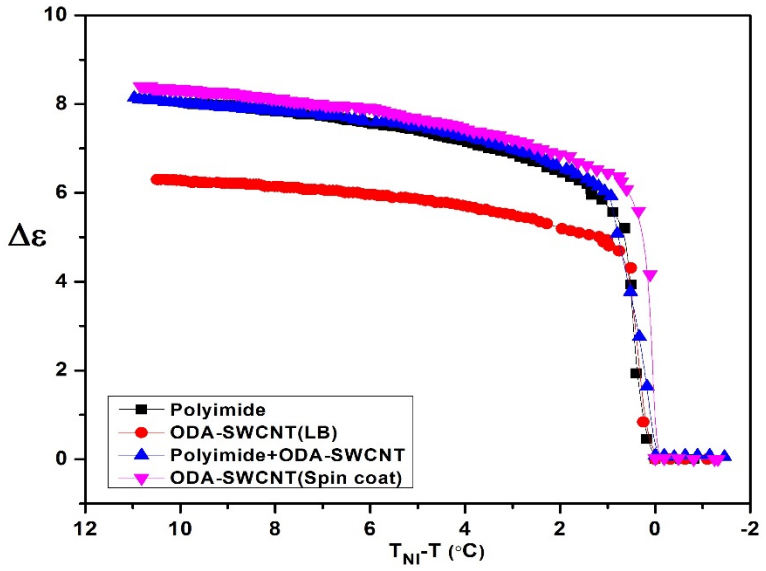

Figure 5.10: Dielectric anisotropy as a function of reduced temperature (T_{NI}-T) for pure 7CB in planar cell fabricated using pure PI, mixture of PI and ODA-SWCNT and only ODA-SWCNT deposited by spin coating as well as LB techniques.

In Figure 5.10, the dielectric anisotropy of all samples as a function of T_{NI}-T is plotted. For the unrubbed cell treated with ODA-SWCNT using spin coating technique, the Δε value is increased by 2 % as compared to that of pure PI alignment layer. The Δε value in cells treated with mixture of ODA-SWCNT and PI cell is found to be close to value of Δε measured in LC cell prepared with pure PI. However, the unrubbed cell prepared using ODA-SWCNT alignment layer with LB technique shows lower value. All samples showed similar temperature dependence trend of Δε.

The variation of V_{th} for all samples as a function of reduced temperature is displayed in Figure 5.11(a). The addition of ODA-SWCNT into PI alignment layer leads to decrease in the V_{th} value regardless of methods used for deposition of alignment layer. The highest reduction in V_{th} value is found in LC cell treated with ODA-SWCNT using spin coating technique. The presence of the ODA-SWCNT in PI alignment layer helps the LC molecules to respond to low applied electric field.

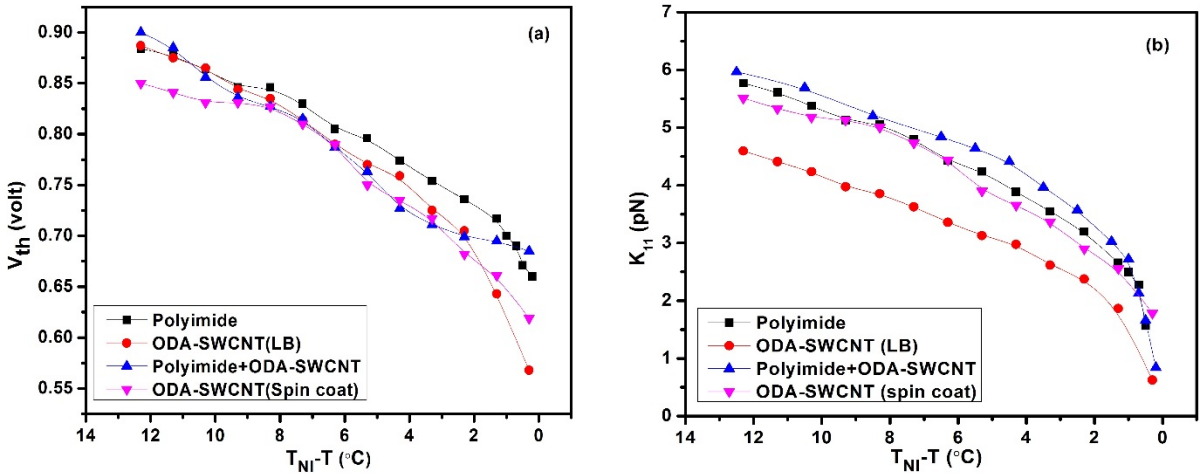

Figure5.11: (a) Threshold voltage (V_{th}) and (b) splay elastic constant (K_{11}) as a function of reduced temperature (T_{NI}-T) for pure 7CB in planar cell fabricated using pure PI, mixture of PI and ODA-SWCNT and only ODA-SWCNT deposited by spin coating as well as LB techniques.

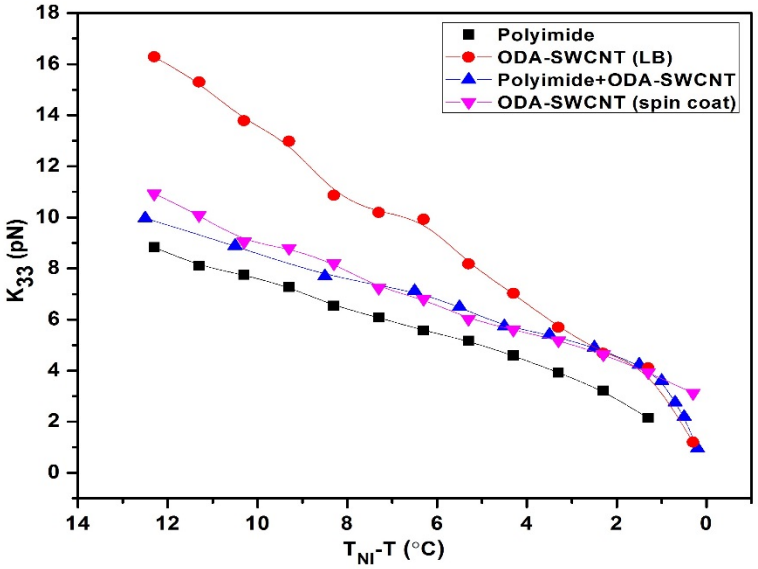

Figure 5.12: Bend elastic constant (K_{33}) as a function of reduced temperature for pure 7CB in planar cell fabricated using pure PI, mixture of PI and ODA-SWCNT and only ODA-SWCNT deposited by spin coating as well as LB techniques.

The variation of K_{11} with temperature is shown in Figure 5.11 (b). The value of K_{11} is decreased by ~30% in the cell treated with only ODA-SWCNT using LB technique, whereas other cells show the K_{11} value comparable to that of pure PI treated cell. The variation of K_{33} as a function of reduced temperature is shown in Figure 5.12. The value of K_{33} increases as a function of T_{NI}-T in all samples. The K_{33} is found to be increased in cells treated with ODA-SWCNT as well as mixtures of PI and ODA-SWCNT used as an alignment layer. The highest increment in K_{33} is

observed in cell treated with only ODA-SWCNT using LB technique. In case of ODA-SWCNT deposited cell using LB method, it is increased by ~30 % as compared to cell prepared using pure PI alignment layer. The increased value of K_{33} in cell treated with ODA-SWCNT using LB technique is consistent with decrease of $\Delta\varepsilon$.

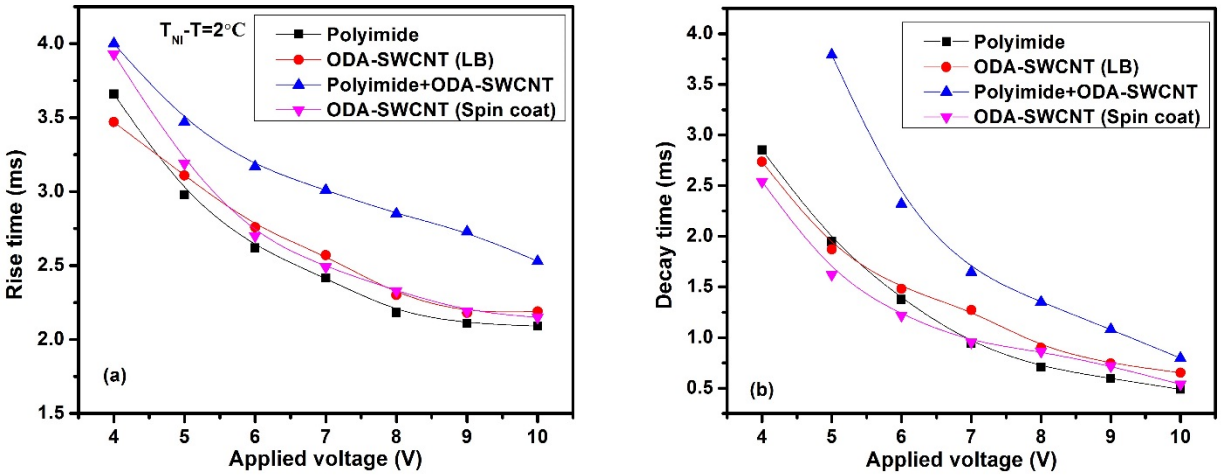

Figure 5.13: (a) Rise time and (b) decay time as a function of applied voltage for pure 7CB in planar cell fabricated using pure PI, mixture of PI and ODA-SWCNT and only ODA-SWCNT deposited by spin coating as well as LB techniques.

The response time behavior of LC is dependent on the temperature and applied voltage. The rise time and decay time as a function of applied voltage for pure 7CB measured at T_{NI}-T = 2°C, are shown in Figure 5.13 (a) and (b), respectively. The response time of the 7CB in the cell treated with only ODA-SWCNT by both LB technique and spin coating technique is comparable to pure PI treated cell, whereas it is slightly increased in cell prepared with mixture of ODA-SWCNT and PI.

The rotational viscosity is important factor in governing the response time. The variation of rotational viscosity as a function of reduced temperature for pure 7CB in planar mode with different alignment layers is shown in Figure 5.14. Using the value of decay time and K_{11} for each sample, the corresponding viscoelastic coefficients are calculated. On addition of ODA-SWCNT into PI alignment layer, the rotational viscosity decreases and thereby affects the rise time of 7CB. The decrease in the rotational viscosity can be attributed to reduction in the free ions due to trapping of ions by ODA-SWCNT, which are present on the surface of substrates [22].

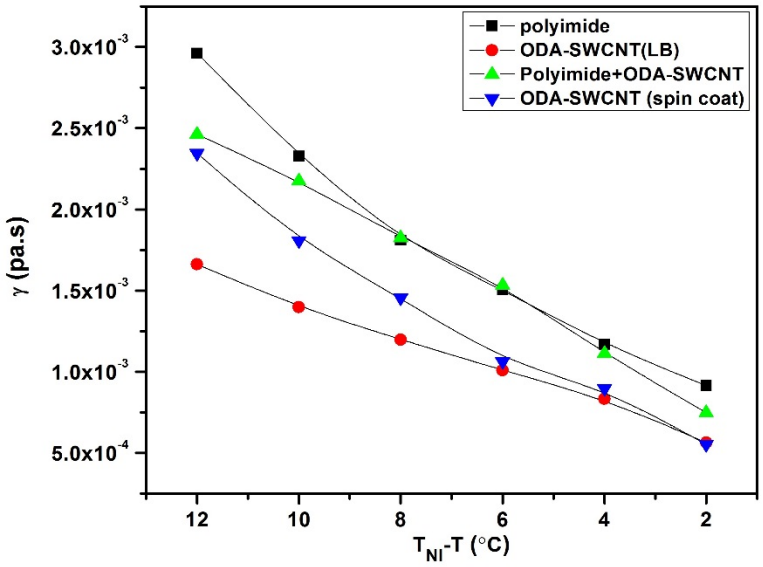

Figure 5.14: Rotational viscosity as a function of reduced temperature for pure 7CB in planar cell fabricated using pure PI, mixture of PI and ODA-SWCNT and only ODA-SWCNT deposited by spin coating as well as LB techniques.

5.5 Conclusions

We have investigated the effect of ODA-SWCNT as an alignment layer on the electro-optic switching characteristics of 7CB in planar alignment geometry. We found that the presence of the ODA-SWCNT in the alignment layer leads to enhanced value of Δε. The rise time and decay time increases due to strong anchoring between 7CB and ODA-SWCNT. The effect of ODA-SWCNT alignment layer deposited using spin coating and LB technique on the V_{th} and response time of pure 7CB has also been investigated. We observed that the Δε value in the cell treated with ODA-SWCNT alignment layer using LB is found to be reduced by ~30% as compared to that of pure PI treated cell. The results indicate that the presence of ODA-SWCNT in PI lead to enhancement of the dielectric anisotropy, hence the order parameter. The physical properties of LC cells prepared with only ODA-SWCNT as alignment layer is comparable to that of pure PI sample. The CNT as an alignment layer can be used for fabricating optical devices with high transmittance of light. Furthermore, it can be used as a built-in heating layer, which can extend the working temperature range of the LCDs [23-24].

References:

1. K. Takatoh, M. Hasegawa, M. Koden, R. Hasegawa, M. Sakamoto, *Alignment Technologies and Application of Liquid crystals*, CRC Press, 99-105, **2005**.

2. W. Lee, C. Y. Wang, Y. C. Shih, Appl. Phys. Lett. 85, 513, **2004**.
3. M. D. Lynch, D. L. Patrick, Nano Lett. 2, 1197, **2002**.
4. J. Kumar, R. K. Gupta, V. Manjuladevi, AIP Conf. Proc. 1536, 693, **2013**.
5. H. Qi, T. Hegmann, J. Mater. Chem. 18, 3288, **2008**.
6. R. Dhar, A. S. Pandey, M. B. Pandey, S. Kumar, R. Dabrowski, Appl. Phys. Express. 1, 121501, **2008**.
7. S. Y. Lu, L. C. Chien, Opt. Express. 16, 12777, **2008**.
8. A. Kumar, A. M. Biradar, Phys. Rev. E. 83, 041708, **2011**.
9. I. Dierking, G. Scalia, P. Morales, J. Appl. Phys. 97, 044309, **2005**.
10. M. Joete, Russell, Oh Soojin, Issac LaRue, Otto Zhou, Edward T. Samulski, Thin Solid Films, 509, 53, **2006**.
11. H. Shimoda, S. J. Oh, H. Z. Geng, R. J. Walker, X. B. Zhang, L. E. McNeil, O. Zhou, Adv. Mater. 14, 899, **2002**.
12. K .J. Lee, H. G. Park, H. C. Jeong, Liq Cryst. 41, 25, **2014**.
13. H. Lee, S. Yang, J. H. Lee, Appl. Phys. Lett. 104, 191601, **2014**.
14. J. Kumar, V. Manjuladevi, R. K. Gupta, S. Kumar, Liq Cryst. 43, 4, **2016**.
15. M. Okulska-Bozek, T. Prot, J. Borycki, J. Kedzierski, Liq Cryst. 20, 349, **1996**.
16. D. W. Berreman, Phys. Rev. Lett. 28, 1683, **1972**.
17. W. Maier and A. Saupe, Z. Naturforsch., A 14, 882, **1959.**
18. Q. Wang, H. Moriyama. *Carbon Nanotube-Based Thin Films: Synthesis and Properties, Carbon Nanotubes - Synthesis, Characterization, Applications*, In Tech, **2011**.
19. L. M. Clayton, A. K. Sikder, A. Kumar, M. Cinke, M. Meyyappan, T. G. Gerasimov, J. P. Harmon, Adv Funct Mater. 15, 101, **2005**.
20. H. Lee, J-H Lee, C. P. Huynh, S. C. Hawkins, M. Musameh, D. H. Kim, H. L. Seung, J. Choi, Liq. Cryst. 42, 3 **2015**.
21. W. Fu, L. Liu, K. Jiang, Q. Li and S. Fan, Carbon. 48, 1876, **2010**.
22. H. Y. Chen, W. Lee, N. A. Clark, Appl. Phys. Lett. 90, 033510, **2007**.
23. W. Q. Fu , Y. Wei , F. Zhu , L. Liu , K. L. Jiang , Q. Q. Li , S. S. Fan, Chin. Phys. B, 19, 088104, **2010**.
24. W. Q. Fu , L. Liu , K. L. Jiang , Q. Q. Li , S. S. Fan, Carbon. 48 ,1876, **2010**.

Chapter 6

Electro-optic and dielectric studies on nanomaterials doped nematic liquid crystal

6.1 Introduction

Liquid crystal (LC) is known to be excellent hosts for carbon nanotubes (CNTs). Having molecular structure similar to CNTs, LCs perfectly incorporate CNTs into own structure. In the previous chapter, we have discussed the effect of octadecylamine functionalized single walled carbon nanotubes (ODA-SWCNT) in the alignment layer of the LC cells. We found that the presence of the ODA-SWCNT in the alignment layer leads to enhanced value of dielectric anisotropy ($\Delta\varepsilon$). The rise time and decay time increases due to strong anchoring between LC and ODA-SWCNT. The physical properties of the LC materials can be suitably altered by incorporating nanomaterials of different aspect ratio like CNTs, graphene and nanoparticles [1-15]. The collective behavior of the LC can be altered by the incorporation of nanomaterials of different shapes and size. In this chapter, we present our investigation on the effect of incorporation of nanomaterials viz. cadmium selenide (CdSe) quantum dots (QDs), titanium dioxide (TiO_2) nanoparticles and polyethylene glycol functionalized single walled CNT (PEG-SWCNT) in a nematic liquid crystals (NLC) on their dielectric property and elastic constant. The collective reorientation of preferred long axis of NLCs on application of external electric and magnetic field makes them a suitable candidate in many switching devices mainly for liquid crystal display (LCD) technology [16, 17]. The performance of LC based devices depend on some physical parameters such as threshold voltage (V_{th}), voltage holding ratio (VHR), birefringence and dielectric anisotropy ($\Delta\varepsilon$) etc. The V_{th} is the key factor for LCD, which determine the power consumption. Reducing V_{th} of LCD is important

for achieving low power consuming devices. The study of nanoparticles doped LCs has been of great interest since they demonstrate remarkable physical properties and have potential applications in display technology [16]. Among these nanomaterials, the semiconducting inorganic nanoparticles, generally known as QDs, have created lot of interest among the researchers. Due to the unique properties such as solution processability, tailoring of band gap and quantum confinement, QDs are widely used in many applications such as optoelectronics, photovoltaics, solar cells and lasers [18]. The director of nematic phase can be reoriented by the application of external electric field using which the nanoscale assemblies of the QDs in the LC matrix can also be manipulated. The inclusion of semiconductor QDs into NLC affects the orientation of the LC molecules from planar to homeotropic depending on the size, nature and concentration of QDs. It was shown that NLC doped with hexadecyleamine capped CdSe QDs, varying in size from 2.5 to 5.2nm shows homeotropic alignment upto 2wt% of dopant whereas cadmium telluride (CdTe) QDs capped with thioglycolic acid, varying in size from 3.2 to 4 nm, shows planar alignment [9, 10]. Basu *et al.* [19] have studied the interaction between cadmium sulfide (CdS) QDs and NLCs and demonstrated the assembly of CdS QDs into nanoscale macroscopic chain-like configurations. Assembly of QDs in LC medium due to self-assembly nature of LC can become a better candidate from application point of view.

The dispersion of different type of nanoparticle such as semiconducting, metallic and QDs into NLCs has improved their electro-optic and physical properties [20-22]. Each type of these nanoparticles has its own effect on tailoring the properties of LC. The insulating nanoparicles can trap ions in the LC material, and this leads to fewer ions in LC matrix, thus abating the screening effect [20]. Chou *et al.* have observed that the doping TiO_2 nanoparticles into NLCs lead to a reduction in the moving-ion density. The amount of the reduced impurity ions related to the size of doped TiO_2 nanoparticles. Under similar doping concentrations, TiO_2 nanoparticles with a smaller average particle size were found to be more efficient in trapping the impurity ions [23].

In this chapter, the electro-optic switching and dielectric properties of NLC doped with nanoparticles, viz., octadecylamine capped CdSe QDs and titanium dioxide (TiO_2) nanoparticles are presented. The NLC was doped with different concentrations of the semiconducting CdSe QDs. The doped samples were found to have a lower V_{th} than that of pure NLC. The value of V_{th} decreases with increasing concentration of the QDs. The dielectric constants and splay elastic constant were measured to understand the cause of the V_{th} reduction. Doping QDs led to increase

in value of Δε in comparison with that of pure NLC. We have also investigated the effect of semiconducting TiO_2 nanoparticles on the dielectric properties of NLC. The enhancement of dielectric anisotropy as well as splay elastic constant (K_{11}) was observed on doping of TiO_2 nanoparticles into NLC. The result showed that the incorporation of nanoparticles into NLC provides a way to improve the performance of LC based devices.

6.2 Materials and methods

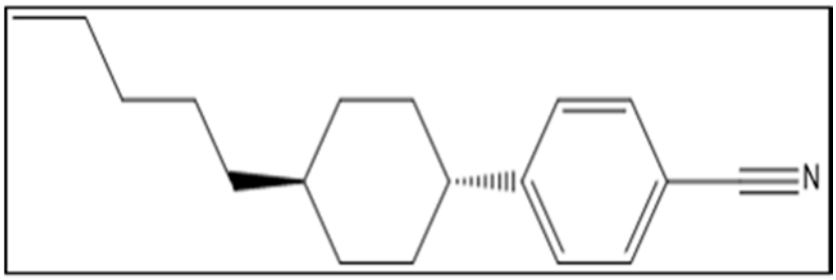

Cr-15.5°C-N-55.3°C-Iso

Figure 6.1: Chemical structure of 4-trans-pentylcyclohexylcyanobenzene (5PCH) and its phase transition temperatures.

The nematic liquid crystal 5PCH (4-trans-pentylcyclohexylcyanobenzene) was procured from Sigma Aldrich. TiO_2 nanoparticles are procured from Sigma Aldrich and polyethylene glycol functionalized single walled CNT (PEG-SWCNT) from Carbon Solution Inc. USA. The size of TiO_2 nanoparticles was ~5 nm. The octadecylamine capped CdSe QDs were synthesized by Sandeep Kumar *et al*. [18], Raman Research Institute, Bengaluru. The size of semiconducting CdSe QDs is 3.5 nm in diameter. The CdSe QDs are dissolved in chloroform solvent. The solution is ultrasonicated for about three hours. The nanocomposite of 5PCH containing CdSe QDs of two different concentrations (1 and 2 wt%) are prepared. The nanocomposites are used in the further studies after evaporating the solvent. The planar LC cells are prepared using polyimide coated indium tin oxide (ITO) coated glass plates. The thickness of LC cells is ~10 μm. The alignment of pure 5PCH and its nanocomposites doped with CdSe QDs is observed using a polarizing optical microscope (Model OLYMPUS BX51). Pure 5PCH as well as CdSe QDs doped (upto 2 wt%) NLC reveal an uniform texture between crossed polarizers indicating a uniform nematic director field. At higher concentration (>2 wt%) of CdSe QDs, the alignment deteriorates in the NLC medium due to formation of cluster of QDs. The Freedericksz threshold voltages (V_{th}) of each sample are estimated through transmittance intensity data. We have measured the V_{th} for CdSe

QDs doped NLC and pure NLC from both transmission and capacitance methods. In capacitance method, the V_{th} in planar aligned cells is estimated from capacitance-voltage (*C-V*) plot wherein the capacitance starts to increase at V_{th} and before V_{th} the capacitance remain constant. The difference between transitions voltages measured from both methods is around 2 %. In order to avoid the effect of any scattering caused by nanoparticles on optical transmittance, we have taken the V_{th} values from capacitance data. The dielectric constant (ε) of each sample is recorded as a function of temperature at a frequency of 4.1 kHz. For measuring parallel component of dielectric constant ($\varepsilon_{\parallel}$), homeotropic cells are prepared.

In another study similarly 5PCH is mixed with 0.5wt% of TiO_2 nanoparticles and studied. A mixture of 5PCH and 0.05 wt% of PEG-SWCNT is prepared. The dielectric constant ($\varepsilon_{\parallel}$, $\varepsilon_{\perp}$) of the pure 5PCH and its mixtures is measured using planar LC cell. The $\varepsilon_{\perp}$ is measured at voltages below the V_{th} at frequency of 4.1 kHz. The $\varepsilon_{\parallel}$ is measured at 5 volt using the same cell. The V_{th} value as well as splay elastic constant (K_{11}) are measured.

6.3 Results and discussion

6.3.1 Effect of CdSe QDs on physical properties of NLC

The parallel and perpendicular components of dielectric constant ($\varepsilon_{\parallel}$, $\varepsilon_{\perp}$) for pure 5PCH and its CdSe QDs nanocomposites as a function of reduced temperature is shown in Figure 6.2. The perpendicular component of dielectric permittivity ($\varepsilon_{\perp}$) is determined directly from the value of capacitance measured at voltages lower than V_{th}. On cooling pure 5PCH from isotropic to nematic state, the dielectric constant $\varepsilon_{\perp}$ significantly decreases at the isotropic to nematic transition temperature (T_{NI}) and on further cooling, the dielectric constant gradually decreases with decreasing temperature. Whereas the dielectric constant $\varepsilon_{\parallel}$ significantly increases at T_{NI} and on further cooling, it increases with decreasing temperature. The value of T_{NI} temperature was determined from discontinuous change of ε value which appeared at 55.1°C, 54.6°C and 53.6°C for pure 5PCH, 1 wt% and 2 wt% of CdSe QDs doped 5PCH, respectively.

The values of both $\varepsilon_{\parallel}$ and ε⊥ increase with increasing concentration of CdSe QDs in 5PCH as compared to the pure 5PCH. The increase in $\varepsilon_{\perp}$ value indicates that the functionalized CdSe QD

particles functionalized with octadecylamine group align themselves along the director of host NLC due to nematic ordering of the NLC at the surface of substrate. On application of external electric field, the dielectric permittivity $\varepsilon_{\parallel}$ of the medium increases due to polarisability of QDs in the system. On increasing the concentration of CdSe QDs, the anisotropy in the dielectric constant is observed in the isotropic phase also. The anisotropy in dielectric constant for 2 wt% CdSe QDs doped 5PCH might be due to aggregation of the QDs and the aggregated QDs possess some polarizability in the isotropic state also.

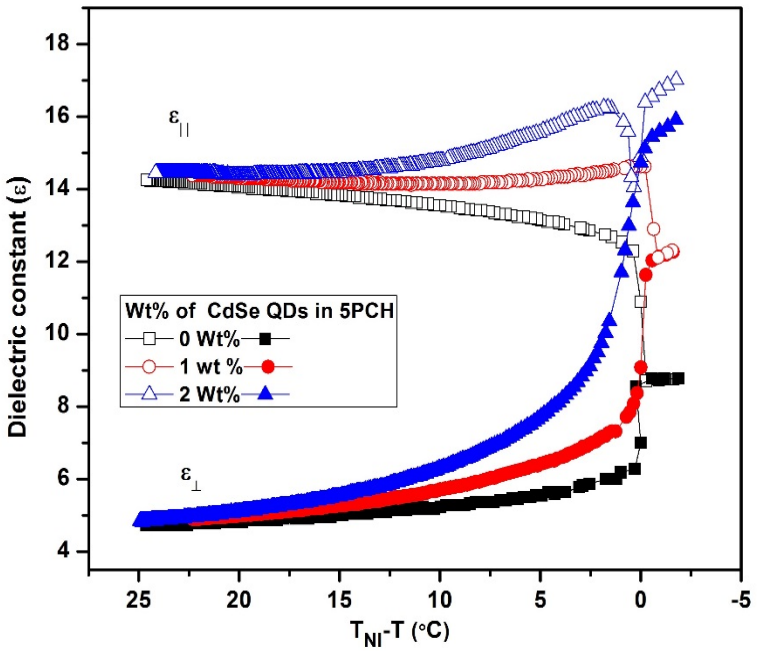

Figure: 6.2: Dielectric constant ($\varepsilon_{\parallel}, \varepsilon_{\perp}$) for pure and CdSe QDs doped NLC as a function of reduced temperature (T_{NI}-T).

The variation of dielectric anisotropy (Δε) as a function of reduced temperature (T_{NI}-T) for pure 5PCH and CdSe QDs doped 5PCH is shown in Figure 6.3. It is observed that on cooling from isotropic state, Δε increases with decreasing temperature. The Δε value increases with increase in concentration of CdSe QDs. The temperature variation of Δε of pure 5PCH is in good agreement with the values reported earlier [24, 25]. The dielectric anisotropy Δε is a measure of order parameter of NLC. Our study suggests that doping CdSe QDs in NLC can lead to enhancement of orientational order due to incorporation of QDs into NLC.

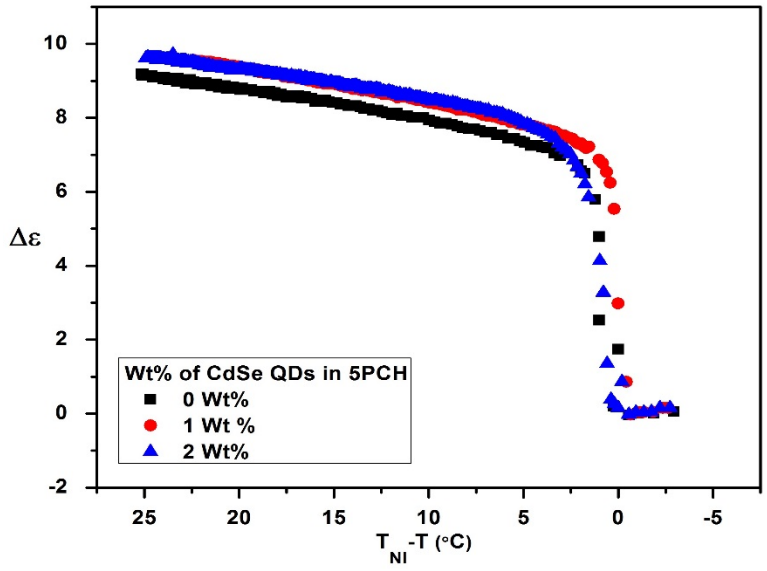

Figure: 6.3: Dielectric anisotropy for pure and CdSe QDs doped NLC as a function of reduced temperature (T_{NI}-T).

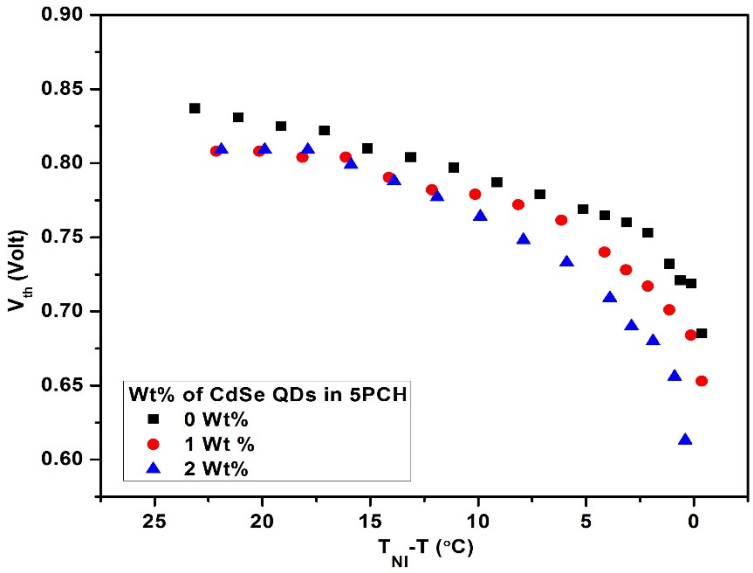

Figure 6.4: Threshold voltage (V_{th}) for pure and CdSe QDs doped NLC as a function of reduced temperature (T_{NI}-T).

The temperature variation of V_{th} in nematic phase for pure 5PCH as well as its nanocomposites doped with CdSe QDs is shown in Figure 6.4. The value of V_{th} at any given temperature decreases with increasing concentration of dopant CdSe QDs. The decrease in V_{th} may be due to the disorder created by incorporation of QDs in nematic which lead to formation of microdomain [9].

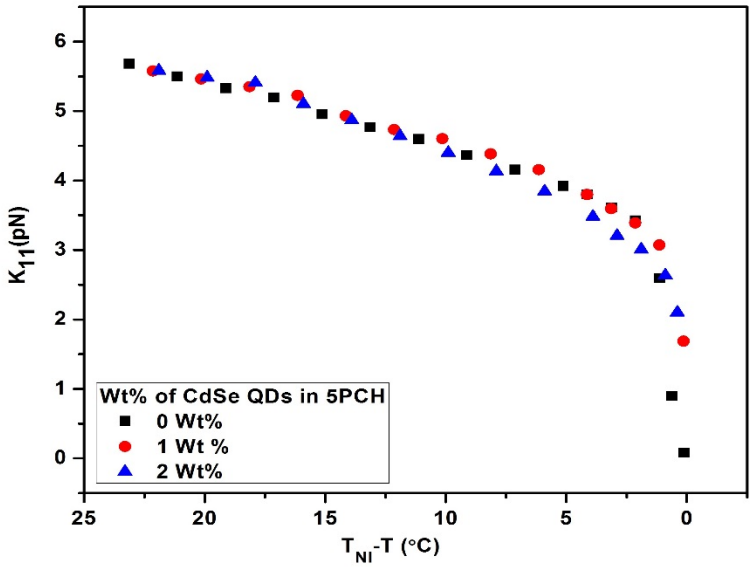

Figure 6.5: Splay elastic constant (K_{11}) for pure and CdSe QDs doped NLC as a function of reduced temperature (T_{NI}-T).

The effect of CdSe QDs on the splay elastic constant (K_{11}) has also been observed. The K_{11} of positive dielectric anisotropic LC material in a planar aligned cell is determined using relation,

$$V_{th} = \pi \sqrt{\frac{K_{11}}{\varepsilon_0 \Delta\varepsilon}} \qquad (6.1)$$

where ε_0 permittivity of free space and $\Delta\varepsilon = \varepsilon_{\parallel} - \varepsilon_{\perp}$, is the dielectric anisotropy of the sample. The equation 6.1 indicates that the V_{th} depends on the value of $\Delta\varepsilon$ and K_{11}. To understand the effect of CdSe QDs on electro-optic proeprties of NLC, we have estimated the K_{11} value with help of equation 6.1. The variation of K_{11} as a function of T_{NI}-T for pure as well as for its nanocomposites doped with CdSe QDs is shown in Figure 6.5. At higher temperature, V_{th} for 2wt% CdSe QDs doped 5PCH is reduced significantly compared to that of pure 5PCH, leading to reduction in the K_{11} for 2wt% CdSe QDs doped 5PCH as compared to that of pure 5PCH. At low temperatures, V_{th} for CdSe QDs doped 5PCH is even though reduced compared to that of pure 5PCH, the increase in $\Delta\varepsilon$ leads to a value of K_{11} which is comparable to that of pure 5PCH.

We have observed that above 2 wt% of CdSe QDs, they start to aggregate and alignment of NLC medium deteriorates. The biggest challenge in achieving a uniform dispersion in thermotropic LCs arises from the fact that these nanoparticles induce distortions of the LC director field, which cost elastic free energy and therefore promote aggregation. This aggregation of

nanoparticles with strong surface boundary conditions allows the LC to reduce the overall free energy due to such distortions induced by individual interacting particles [26]. The aggregation of nanoparticles might not be always disadvantageous for device application. This situation may be preferred, if the aggregates are nano-scale and anisotropic.

6.3.2 Effect of TiO_2 nanoparticles on physical properties of NLC

In this section, we are presenting the result of electro-optical and physical properties of semiconducting TiO_2 nanoparticles and PEG-SWCNT doped 5PCH. TiO_2 nanoparticles are spherical particles and CNTs exhibit the shape anisotropy like cylinders. The incorporation of different shape anisotropic nanomaterials in the LC matrix can introduce different level of defects and ordering. Such perturbation of the LC medium has significant effect on their electro-optic and dielectric properties. Considering the shapes of nanomaterials e.g., spherical and rod shape (uniaxial), the dielectric permittivity and elastic constant of the nanocomposites of 5PCH is discussed in this chapter. We observed that small amount of TiO_2 nanoparticles has brought appreciable change in the dielectric anisotropy of 5PCH. Whereas, doping PEG-SWCNT into 5PCH reduces the dielectric anisotropy.

The effect of nanomaterials with different structure on the electro-optical properties of NLC has been reported [10, 22, 27]. They have used fullerene C_{60}, C_{70}, SWCNTs, multi-walled CNTs (MWCNTs) and graphene. Interestingly, fullerene balls were found to be the best compatible material for optical characteristics and reorientation of LC molecules, while the CNTs induce some reorientation in LC media, and graphene layers are good barriers to preserve reorientation.

The variation of dielectric constant ($\varepsilon_{\parallel}, \varepsilon_{\perp}$) with temperature for pure 5PCH and its nanocomposites of TiO_2 nanoparticles and PEG-SWCNT is shown in Figure 6.6. For TiO_2 nanoparticles doped sample, the $\varepsilon_{\parallel}$ value is found to be higher than that of pure 5PCH, whereas for PEG-SWCNT doped sample, the $\varepsilon_{\parallel}$ values are somewhat smaller than the values for pure 5PCH. The $\varepsilon_{\parallel}$ is enhanced by ~6% in the sample with TiO_2 nanoparticles doped 5PCH as compared to pure 5PCH. The dispersion of nanoparticles enhances the dielectric anisotropy of the NLCs. The $\varepsilon_{\perp}$ is similar to that of pure 5PCH at low temperatures but on increasing the temperature, it increases for doped sample.

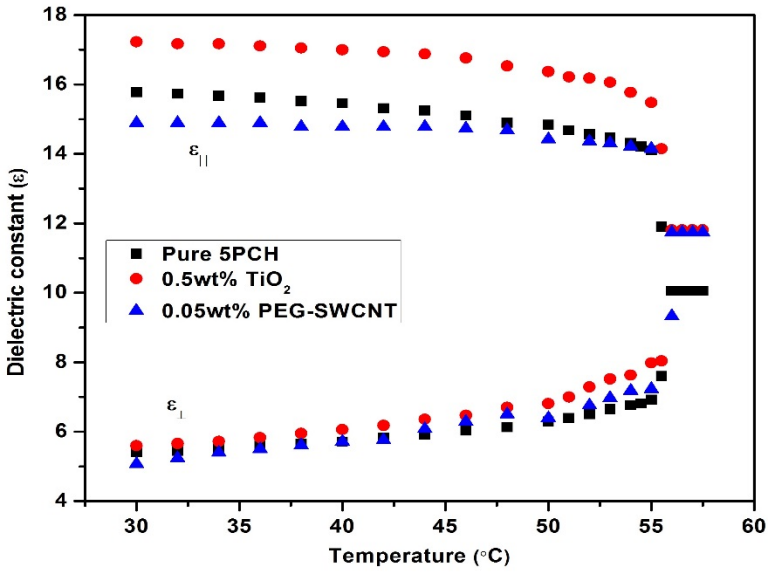

Figure 6.6: Dielectric constant ($\varepsilon_{\parallel}, \varepsilon_{\perp}$) for pure 5PCH and its nanocomposites of TiO_2 nanoparticles and PEG-SWCNT as a function of temperature.

The dielectric constant is measured from the voltage-dependent capacitance measurement. The measurement indicates that the existence of a minute amount of PEG-SWCNT does not affect the cell capacitance, whereas the V_{th} was greatly reduced due to the ion trapping by CNTs. In case of PEG-SWCNT doped 5PCH, the dielectric constant $\varepsilon_{\parallel}$ is similar to that of pure 5PCH near the T_{NI} transition temperature but on decreasing the temperature, it is slightly reduced. The properties of functionalized CNT depend on the functionalization method and on the functionalization group. PEG functionalized CNT is prepared by wrapping method which is different from the covalently functionalized ODA-SWCNT. polyethylene glycol functionalized CNT is biocompatible material. The interaction between PEG functionalized CNT and 5PCH is less. Hence, the PEG-SWCNT can not impart any orientational order onto 5PCH which can lead to decrease in $\varepsilon_{\parallel}$ values.

The dielectric anisotropy is estimated from temperature dependence of dielectric constant ($\varepsilon_{\parallel}, \varepsilon_{\perp}$). The variation of $\Delta\varepsilon$ as a function of temperature for pure 5PCH and its nanocomposites of TiO_2 and PEG-SWCNT is shown in Figure 6.7. The small concencetration of TiO_2 nanoparticles in 5PCH has enhanced the $\Delta\varepsilon$ significantly. The increase in $\Delta\varepsilon$ in TiO_2 nanoparticles doped 5PCH sample is due to increase in $\varepsilon_{\parallel}$ values. The dielectric anisotropy of LC material is also related to the order parameter. The dispersed TiO_2 nanoparticles change the orientation of molecules in the LC medium. The enhanced $\Delta\varepsilon$ suggests that doping TiO_2 nanoparticles in 5PCH can lead to

enhancement of orientational order due to interaction between TiO_2 nanoparticles and 5PCH. The effect of TiO_2 nanoparticles can also be seen at the temperature above the T_{NI}. In isotropic state, the dielectric constant $\varepsilon_{\parallel}$ and $\varepsilon_{\perp}$ values for doped samples are found to be higher than pure 5PCH.

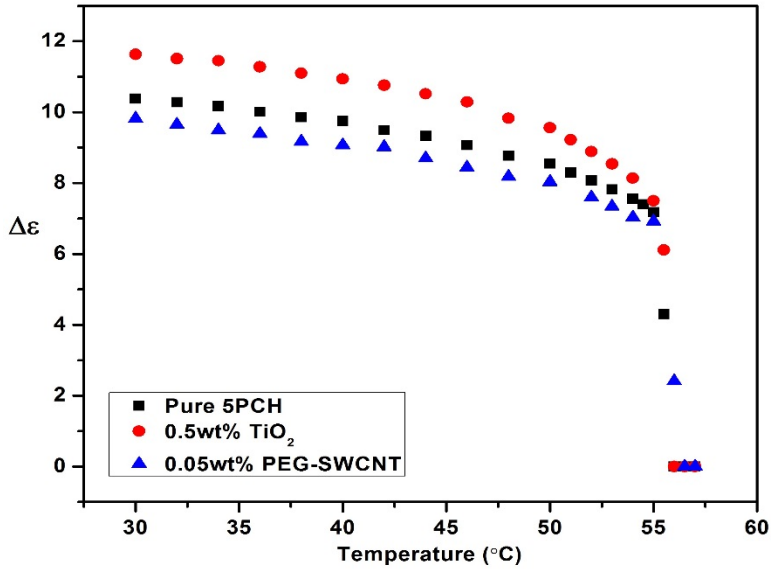

Figure 6.7: Dielectric anisotropy (Δε) for pure 5PCH and its nanocomposites of TiO_2 nanoparticles and PEG-SWCNT as a function of temperature.

The temperature variation of V_{th} for pure 5PCH as well as TiO_2 nanoparticles and PEG-SWCNT doped 5PCH is shown in Figure 6.8. On addition of TiO_2 nanoparticles, the V_{th} value is reduced. The V_{th} value for TiO_2 nanoparticles doped 5PCH is reduced by ~2% as compared to that of pure 5PCH. The TiO_2 nanoparticles are randomly distributed in LC medium. The dispersed TiO_2 nanoparticles in LC medium can trap the ion impurities which are available in the LC cell. These ions impurities cause the screening effect. When a voltage is applied across the LC cell, such ions begin to move and finally are adsorbed by the alignment layers [28]. After dispersing the TiO_2 nanoparticles, such ions are trapped by nanoparticles and less number of ions reach at alignment layer. The traping of ion impuirites by TiO_2 nanoparticles might be reason for decreasing V_{th}. It was suggested that the reduction of V_{th} in a system of NLC and nanoparticles is due to interaction between ion impurities and nanoparticles [29]. The trapping of ion impurities by nanoparticles cause the screening effect less effective, which allow the LC molecules to experience a relatively larger effective voltage within the cell.

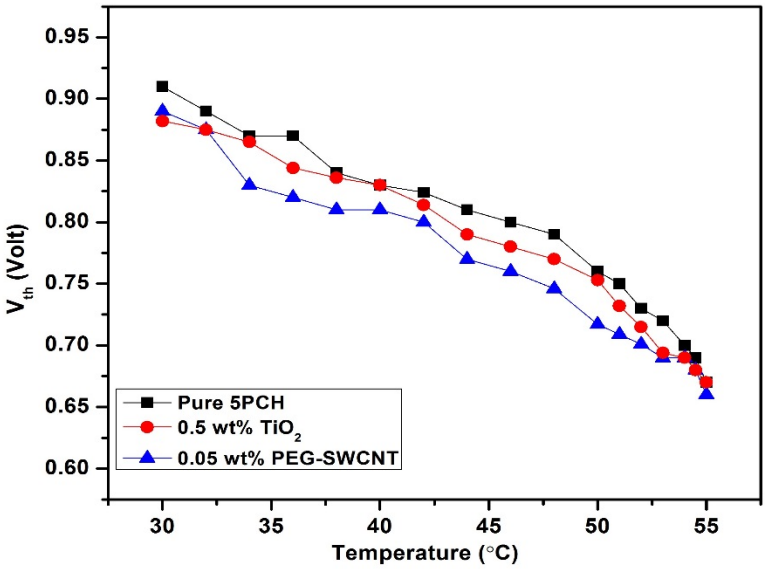

Figure 6.8: Threshold voltage (V_{th}) for pure 5PCH and its nanocomposites of TiO_2 nanoparticles and PEG-SWCNT as a function of temperature.

In case of PEG-SWCNT doped 5PCH, V_{th} decreases as compared to both pure 5PCH and TiO_2 nanoparticles doped 5PCH and it is reduced by ~4% as compared to pure 5PCH. The reduction in the V_{th} may be due to decrease of K_{11}. Doped PEG-SWCNT favor the splay deformation in NLC medium which results in decrease of V_{th} value. Chen *et al.* [20] reported that doping insulating nanoparticles such as ZnO, TiO_2, and Si_3N_4 in NLCs leads to a reduction in the moving-ion density in LC cells and drastically reduces the transient currents as well as threshold voltage.

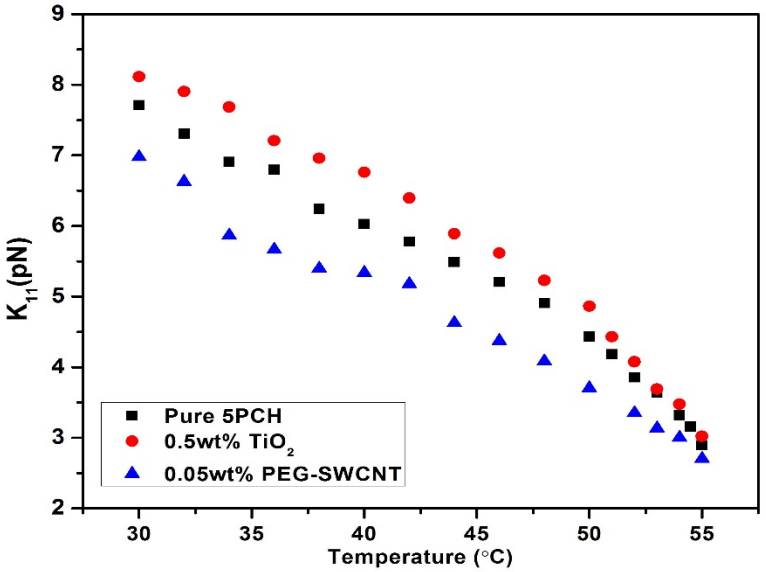

Figure 6.9: Splay elastic constant (K_{11}) for pure 5PCH and its nanocomposites of TiO_2 and PEG-SWCNT as a function of temperature.

In Figure 6.9, variation of K_{11} as a function of temperature for pure 5PCH and nanocomposites of 5PCH doped with TiO_2 nanoparticles and PEG-SWCNT is shown. The value of K_{11} increases with the inclusion of TiO_2 nanoparticles in 5PCH. The result suggests that the increase value of K_{11} is due to increase in $\Delta\varepsilon$. Near T_{NI}, splay elastic constant value for TiO_2 nanoparticles doped 5PCH is comparable to pure 5PCH. On decreasing the temperature, K_{11} starts to increase for doped sample which indicates that the order parameter is improved.

The physical properties of nanomaterial doped LC medium are strongly dependent on the molecular structure and elastic properties of the LC as well as on the size and shape of the nanoparticles used. We find that the ability to reduce the V_{th} and enhanced $\Delta\varepsilon$ is apparently not dependent on the type of nanoparticles. In both type of nanoparticles, viz., CdSe QDs and TiO_2 nanoparticles doped 5PCH, the V_{th} is reduced which suggests that the impurity ions are physically trapped by the polarized nanoparticles by coulomb force.

6.4 Conclusions

The nanocomposites of 5PCH and CdSe QDs were prepared and the alignment were found to be uniform and stable upto 2 *wt* %. The addition of QDs with concentrations 1 and 2 *wt* % into NLC favors homogeneous alignment. The doped LC cells found to have lower V_{th} than pure 5PCH. The doping of CdSe QDs into 5PCH have significantly enhanced the dielectric anisotropy and a minor shift in the transition temperatures has been observed. Improved dielectric anisotropy in the mixtures of CdSe QD and 5PCH nanocomposite systems indicates that QDs align themselves along with the average direction of 5PCH molecules. In case of TiO_2 doped NLC, the V_{th} is reduced and dielectric anisotropy is enhanced due to incorporation of nanoparticles into NLC, whereas for PEG-SWCNT doped 5PCH, dielectric anisotropy is somewhat smaller than that of pure 5PCH. These mixtures of nanoparticles and NLC can provide an opportunity to develop LC based optoelectronic devices with improved electro-optic switching.

References:

1. R. Saito, G. Dresselhaus, M. S. Dresselhaus, *Physical Properties of Carbon Nanotubes*, Imperial College Press, London, **2001**.
2. H. Qi, B. Kinkead, T. Hegmann, Adv. Funct. Mater. 18, 212, **2008**.
3. Y. Williams, K. Chen, J. H. Park, I. C. Khoo, B. Lewis, T. E. Mallouk, Proc. SPIE-Int. Soc. Opt. Eng. 5936, 225, **2005**.

4. Y. S. Ha, H. J. Kim, H. G. Park, D. Shik, Opt. Exp. 20, 6448, **2012**.
5. A. K. Garg, V. K. Agrawal, B. Bahadur, Mol. Cryst. Liq. Cryst. 130, 11, **1985**.
6. T. Zhang, C. Zhong, J. Xu, Jpn. J. Appl. Phys. 48, 055002, **2009**.
7. X. Tong, Y. Zhao, J. Am. Chem. Soc. 129, 6372, **2007**.
8. H. L. Lee, I. A. Mohammed, M. Belmahi, M. B. Assouar, H. Rinnert, M. Alnot, Materials, 3, 2069, **2010**.
9. B. Kinkead, T. Hegmann, J. Mater. Chem. 20, 448, **2010**.
10. H. Qi, T. Hegmann, J. Mater. Chem. 18, 3288, **2008**.
11. U. B. Singh, R. Dhar, R. Dabrowski, M. B. Pandey, Liq. Cryst. 41, 953, **2014**.
12. J. Mirzaei, M. Urbanski, K. Yu, H.-S. Kitzerow, T. Hegmann, J. Mater. Chem. 21, 12710, **2010**.
13. T. Joshi, A. Kumar, J. Prakash, A. M. Biradar, Appl. Phys. Lett. 96, 253109, **2010**.
14. G. A. Shandryuk, E. V. Matukhina, R. B. Vasil'ev, A. Rebrov, G. N. Bondarenko, A. S. Merekalov, A. M. Gas'kov, R. V. Talroze, Macromolecules. 41, 2178, **2008**.
15. V. Manjuladevi, R. K. Gupta, S. Kumar, J. Mol. Liq. 171, 60, **2012**.
16. J. W. Doane, Liquid Crystals: *Applications and Uses*; World Scientific, Singapore, **1990**.
17. I. Dierking, G. Scalia, P. Morales, J. Appl. Phys. 97, 044309-1, **2005**.
18. S. Kumar, L. K. Sagar, Chem. Commun. 47, 12182, **2011**.
19. R. Basu, G. S. Iannacchione, Phys. Rev. E 80, 010701, **2009**.
20. W. T. Chen, P. S. Chen, C.Yu Chao, Japan. J. Appl. Phys. 48, 015006, **2009**.
21. R. Manohar, S. P. Yadav, A. K. Srivastava, A. K. Misra, K. K. Pandey, P. K. Sharma, A. C. Pandey, Japan. J. Appl. Phys. 48.101501, **2009**.
22. C. W. Lee, W. P. Shih, Mater. Lett. 64, 466, **2010**.
23. T. R. Chou, J. H., W. T. Chen, and C. Y. Chao, Japan J. Appl. Phys. 53, 071701, **2014**.
24. S. Sen, K. Kali, S. K. Roy, S. B. Roy, Mol. Cryst. Liq Cryst. 126, 269, **1985**.
25. L. Pohl, R. Eidenschink, G. Krause, D. Erdmann, Phys. Lett. A. 60, 421, **1977**.
26. Q. Liu, Y. Yuan and I. Smalyukh, Nano Lett. 14, 7, 4071, **2014**.
27. S. Eren, M. Okutan, O. Köysal, Y. Yerli, Chin. Phys. Lett. 25, 212, **2008**.
28. H. Mada, K. Osajima, J. Appl. Phys. 60, 3111, **1986**.
29. W. K. Lee, J. H. Choi, H. J. Na, J. H. Lim, J. M. Han, J. Y. Hwang, D. S. Seo, Opt Lett. 34, 3653, **2009**.

Chapter 7

Effect of ODA-SWCNT on the dielectric property of a chiral smectic liquid crystal

7.1 Introduction

The chiral molecules in liquid crystal (LC) material induce spontaneous polarization perpendicular to the tilt plane in smectic-C phase because of the chiral symmetry breaking. This polarization induces more interesting phases called chiral smectic-C* (SmC*) variant phases [1-3]. Similar to the smectic-C, the director in SmC* phase also makes a tilt angle with respect to the smectic layer normal. The chirality of the molecules induces a non-zero azimuthal twist from one layer to the next layer, which is responsible for producing a spiral twisting of the molecular axis along the layer normal.

The antiferroelectric phase SmC_A^* was first observed in LCs in 1989 [4]. The antiferroelectric SmC_A^* LC phase is formed when the molecules in alternate layers tilt in opposite directions, the dipole contribution also reverse in direction from one layer to the next. In addition to the SmC_A^* phase, several different SmC* subphases have been identified and studied [2]. Many smectic phases i.e. SmC_A^* (antiferroelectric), $SmC*$ (ferroelectric), SmC_{FI2}^* (intermediate), SmC_{FI1}^* (intermediate) and SmC_α^* (incommensurate) are observed in chiral LC materials. These subphases, whose projections onto the smectic layer plane are shown in Figure 7.1. The molecules in these $SmC*$ variant phases are uniformly tilted from the layer normal but different interlayer orientational structures yield different phases [1, 2]. The existence of a new mesophase (SmC_α^*) intermediate between SmA and $SmC*$ was reported by Fukui *et al*. [5]. Similar to the SmC_A^* and $SmC*$ phases, the LC molecules in the SmC_α^* phase form a layered structure and have a finite tilt relative to the layer normal but no long range positional order. The SmC_α^* phase has a temperature-dependent periodicity ranging from three to eight layers [6]. The SmC_{FI2}^* and SmC_{FI1}^* are ferrielectric phases with four and three layer periodicity of their molecular tilt directions,

respectively. The physical origin of order in chiral LCs is the competition between the polar and steric interactions of molecules. The nearest neighbor ferroelectric interactions favor the $SmC*$ structure, but the next-nearest-neighbor antiferroelectric interactions favor a structure similar to the SmC^*_{FI2} phase.

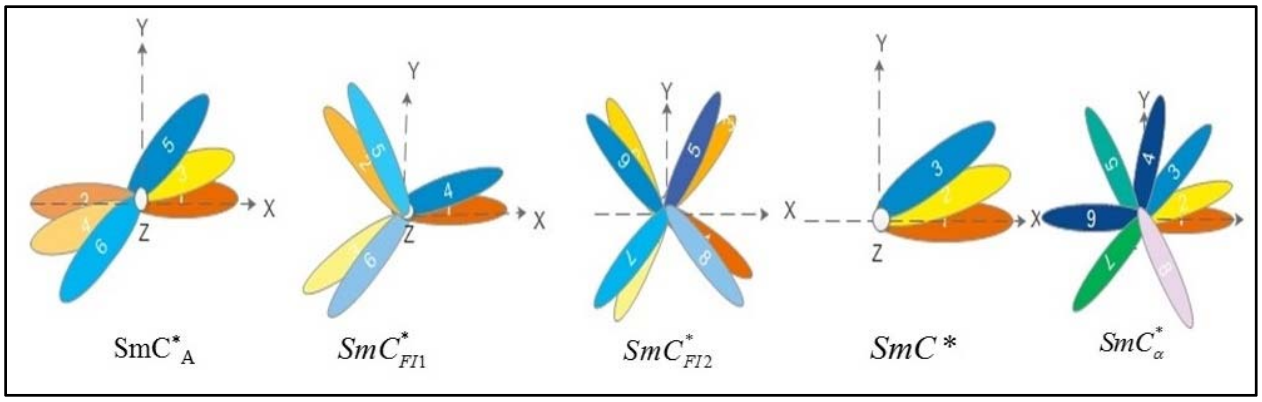

Figure 7.1: The five chiral smectic-C^*_{tilted} subphases drawn in the same order as usually observed upon heating. Ellipses, numbered by layer indices, represent the projections of the molecules onto the smectic layer plane [7].

Among antiferroelectric LC materials, a typical order of appearance of mesophases on cooling is the following: SmA- SmC^*_α - $SmC*$ - SmC^*_{FI2} - SmC^*_{FI1} -SmC*A with some of these phases are missing in many compounds [8]. Laux *et al*. have reported an unusual phase sequence in 10OHFBBB1M7 (10OHF) which has following phase sequence SmA- SmC^*_α - SmC^*_{FI2} - $SmC*$ on cooling from isotropic state [9]. The addition of a single extra CH_2 group to the achiral alkyl chain of 10OHF molecule can modify the behavior of the material [10]. Wang *et al*. [11] have also reported the existence of a phase sequence reversal in a compound 10OHF using the resonant x-ray diffraction techniques. They reported that in the pure 10OHF compound, the high-temperature SmC^*_{FI2} phase is metastable and both $SmC*$ and SmC^*_{FI2} phases are monotropic, i.e., they exist only upon cooling. The stability of $SmC*$ variant phases was checked by mixing them with other LC compound. Sandhya *et al*. [12] have reported that the both $SmC*$ and SmC^*_{FI2} of 10OHF are monotropic in the pure sample while these become thermodynamically stable in a binary mixtures with the compound 9OTBBB1M7 (C9). The electro-optical and structural properties of intermediate phase of antiferroelectric compounds seem to change as a function of temperature and applied electric field [13, 14]. Electro-optical measurements on $SmC*$ variant phases were

carried out soon after their discovery to show the ferro-, ferri- and antiferroelectric switching behavior of these phases, which enables potential applications in fast electro-optical switching applications [14]. The effect of carbon nanotubes (CNTs) on the phase sequence and dielectric property of the intermediate phases of antiferroelectric LC compounds has not been studied yet.

In this chapter, we present the experimental study of the dielectric permittivity of Octadecylamine functionalized single walled CNTs (ODA-SWCNT) doped 10OHF. Dielectric measurements carried out for the cooling cycle confirm that SmC^*_{FI2} phase exists over a higher temperature range than Sm*C** phase. The dielectric permittivity increases with increasing concentration of ODA-SWCNT. The presence of ODA-SWCNT (≤ 0.15 wt%) in 10OHFBBB1M7 (10OHF) has not altered the phase sequence but the dielectric permittivity increases with increasing concentration of ODA-SWCNT. On doping ODA-SWCNT in 10OHF, all variants of smectic phase were present all the way between *SmA* and crystallization, while SmC^*_{FI2} is suppressed at low voltage. However, at high voltage, SmC^*_{FI2} is revived with enhanced dielectric permittivity.

7.2 Materials and methods

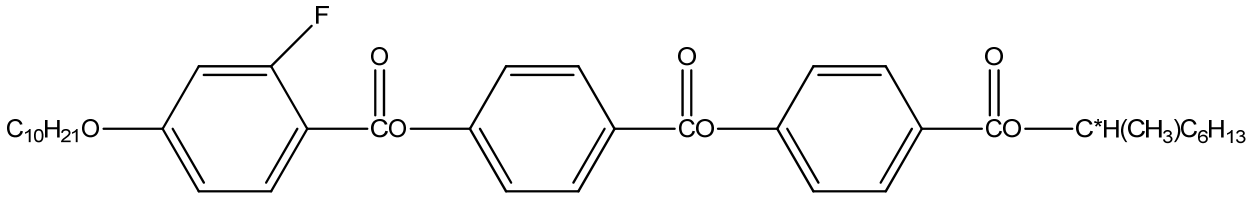

Iso- 120.7°C- *SmA* -82.5°C- SmC^*_α -72.9°C- SmC^*_{FI2} -61.4°C-SmC∗-55.5°C- Cr.

Figure 7.2: Chemical structure of the compound 10OHF and its phase transition temperature.

The liquid crystal 10OHFBBB1M7 (10OHF) was synthesized by S Kumar *et al*., Raman Research Institute, Bengaluru. The 10OHF compound belongs to benzoate ester series. Octadecylamine functionalized single walled CNT (ODA-SWCNT) was purchased from Carbon Solutions Inc. The compound 10OHF shows unusual phase sequence reversal wherein SmC^*_{FI2} phase occurring at higher temperature than the SmC* phase. The other homologs of 10OHF (namely, 9-, 11- and 12OHF) do not show reversed phase sequence behavior [15]. We have prepared nanocomposites of ODA-SWCNT and 10OHF. The nanocomposites of ODA-SWCNT with weight percent of 0.5, 0.1 and 0.15 in 10OHF are prepared. The planar aligned cells of thickness of around 8μm are prepared using PI2555 (PI) coated ITO plates. The LC cell filled with sample is mounted in a hot-

stage for dielectric measurements. The temperature of sample is controlled using a hot stage with an accuracy of ± 0.1 °C. The dielectric measurements are carried out for pure 10OHF as well as its nanocomposites with ODA-SWCNT. A lock-in amplifier (SRS, model 830) is used for conducting the dielectric measurements. We have measured the dielectric permittivity as a function of applied voltages and temperature ranging from 35ºC to 123ºC.

7.3 Results and discussion

Figure 7.3 illustrates the temperature dependence of the dielectric permittivity (ε) of pure 10OHF at 1 and 5 volt at 1 kHz frequency on cooling from isotropic liquid phase. The 10OHF shows the unusual reversed phase sequence, SmC*– SmC^*_{FI2} – SmC^*_{α} –SmA. The measured dielectric permittivity values for pure 10OHF are in good agreement with those values of reported in literature [12]. The permittivity in SmC* phase is the highest, which indicates the maximum helix strength in the LC sample. It decreases sharply near SmC* to SmC^*_{FI2} phase transition and has very low value within the temperature range of 61 to 70°C because the tilt direction of molecules in one layer is opposite to that in adjacent layer. The polarization in individual layers cancels out with each other in a four layered unit cell, which indicates the antiferroelectric behaviour of molecules in SmC^*_{FI2} phase [12].

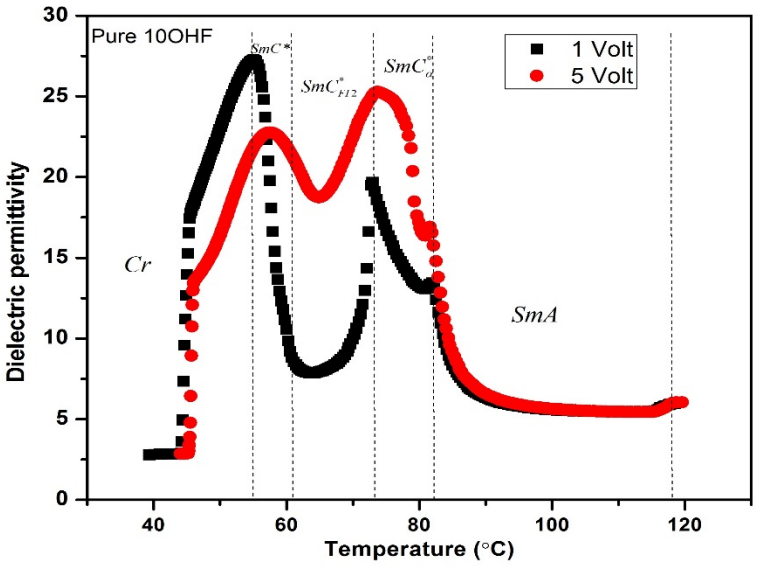

Figure 7.3: Temperature dependence of the dielectric permittivity at 1 and 5 volt at a frequency of 1 kHz for pure 10OHF in the cooling mode.

The effect of applied voltage on the dielectric permittivity is noticeable in the SmC^*_{FI2} and SmC^*_{α} phase as shown in Figure 7.3. However, there is no change in the dielectric permittivity in the *SmA* phase. At high voltage, the short helix of SmC^*_{FI2} transforms to helical SmC*. The SmC^*_{FI2} and SmC^*_{α} phases show the bistable switching behavior resulting in increase in the dielectric permittivity value. Figure 7.4 shows the variation of dielectric permittivity for the nanocomposites of 10OHF with ODA-SWCNT as a function of temperature at 1 volt with frequency of 1 kHz. On increasing the concentration of ODA-SWCNT, the dielectric permittivity increases in all chiral smectic phases at given temperature.

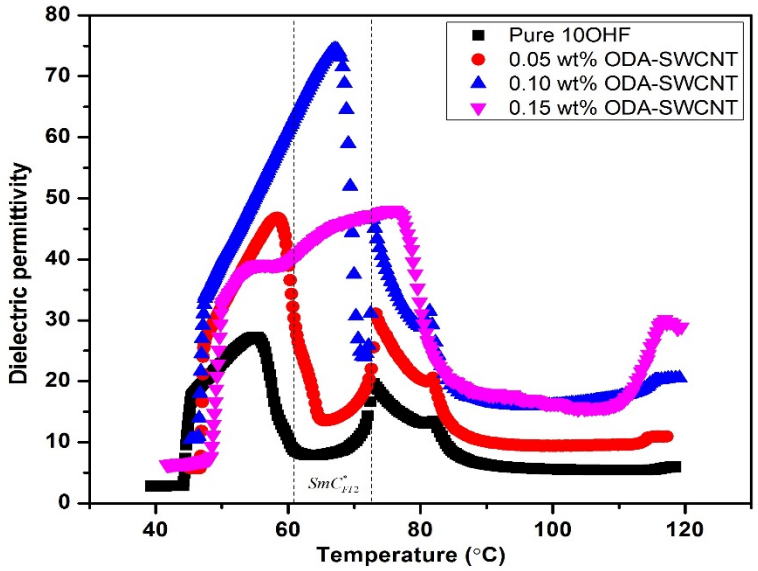

Figure 7.4: Temperature dependence of dielectric permittivity at 1 volt with 1 kHz for pure 10OHF and its ODA-SWCNT nanocomposites in the cooling mode.

The dielectric measurement is carried out in the cooling mode. It is observed that the value of dielectric permittivity increases with increasing concentration of ODA-SWCNT in 10OHF. The value of dielectric permittivity in *SmA* phase is found to be lowered than other variant phases. On further cooling the sample, it starts to increase in SmC^*_{α} phase because helix starts winding and at the higher temperature of SmC^*_{α} phase, the permittivity starts to decrease. In the SmC^*_{FI2} phase, permittivity sharply decreases due to antiferroelectric behavior. The dielectric permittivity is increased by 66% , 133% and 146% for 0.05, 0.1 and 0.15wt% ODA-SWCNT doped 10OHF sample in *SmC** phase as compared to that of pure 10OHF and the trend also continues in the other phases but with a smaller difference. The dielectric permittivity is enhanced due to the

incorporation of CNTs. In addition to increase in the dielectric constant, we observed that the range of SmC^*_{FI2} phase decreases with the increase in the concentration of ODA-SWCNT. In case of highest concentration of ODA-SWCNT, SmC^*_{FI2} phase almost disappears. It suggests that at higher concentration CNTs do not favor the four layer unit cell structure instead a ferroelectric behavior is favoured. On heating the sample from the crystallization state both SmC^*_{FI2} and Sm*C** disappear and the sample directly goes into SmC^*_{α} phase. Both Sm*C** and SmC^*_{FI2} phase are monotropic, i.e., it exists only during the cooling mode in all ODA-SWCNT nanocomposites of 10OHF.

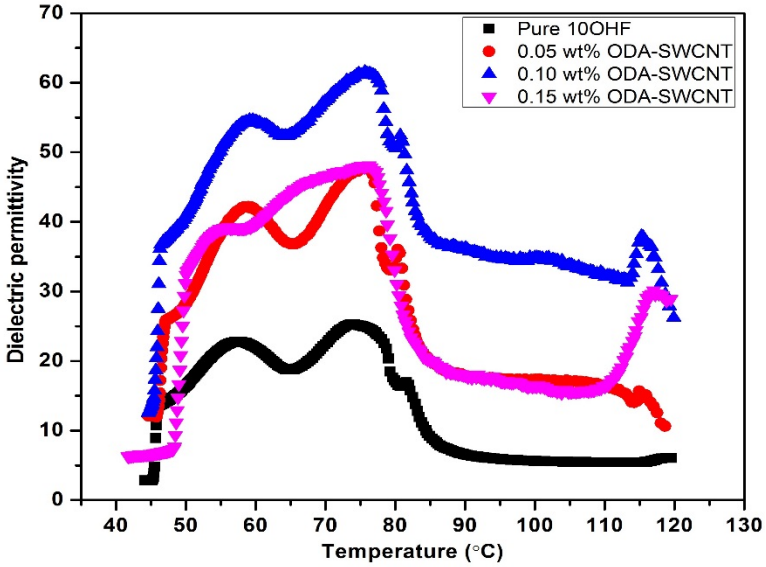

Figure 7.5: Temperature dependence of dielectric permittivity at 5 volt at 1 kHz for pure 10OHF and its ODA-SWCNT nanocomposites in the cooling mode.

The temperature variation of the dielectric permittivity for pure 10OHF and varying concentration of ODA-SWCNT is shown in Figure 7.5. The dielectric permittivity is measured at 5 volt of 1 kHz frequency. The dielectric permittivity increases systematically with increasing concentration of ODA-SWCNT. The dielectric permittivity is found to be 23, 42, 55 and 47 for pure 10OHF, 0.05wt%, 0.10wt% and 0.15wt% ODA-SWCNT doped 10OHF at 70°C, respectively. At 1 volt, we observed that with increasing concentration of ODA-SWCNT in 10OHF, the temperature range of SmC^*_{FI2} starts to decrease, whereas at 5 volt there is no change in the temperature range of SmC^*_{FI2} phase. The results suggest that at low voltage, dispersed ODA-SWCNT destabilizes the

four layer structure of SmC^*_{FI2} whereas at 5 volt they not only favor four layer structure but also contribute to the dipole moment of 10OHF.

To investigate the stability of layered smectic phase (SmC^*_{FI2}), we measured the dielectric permittivity of the sample as a function of applied voltage at a frequency of 1 kHz as shown in Figure 7.6. The dielectric measurement is carried out at 72°C, which is corresponding to SmC^*_{FI2} phase.

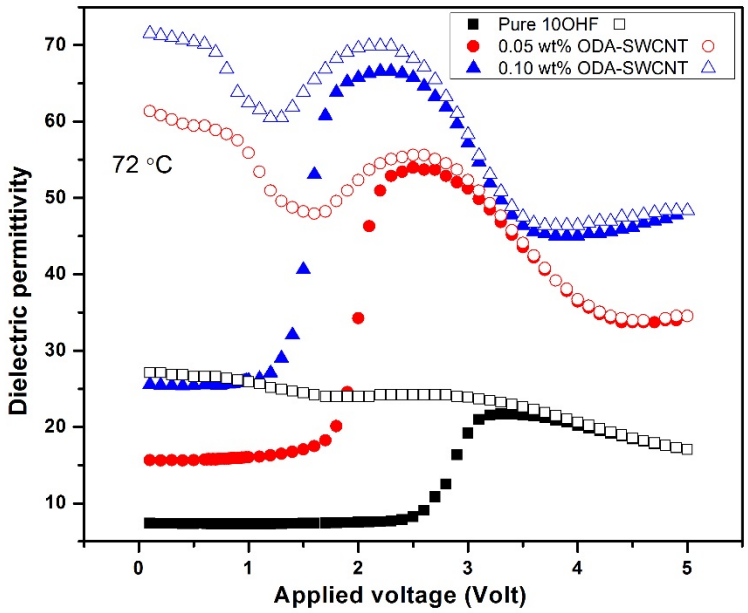

Figure 7.6: Dielectric permittivity for the pure 10OHF and its ODA-SWCNT nanocomposites at a frequency of 1 kHz as a function of applied voltage at a temperature of 72°C. Open and closed symbols represent the decreasing and increasing voltage, respectively.

In order to measure the dielectric permittivity, the LC sample was cooled to SmC^*_{FI2} from isotropic liquid phase without applying voltage across the cell. After reaching the temperature to SmC^*_{FI2}, voltage is applied across the cell upto 5 volt in step of 0.1 volt and decreased back to 0 V for measuring the dielectric permittivity. The dielectric permittivity of pure 10OHF starts to increase at 2.5 volt and the layered smectic phase (SmC^*_{FI2}) transforms to *SmC** phase at high voltage. On reversing the applied voltage from 5 volt to 0 volt, *SmC** phase does not return to SmC^*_{FI2} phase. Similar trend is observed for ODA-SWCNT doped samples, which indicates the bistable switching of the chiral LC molecules. The threshold voltage decreases with increasing

concentration of ODA-SWCNT. For the sample with 0.05 wt% and 0.1 wt% ODACNT, the threshold voltage is found to be 1.8 and 1.4 volt, which is very low as compared to that of pure sample (2.5 volt). It means that the low electric field is required to change to ferroelectric state in case of ODA-SWCNT doped sample as compared to pure sample. In the SmC^*_α phase, the dielectric permittivity remains almost same in both the direction of applied voltage. Hence, we can conclude that SmC^*_{FI2} phase is metastable. It has been observed that the temperature range of SmC^*_{FI2} phase decreases with the addition of ODA-SWCNT in 10OHF whereas, the dielectric permittivity increases in the SmC^*_{FI2} phase.

7.4 Conclusions

The effect of doping of ODA-SWCNT on the dielectric permittivity of 10OHF has been investigated. The experimental results showed that in the nanocomposites of 10OHF and ODA-SWCNT, the temperature range of SmC^*_{FI2} phase with four-layer unit cell decreases at an applied 1 volt. For the sample with highest concentration of ODA-SWCNT, SmC^*_{FI2} is almost disappeared at 1 volt whereas at 5 volt there is no change in the temperature range of SmC^*_{FI2} phase. Investigations on the 10OHF sample confirm the existence of unusual phase reversal SmC^*_α - SmC^*_{FI2} - SmC^* upon cooling from isotropic state. Both SmC* and SmC^*_{FI2} are monotropic i.e they exist only during the cooling cycle even in all ODA-SWCNT nanocomposites of 10OHF. The dispersion of ODA-SWCNTs in 10OHF enhanced the dielectric permittivity so it may be useful for designing the novel electro-optic devices.

References:

1. R. B. Meyer, L. Liebert, L. Strzelecki, P. Keller, J. Phys. Lett. 36, L69, **1975**.
2. A. Fukuda, Y. Takanishi, T. Isozaki, K. Ishikawa, H. Takezoe, J. Mater. Chem. 4, 997, **1994**.
3. H. Takezeo, E. Gorecka, M. Cepic, Rev. Mod. Phys. 82, 897, **2010**.
4. A. D. L. Chandani, E. Gorecka, Y. Ouchi, H. Takezoe, A. Fukuda, Jpn. J. Appl. Phys., Part 128, 1265, **1989**.
5. M. Fukui, H. Orihara, Y. Yamada, N. Yamamoto, Y. Ishibashi, Jpn. J. Appl. Phys. Part 2 28, L849, **1989**.
6. P. Mach, R. Pindak, A. M. Levelut, P. Barois, H. T. Nguyen, H. Baltes, M. Hird, K. Toyne, A. J. Seed, J. W. Goodby, C. C. Huang, and L. Furenlid, Phys. Rev. E. 60, 6793, **1999**.

7. M. Rajili, A. Gharbi, T. Othman, Phys. Rev. E 89, 022507, **2014**.
8. L. S. Hirst, S. J. Watson, H. F. Gleeson, P. Cluzeau, P. Barois, R. Pindak, J. Pitney, A. Cady, P. M. Johnson, C. C. Huang, A. M. Levelut, G. Srajer, J. Pollmann, W. Caliebe, A. Seed, M. R. Herbert, J. W. Goodby, M. Hird, Phys. Rev. E. 65, 041705, **2002**.
9. V. Laux, N. Isaert, V. Fay, H. T. Nguyen, Liq Cryst. **27**, 1, **2000**.
10. A. Cady, D. A. Olson, X. F. Han, H. T. Nguyen, C. C. Huang, Phys. Rev. E 65, 03070, **2002**.
11. S. T.Wang, Z. Q. Liu, B. K. McCoy, R. Pindak, W. Caliebe, H. T. Nguyen, C. C. Huang, Phys. Rev. Lett. 96, 097801, **2006**.
12. K. L. Sandhya, J. K. Song, Yu. P. Panarin, J. K. Vij, S. Kumar, Phys. Rev. E **77**, 051707, **2008**.
13. Y. Takanishi, K. Hiraoka, V.K. Agrawal, H. Takezoe, A. Fukuda, M. Matsushita, Jpn. J. Appl. Phys. 30, 2023, **1991**.
14. K. Hiraoka, Y. Takanishi, K. Skarp, H. Takezoe, A.Fukuda, Jpn. J. Appl. Phys. **30**, L1819, **1991**.
15. B. K. McCoy, Z. Q. Liu, S. T. Wang, Lidong Pan, Shun Wang, H. T. Nguyen, R. Pindak, C. C. Huang, Phys. Rev. E 77, 061704, **2008**.

Chapter 8

Nanoparticles and ionic liquid in columnar discotic liquid crystalline material

The present chapter deals with the studies on the dielectric permittivity and conductivity in thermotropic columnar liquid crystalline phase formed by triphenylene based discotic molecules. The discotic liquid crystal (DLC) and its nanocomposites are characterized using various techniques like differential scanning calorimetry, dielectric measurement, and current-voltage (*I-V*) characteristics measurement. The electrical conductivity of the nanomaterial doped DLC is observed to be enhanced by several orders of magnitude compared to that of pure DLC. The dielectric and conductivity studies of DLC doped with ionic liquids are also presented in this chapter.

8.1 Introduction

The discotic liquid crystal molecules consist of a poly aromatic core with flexible aliphatic chains. [1]. Due to the strong π–π interaction between the aromatic cores and the weak interaction between the flexible aliphatic chains, the molecules can stack one over the other, forming columns. These columns of discs can then self-organize into different lattices, for example, hexagonal lattice (Col_h), rectangular lattice (Col_r) and oblique lattice (Col_{ob}). Due to the strong π–π interaction between the cores, the typical core-core distance between the two molecules in the columnar phase is 0.35 -0.5nm. The column-column distance is around 2-4 nm depending on the length of the aliphatic substitution on the core groups [2-4]. These alkyl chains should be of sufficient length in order to provide necessary flexibility for the discotic molecules to form columnar phases.

In addition to the technologically important nematic phase exhibited by calamitic rod shaped LC molecules, the columnar phase exhibited by discotic LCs are also very interesting. The DLC in columnar phase can be considered as an organic semiconducting material. Columnar LCs can be used for one-dimensional transportation of charge, ion, and energy [5-7]. Due to the strong core-core interaction, the molecules stack one above other creating a channel. Charge movement in these materials is expected to be quasi-1-dimensional, as the conducting core of the discotic

molecule is surrounded by insulating aliphatic chains. This one-dimensional conductivity is important for a variety of applications in the areas including solar cells, photovoltaic cells, organic light emitting diodes (OLED) and field effect transistors (FET) [8-10].

In particular, the formation of self-organized monodomain in macroscopic scale plays key roles for the enhancement of properties of DLCs, i.e. fast charge (electron and hole) transports through columns. Due to very high band gap (~4ev), DLCs behave as insulator at normal conditions. One approach to enhance the conductivity of these supramolecular systems is the addition of a small quantity of either electron donors or electron acceptors. On doping appropriately, the conductivity can be enhanced by several orders of magnitude. Trinitrofluorenone, [11, 12], iodine [12], aluminium chloride [13-15], quantum dots [16] and gold nanoparticles (NPs) [17, 18] are some of the most studied dopants in the columnar liquid crystalline matrix. These dopants at low concentrations preserve the columnar phase with enhancement in the electrical conductivity by several orders of magnitude.

Remarkably, electrical conductivity was enhanced by six orders of magnitude upon doping of 1% discotic-functionalized gold nanoparticles (GNPs) into hexaheptyloxy-triphenylene DLC. It was suggested that the randomly distributed GNPs can form charge transfer complexes when sandwiched between discotic cores, thus enhancing the conductivity of the system [17]. Holt *et al.* [18] have observed an enhancement in electrical conductivity in the hexagonal columnar phase of a triphenylene-based DLC upon doping with methylbenzene thiol-covered GNPs. The enhancement in the conductivity was due to formation of small chain-like aggregates of gold NPs.

Ionic liquids are functional isotropic liquids exhibiting high ionic conductivity [20]. The ionic liquids have emerged as promising materials with unique properties such as tunable polarity, high thermal stability, negligible vapor pressure, and recyclability [21]. Their high polarity and the ability to solubilize in both inorganic and organic compounds can result in both enhanced reaction rate and higher selectivity of chemical process in contrast with conventional material. Such materials have considerable potentials as electrolytes for batteries and capacitors. In the present chapter, the electrical conductivity study provides information on the effect of doping ionic liquids into DLC on the transport properties of charge carriers.

In the present chapter, we present the results of dielectric permittivity and conductivity measurement of pure and nanoparticles doped triphenylene based DLC. The nanocomposites of

zinc sulfide (ZnS) nanoparticles and BMIM-BF_4 (1-Butyl-3-methylimidazolium tetrafluoroborate) ionic liquid with decyloxytriphenylene DLC (TP10) are prepared. The concentration of ZnS nanoparticles are 2 and 5 wt% in TP10. With this low concentration of ZnS nanoparticles, the conductivity of the nanocomposite is enhanced significantly. It has been observed that with the increase in concentration of ZnS nanoparticles, the Col_h–isotropic liquid transition temperature decreases but the crystal–Col_h transition temperature does not change significantly. Electrical conductivity increases by ~90% for the highest concentration of ZnS (5 *w*t%) nanoparticles as compared to that of pure TP10. The ionic liquid also has great impact on the dielectric permittivity and conductivity of pure TP10.

8.2 Materials and methods

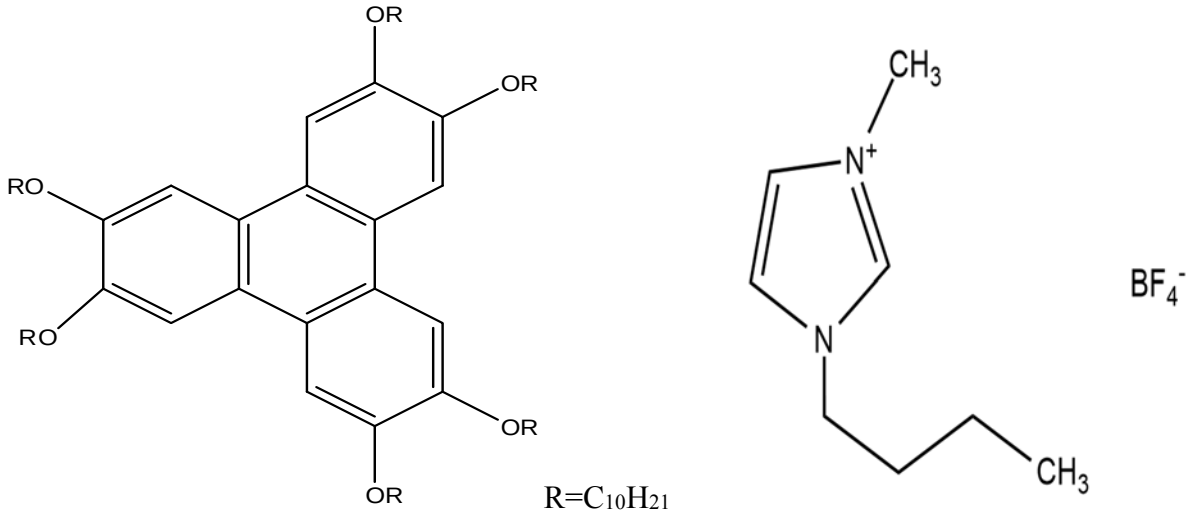

Figure 8.1: Chemical structure of TP10 [hexakis(decyloxy)triphenylene] and 1-Butyl-3-methylimidazolium tetrafluoroborate (BMIM-BF_4).

The hexakis(decyloxy)triphenylene (TP10) was synthesized by Prof. S Kumar of Raman Research Institute, Bangaluru. The phase sequence of TP10 is Cr-45°C-Col_h-69°C-Iso. The ionic liquid 1-butyl-3-methylimidazolium tetrafluoroborate (BMIM-BF_4) was provided by Prof. Anil Kumar of BITS, Pilani. The chemical structure of TP10 and BMIM-BF_4 is shown in Figure 8.1. The nanocomposites of TP10 with ZnS nanoparticles and ionic liquid BMIM-BF_4 (1-Butyl-3-methylimidazolium tetrafluoroborate) are prepared and characterized using differential scanning calorimetry and *I-V* measurement. The ZnS nanocomposites of TP10 as well as BMIM-BF_4 nanocomposites of TP10 DLC were prepared by dispersing the components in organic solvent.

After complete evaporation of organic solvent, the nanocomposites were used for further studies. The sandwiched type LC cells were prepared using indium tin oxide (ITO) coated glass plates. LC cells of ~8 μm thickness were prepared using polyimide (PI) coated ITO substrates. The PI coated ITO plates were rubbed unidirectionally using a soft cloth. The dielectric measurement on the nanocomposites of TP10 DLC at an applied 5V with frequency of 4.1 kHz was carried out in cooling mode. Slow cooling of sample from the isotropic phase generally yields spontaneous homeotropic alignment (column axis normal to the glass plates) of DLCs in LC cells.

The *I-V* measurement on pure TP10 and its nanocomposites was carried out using a Keithley source meter (Model 2400). The conductivity was measured in columnar hexagonal phase (Col_h) and the temperature is controlled using a hot stage with an accuracy of ± 0.1 °C. The silicon substrates deposited with gold electrodes were used and gap between electrodes was around 13 μm. The DLC TP10 and its nanocomposites were placed between the electrodes and voltage was applied in the in-plane geometry.

8.3 Results and discussions

8.3.1 Effect of ZnS nanoparticles on physical properties of TP10

The transition temperatures of pure TP10 and its ZnS nanocomposites are determined by differential scanning calorimetry (PerkinElmer, model DSC-4000) at a scanning rate of 5 °C per minute and the data is shown in Figure 8.2.

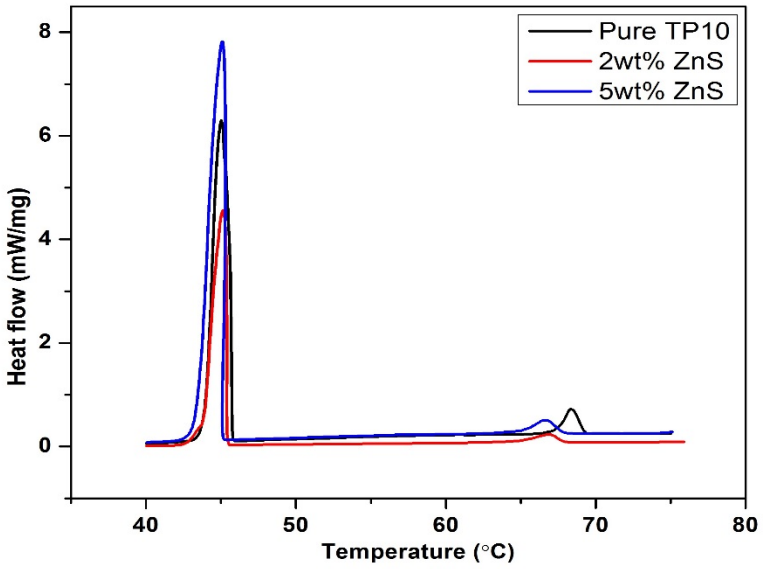

Figure 8.2: DSC curves for pure TP10 and its nanocomposites with 2 and 5 *w*t% of ZnS.

The isotropic liquid to Col_h mesophase (Col_h – Iso) transition temperature appears at 69°C for pure TP10. On cooling the sample, the crystalline state appeared at 45°C. On inclusion of ZnS nanoparticles into TP10, the Col_h - Iso transition temperature significantly decreases but crystal-to- Col_h mesophase transitions were less affected. The Col_h - Iso transition temperature was 69°C, 66.5°C and 66°C for pure TP10, 2 and 5 *wt*% of ZnS nanocomposites of TP10, respectively. With increase in the concentration of ZnS nanoparticles beyond 5 *wt*% , tendency of phase segregation and hence, a significant decrease of the Col_h - Iso transition temperature were observed.

The variation of dielectric permittivity for pure TP10 and its ZnS nanocomposites is shown in Figure 8.3. The presence of ZnS nanoparticles does not affect the permittivity of pure TP10 near the Col_h - Iso transition temperature but at low temperature in the Col_h phase, it decreases with increasing concentration of ZnS nanoparticles. For 5 *wt*% of ZnS nanocomposites of TP10, ε is reduced by 2% at 60°C as compared to that of pure TP10. The presence of ZnS nanoparticles disturbing the Col_h charge transfer along the column, it is possible that the addition of ZnS nanoparticles disrupt the ordering of columns as the temperature decreases and results in decreasing the capacitance.

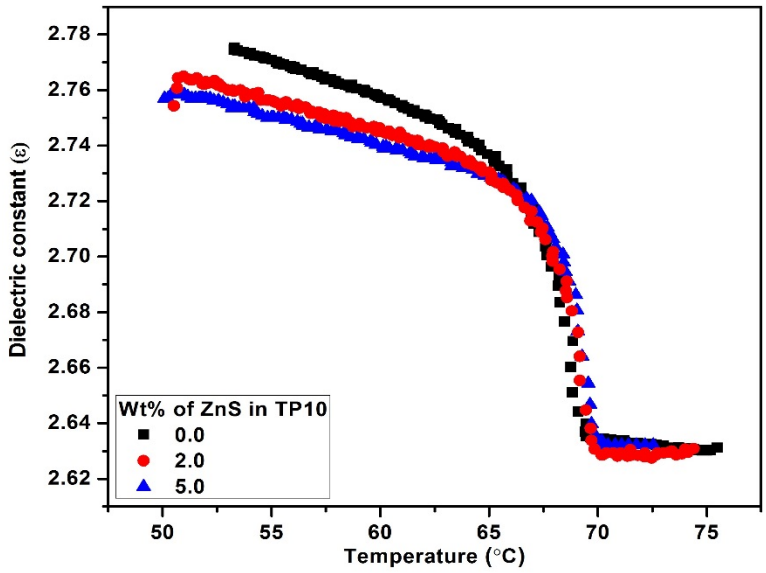

Figure 8.3: Variation of dielectric constant of pure TP10 and its ZnS nanocomposites as a function of temperature.

Conductivity of the pure TP10 and its ZnS nanocomposites as a function of temperature is shown in Figure 8.4. The incorporation of the ZnS nanoparticles in the columnar material leads to

the enhancement of the conductivity. The highest conductivity 2×10^{-7} Sm^{-1} is achieved for 5 *w*t% ZnS nanocomposites at 53°C. Even in the isotropic phase, an enhancement in the conductivity due to the incorporation of ZnS was also observed. The variation of conductivity in Col_h phase of pure TP10 is not as much as observed in case of 5wt% of ZnS nanocomposites of TP10. The result suggests that the ZnS nanoparticles are distributed in the columnar phase. Shen *et al.* [22] have observed a similar enhancement of conductivity in a system of DLC doped with functionalized gold nanoparticles (GNPs).

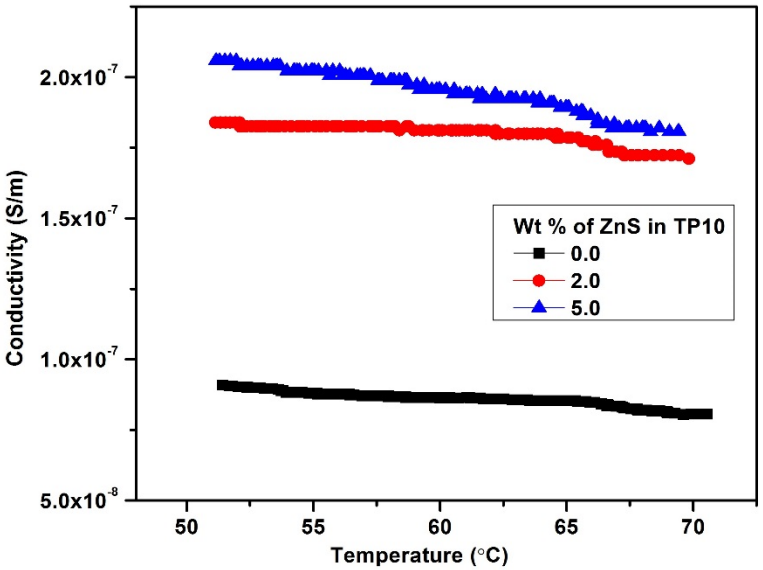

Figure 8.4: Conductivity of pure TP10 and its ZnS nanocomposites as a function of temperature.

In order to understand the effect of ZnS nanoparticles on the conductivity of TP10, the *I-V* curve measurement in the in-plane geometry was carried out and is shown in Figure 8.5. The current is measured as a function of applied voltage at 65°C in Col_h phase. At low voltage, the *I-V* characteristics of ZnS nanocomposites of TP10 is similar to that of pure TP10. On further increasing voltage, the current starts to increase rapidly in case of ZnS doped sample as compared to that of pure TP10. The measurement of *I-V* characteristics also confirm that the on addition of ZnS nanoparticles into TP10 enhances the conductivity.

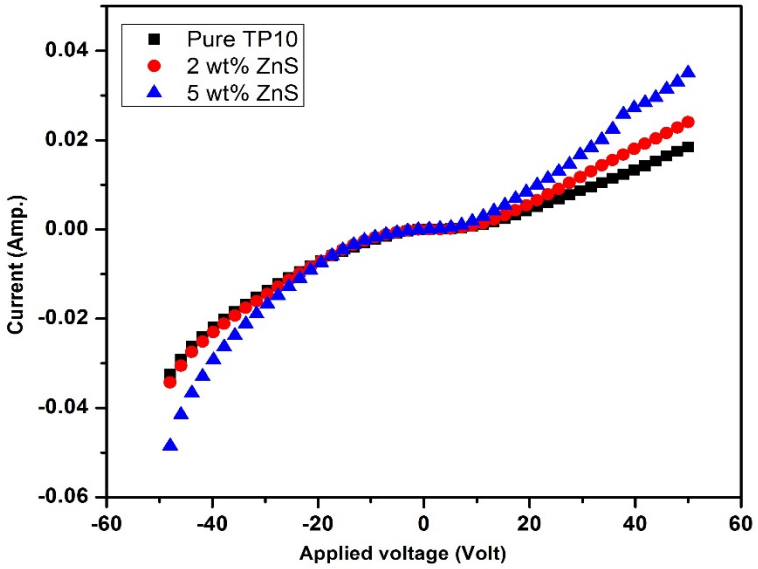

Figure 8.5: *I-V* characteristics of pure TP10 and its ZnS nanocomposites in columnar phase in plane geometery.

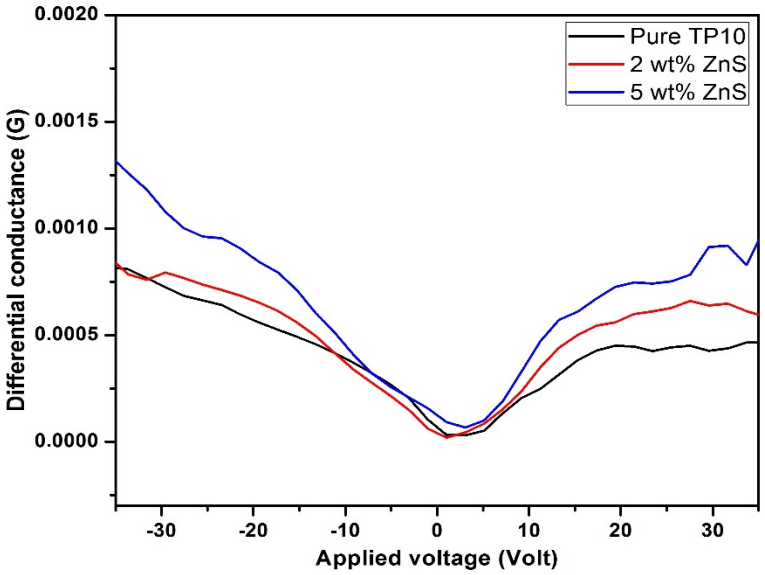

Figure 8.6: Conductance of pure TP10 and its ZnS nanocomposites in columnar phase.

The differential conductance (G=dI/dV) is calculated from *I-V* measurement. For pure TP10 and 2*wt*% of ZnS nanocomposites of TP10 DLC, the differential conductance is almost similar at V=0 volt, whereas for 5 wt% of ZnS nanocomposites of TP10 DLC, the value of G is increased.

8.3.2 Effect of ionic liquid on the dielectric permittivity and conductivity of TP10

The transition temperatures of pure TP10 and its BMIM-BF_4 nanocomposites are determined by DSC at a scanning rate of 5 °C per minute and the data is shown in Figure 8.7. We observed a shift in Col_h - Iso transition temperature as the concentration of BMIM-BF_4 increases; which appeared at 69°C, 67°C and 66.5°C for pure TP10, 2.5% and 4.5% *w*t% of BMIM-BF_4, respectively. It means Col_h of the pure TP10 is highly ordered structure as compared to the doped BMIM-BF_4. This suggests a possible destabilisation of columnar phase in case of BMIM-BF_4 nanocomposites of TP10.

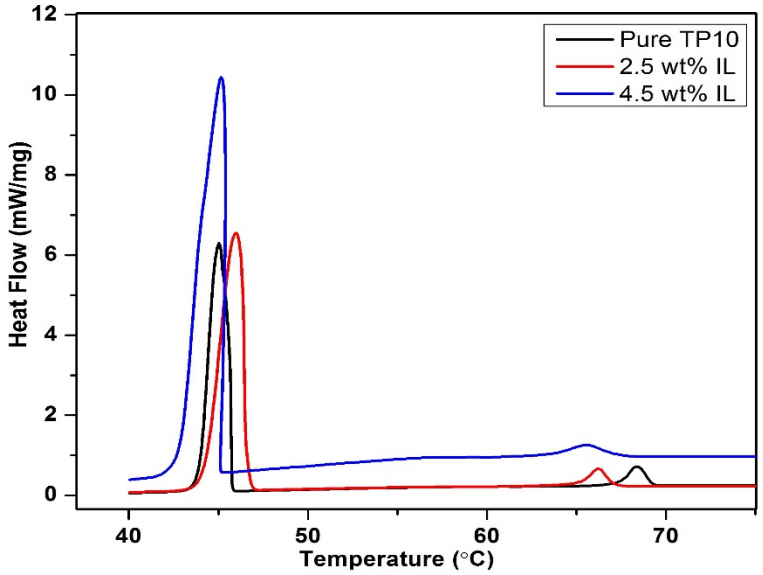

Figure 8.7: DSC curves for pure TP10 and its nanocomposites with 2.5 and 4.5 *w*t% of ionic liquid (IL) BMIM-BF_4.

The temperature variation of dielectric constant of TP10 and its mixtures with BMIM-BF_4 is shown in Figure 8.8. The dielectric constant of all samples is measured at 5 volt. On addition of BMIM-BF4 into TP10, the dielectric constant increases as compared to that of pure TP10. At low concentration (2.5 *w*t%) of BMIM-BF_4, the dielectric constant is similar to that of the TP10 whereas on increasing the amount of BMIM-BF4, it increases significantly. The dielectric constant ε of 4.5 wt% of BMIM-BF_4 nanocomposite at 65°C is 5.4 whereas, for pure TP10 ε value is 2.6. The presence of ions at the surface of substrate leads to increase in capacitance of material, hence the ε increases. At higher concentrations of BMIM-BF_4 in TP10, the variation of dielectric constant

as a function of temperature is different from that of observed at low concentration of BMIM-BF_4 in TP10 as well as pure TP10. When the concentration of BMIM-BF_4 is increased above 3.5 wt%, they tend to disrupt the columns and induce defects in it. Large size of the aggregated ionic liquids (ILs) disturbs the packing of the molecular discs as they cannot be adjusted between flexible chains without disturbing columns. This leads to decrease the dielectric constant at low temperature.

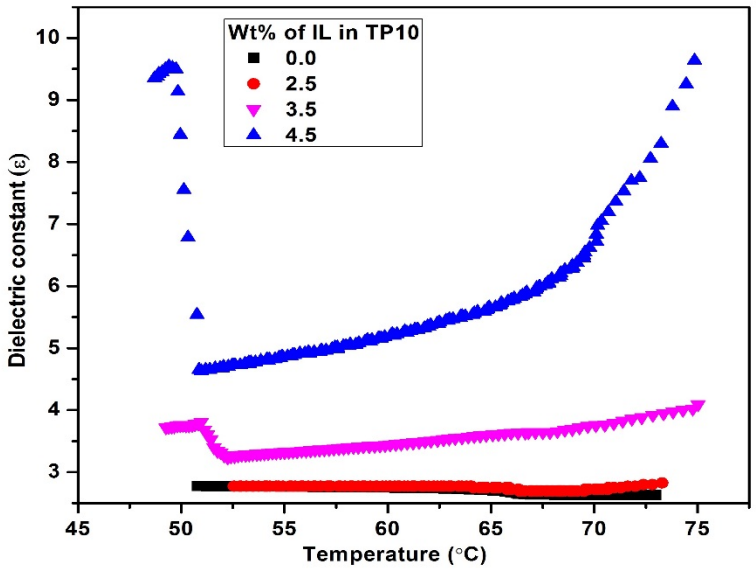

Figure 8.8: Variation of dielectric constant of pure TP10 and its BMIM-BF_4 nanocomposites as a function of temperature.

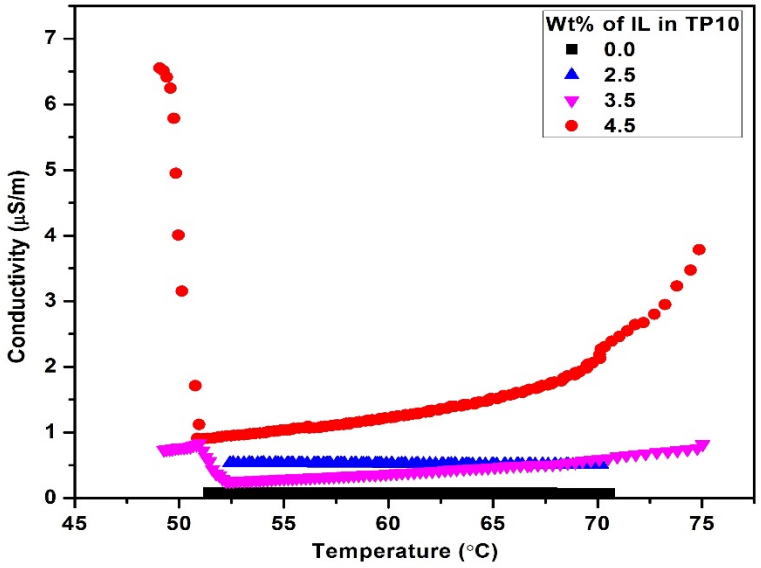

Figure 8.9: Conductivity of pure TP10 and its BMIM-BF_4 nanocomposites as a function of temperature.

The conductivity of pure TP10 and its BMIM-BF_4 nanocomposites as a function of temperature is shown in Figure 8.9. In case of highest concentration (4.5 *w*t%) of BMIM-BF_4 into TP10, the conductivity is increased significantly in the Col_h phase relative to pure TP10. The variation in the conductivity of pure TP10 as well as low concentration of BMIM-BF_4 as a function of temperature is not observed in Col_h phase. However, in case of highest concentration with 4.5 *w*t% of BMIM-BF_4, the conductivity starts to decrease unlike rest of the samples, on approaching the temperature to Iso-Col_h transition. It is possible that BMIM-BF_4 are randomly dispersed in the bulk nanocomposite but begin to aggregate within the Col_h phase upon increasing the concentration of BMIM-BF_4.

The dielectric permittivity and conductivity of BMIM-BF_4 nanocomposites of TP10 is also measured in LC cells whose substrates were treated with mixture of Hexakis(pentyloxy)triphenylene (HAT5) and graphene compound. The mixtures of HAT5 and graphene are prepared with 50-50 *w*t% of both compounds. This mixture is deposited on indium tin oxide (ITO) coated glass plates using Langmuir – Blodgett film deposition technique. The monolayer of a mixture of HAT5 and graphene is deposited onto ITO plates at target surface pressure (π_t) 15mN/m. We used LB film of mixed monolayer of HAT5 and graphene as an aligning layer and then LC cells were prepared. Both dielectric constant and conductivity of BMIM-BF_4 nanocomposites of TP10 are enhanced with respect to value observed for pure TP10. The variation of dielectric constant for TP10 and its BMIM-BF_4 nanocomposites as a function of temperature in the cells treated with mixture of HAT5 and graphene is shown in Figure 8.10. In case of BMIM-BF_4 nanocomposites of TP10 samples, dielectric constant is found to be higher than the pure TP10. Dielectric constant ε of pure TP10, 2.5 and 4.5 *wt*% of BMIM-BF_4 nanocomposites of TP10 are found to be 2.64, 4.6 and 7.8 at 65°C, respectively. The value of ε in isotropic phase increases with the increase in concentration of BMIM-BF_4 in TP10. This feature suggests that there is an additional dipolar contribution from the BMIM-BF_4 to the total permittivity of the medium. In case of BMIM-BF_4 doped samples, on cooling from isotropic state, the variation of ε as a function of temperature shows a decreasing trend. It might be due to aggregation of ILs which causes the decrease in the order of DLC as confirmed by conductivity studies.

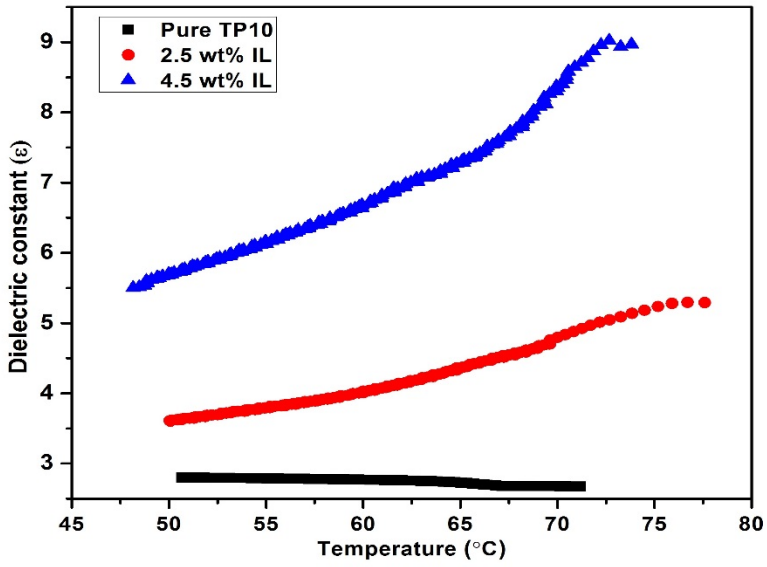

Figure 8.10: Variation of dielectric constant of TP10 and its BMIM-BF4 nanocomposites as a function of temperature in the cells treated with mixture of HAT5 and graphene.

The mixture of HAT5 and graphene is used as an alignment layer because the structure of graphene is somewhat similar to DLC with aromatic rings, which may help to align the DLC molecules. The column axes of TP10 molecules align normal to plane of substrate due to π–π interaction between TP10 and graphene. The conductivity measured for TP10 and its BMIM-BF_4 nanocomposites in the cell treated with mixtures of HAT5 and graphene is found to be higher than that of measured in the cell treated with polyimide. It suggests that the presence of HAT5 and graphene in the alignment layer not only leads to an increase in the conductivity but also improves the alignment of DLC molecules.

Conductivity of pure TP10 and its BMIM-BF_4 nanocomposites as a function of temperature in the cells treated with mixture of HAT5 and graphene is shown in Figure 8.11. The addition of BMIM-BF_4 leads to change in the conductivity value in isotropic phase relative to the pure TP10 sample. The highest measurable value of the conductivity with the highest concentration is about 5×10^{-6} S/m in the isotropic state. At high temperature, some ionization might take place providing further increase in number of charge carriers leading to increase in the electrical conductivity. In case of highest concentration of IL, conductivity increases by an order of magnitude compared to that of pure TP10 in Col_h mesophase. However, in doped samples, it decreases as the temperature decreases in the Col_h phase. On decreasing the temperature from isotropic liquid phase to Col_h mesophase, initially conductivity is high when alignment is good but when temperature further

decreases, perhaps due to aggregation of ILs, alignment deteriorates and hence conductivity decreases.

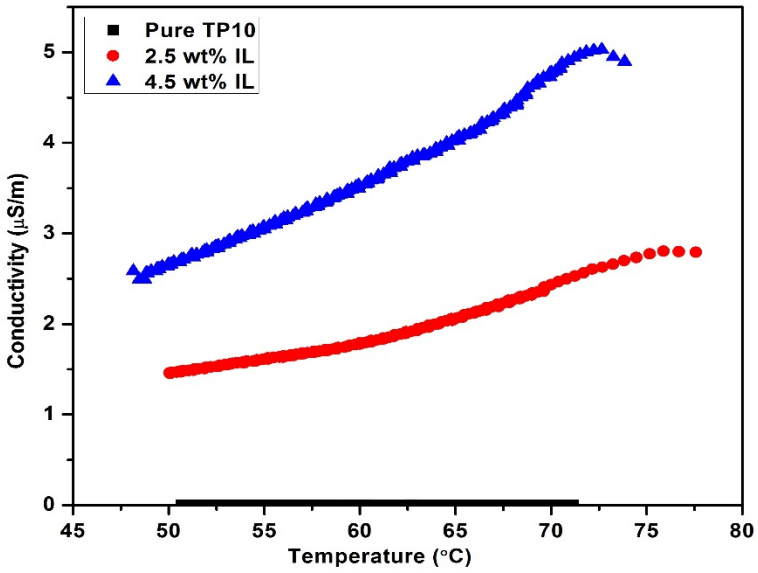

Figure 8.11: Conductivity of pure TP10 and its BMIM-BF4 nanocomposites as a function of temperature in the cells treated with mixture of HAT5 and graphene.

8.4 Conclusions

Effects of ZnS nanoparticles and ionic liquid BMIM-BF_4 of different concentrations in discotic liquid crystal (TP10) on the dielectric constant and conductivity are studied. DSC studies show appreciable depreciation of the Col_h to isotropic liquid transition temperature, while only minor change in the crystal to Col_h or Col_h to crystal transition temperatures has been observed. We observed that conductivity in the TP10 mixed with ILs is found to be higher than that of ZnS doped TP10. The dielectric constant also increases in the TP10 mixed with ILs. The highest concentration, i.e. 4.5 *wt*% of ILs showed a decreasing trend of conductivity when cooled, in the columnar phase. We also observed that the conductivity measured for mixtures of IL and TP10 in the cell treated with mixtures of HAT5, and graphene is found to be higher than that of measured in the cell treated with polyimide. It suggests that the presence of HAT5 and graphene in the alignment layer not only increase the conductivity but also improve the alignment of DLC mesogens. Observed results of the inorganic–organic composite system is extremely useful for many device applications such as one dimensional conductor, photovoltaic solar cell, photoconduction and light emitting diodes.

References:

1. S. Chandrasekhar, B. K. Sadashiva, K. A. Suresh, Prarnana J. Phys., 9,471, **1977**.
2. S. Kumar, Chem. Soc. Rev. 35, 83, **2006**.
3. S. Segeyev, W. Pisula, Y. H. Greets, Chem. Soc. rev. 36, 1902, **2007**.
4. C. Kavitha, B. S. Avinash, S. Kumar, Mater Chem Phys. 133, 635, **2012**.
5. R. J. Bushby, O.R. Lozman, Solid State Mater. Sci. 6, 569, **2002**.
6. C. F. Van Nostrum, R. J. M. Nolte, Chem. Commun. 2385, **1996**.
7. L. S. Mende, A. Fechtenkotter, K. Mullen, E. Moons, R. H, Friend, J. D. Macken, Science. 293, 1119, **2001**.
8. I. Seguy, P. Destruel, H. Bock, Synth. Met. 111, 15, **2000**.
9. T. D. Choudhury, N. V. S. Rao, R. Tenent, J. Phys. Chem. B.115,609, **2011**.
10. S. Supreet, R. Pratibha, S. Kumar, Liq. Cryst. 41, 933, **2014**.
11. S. Chandrasekhar and V. S. K. Balagurusamy, Proc. R. Soc. Lond. A, 458, 1783, **2002**.
12. G. B. M. Vaughan, P. A. Heiney, J. P. Mccauley. Jr., Phys. Rev. B, 46, 2787, **1992**.
13. N. Boden, R. J. Bushby, J. Clements, J. Chem. Phys. 98, 5920, **1993.**
14. N. Boden, R. J. Bushby, J. Clements, J. Mater. Sci. Mater. Electronics, 5, 83, **1994**.
15. N. Boden, R. J. Bushby, J. Clements, M. V. Jesudason, P. F. Knowles, G. Williams, Chem. Phys. Lett. 152, 94, **1988**.
16. N. Yadav, S. Kumar, R. Dhar, RSC Adv. 5, 78823, **2015**.
17. S. Kumar, S. K: Pal, P. S. Kumar, V. Lakshminarayanan, Soft Matter. 3, 896, **2007**.
18. L. A. Holt, R. J. Bushby, S. D. Evans, A. Burgess, G. Seeley, J. Appl. Phys. 103, 063712, **2008**.
19. H. Zhao, S. V. Malhotra, Aldrichimica Acta. 35, 75, **2002**.
20. V. S. K. Balaguruswamy, S. K. Prasad, S. Chandrasekhar, S. Kumar, M. Manickam, C. V. Yelamaggad, Prarnana J. Phys. 53, 3, **1999**.
21. P. Wasserscheid, W. Keim, Angew. Chem. Int. Ed. Engl. 39, 21, **2000.**
22. Z. Shen, M. Yamada, M. Miyake, J. Am. Chem. Soc.129,14271, **2007**.

Chapter 9

Conclusions and future scope of our studies

9.1 Conclusions

Liquid crystals (LCs) are the fourth state of matter whose order lies between that of 3-dimensioanlly ordered solids and completely disordered fluids. The LCs are classified into two categories viz., thermotropic and lyotropic. The phases of thermotropic LCs are driven as a function of temperature. The thermotropic LC material can exhibits many phases as a function of temperature. Nematic liquid crystal (NLC) is the simplest among the LC phases which possesses orientational order but no positional order. The average collective orientation direction of the molecules is known as director of the NLC. Electric field induced director reorientation of the NLC make them interesting candidate from application point of view. We have investigated the effect of nanomaterials on the physical properties mainly dielectric constant (ε), threshold voltage (V_{th}), elastic constants and optical response time of LCs. The measurement of these physical parameters is essential as these parameters govern the performance of LC based devices. This thesis mainly focuses on the dielectric and electro-optic properties of LCs doped with nanomaterial.

A systematic study on functionalized carbon nanotube (CNT) doped LC exhibiting nematic phase as well as smectic A phase has been discussed in chapter 3. We observed that the Freedericksz threshold voltage, V_{th} value of octadecylamine functionalized SWCNT (ODA-SWCNT) nanocomposites of n-octyl cyanobiphenyl (8CB) in the nematic phase is enhanced as compared to that of pure 8CB. The dielectric anisotropy as a function of reduced temperature ($T-T_{NI}$) decreases with increase in concentration of ODA-SWCNT. The elastic constants (K_{11} and K_{33}) of nanocomposites of 8CB doped with ODA-SWCNT as a function of temperature are estimated. We found that the ratio of bend to splay elastic constants (K_{33}/K_{11}) of ODA-SWCNT nanocomposite of 8CB is enhanced considerably as compared to that of pure LC near to the nematic to smecticA

transition temperature. The temperature range of smecticA phase increases with increase in concentration of ODA-SWCNT. The electro-optic response rise time increased at low concentration of ODA-SWCNT (≤0.05 *wt*%) indicating the presence of ODA-SWCNT at the alignment layer. At higher concentrations (>0.05 *wt* % and ≤ 0.15 *wt*%) of ODA-SWCNT the rise time decreases due to formation of the large size nematic domains around the ODA-SWCNT dispersed in the nematic medium. At the lower concentration of ODA-SWCNTs (0.05 *wt*%), the anchoring of the nanotubes at the LC-electrode interface is favoured. At higher concentration of the ODA-SWCNTs, in addition to the anchoring at the interface, the nanotubes, which are dispersed in the LC medium increases the orientational ordering.

In general, twisted nematic (TN) cells are used for the commercial LCDs. The effect of ODA-SWCNT on the response characteristics, i.e., rise time and decay time of a NLC in TN mode has been presented in chapter 4. The optical response time of ODA-SWCNT nanocomposites of 4-trans-pentylcyclohexylcyanobenzene (5PCH) was reduced compared to that of pure 5PCH, whereas an enhancement in the value of threshold electric field (E_{th}) was observed. A fast response time is observed with increase in concentration of ODA-SWCNT in 5PCH.

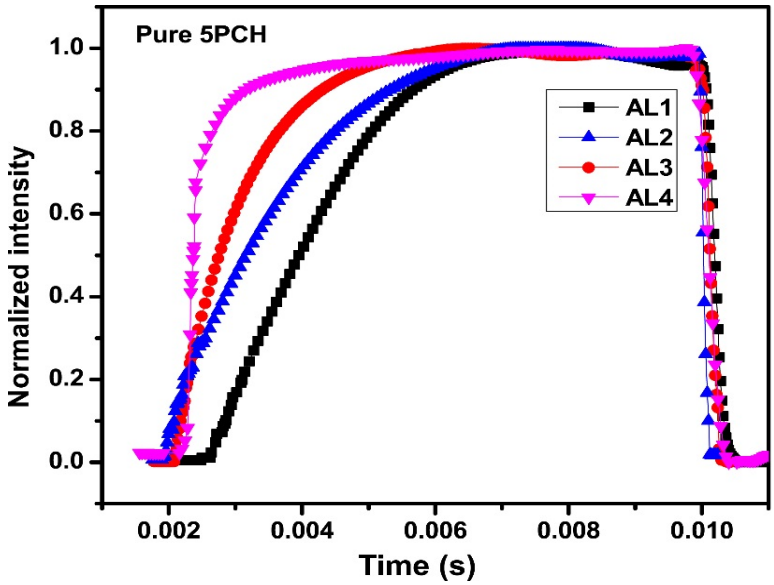

Figure 9.1: Measured oscillogram for 5PCH in TN cells prepared with pure PI and mixtures of PI and ODA-SWCNT as the alignment layers at an applied voltage of 10V. AL1, AL2, AL3 and AL4 correspond to LC cell prepared with pure PI, 0.16, 0.33 and 0.66 µg of ODA-SWCNT in 1 ml PI solution, respectively.

The optical response of pure 5PCH in TN cells prepared using mixtures of polyimide (PI) and ODA-SWCNT as alignment layer is investigated. The optical response time of pure 5PCH in a TN cell fabricated with a mixture of PI and ODA-SWCNT reduces by ~ 75 % compared to the one prepared using pure PI alignment layer as shown in Figure 9.1. The presence of ODA-SWCNT in the alignment layer enhances the surface anchoring of the NLC molecules leading to increase in elastic constant and reduction in the rotational viscosity of the NLC, which leads to a reduction in the optical response time of NLC. The surface roughness of ODA-SWCNT incorporated PI alignment layer treated substrate was reduced compared to that of pure PI treated substrate. The π-π interaction between the ODA-SWCNT, NLC and the PI alignment layer leads to enhanced surface anchoring of the NLC molecules at the substrate. This strong surface anchoring gives rise to increase in elastic constant, which gets reflected as reduction in the optical response time of NLC. Our investigation on TN cells prepared using mixture of ODA-SWCNT and PI alignment layer indicates that the increase in E_{th} might be due to strong anchoring between LC and ODA-SWCNT.

We have investigated the effect of ODA-SWCNT as an alignment layer on the electro-optic switching characteristics of 4-heptyl-4′-cyanobiphenyl (7CB) in planar aligned geometry. The results are presented in chapter 5. We found that the presence of the ODA-SWCNT in the alignment layer enhances the dielectric anisotropy. The rise time and decay time increases due to strong anchoring between 7CB and ODA-SWCNT. The effect of alignment layer of ODA-SWCNT deposited using spin coating and Langmuir-Blodgett (LB) technique on the V_{th} and response time of pure 7CB has been investigated. We observed that the dielectric anisotropy in the cell treated with LB film of ODA-SWCNT is found to be reduced as compared to pure PI treated cell. The response time of LC cells treated with only ODA-SWCNT is comparable to pure PI sample. The CNT as an alignment layer, can be employed for the fabrication of optical device with high transmittance of light.

In chapter 6, the effect of incorporation of octadecylamine capped cadmium selenide quantum dots (CdSe QDs), titanium dioxide (TiO_2) nanoparticles and polyethylene glycol functionalized single walled CNT (PEG-SWCNT) in 5PCH on their dielectric permittivity, and elastic constant is presented. The 5PCH was doped with different concentrations of the CdSe QDs. As QDs have shown their potential to tune the alignment of LC molecules, therefore the alignment of NLC

molecules on incorporation of CdSe QDs have been studied. The addition of the QDs at low concentrations into 5PCH favors homogeneous alignment. The QDs doped 5PCH is found to have a lower V_{th} than that of pure 5PCH. The value of V_{th} decreases with increasing concentration of the QDs. The dielectric permittivity is estimated as a function of temperature in both planar and homeotropic geometry. Doping QDs leads to increase in the dielectric anisotropy in comparison with that of pure 5PCH. Improved dielectric anisotropy in CdSe QD doped 5PCH indicates the self-assembly of QDs which can align themselves along with the average direction of NLC molecules (director). In addition to QDs, we investigated the electro-optical and physical properties of nanocomposites of 5PCH with semiconducting TiO_2 nanoparticles and PEG-SWCNT dopants. The incorporation of different shape anisotropic nanomaterials in the LC matrix can introduce different level of defects and ordering. Such perturbation of LC medium has significant effect on their electro-optic and dielectric properties. Considering the shapes of nanomaterials e.g., spherical and rod shape (uniaxial), the dielectric permittivity and elastic constant of the nanocomposites of 5PCH is discussed in chapter 6. In case of TiO_2 doped 5PCH, the V_{th} is reduced whereas dielectric anisotropy is enhanced. For PEG-SWCNT doped 5PCH, V_{th} is reduced, however, the dielectric anisotropy is slightly reduced compared to pure 5PCH. These nanocomposites of NLC provide an opportunity to develop LC based optoelectronic devices with improved electro-optic switching.

In chapter 7, the effect of ODA-SWCNT on the dielectric permittivity of a LC, which exhibits unusual smectic phase sequence is presented. The compound, 10OHFBBB1M7 (10OHF) which exhibits following phase sequence: SmA- SmC^*_α - SmC^*_{FI2} - $SmC*$ on cooling from isotropic state. The SmC^*_{FI2} is ferrielectric phase with four layer periodicity of their molecular tilt directions. The stability of $SmC*$ variant phases is checked by doping them with ODA-SWCNT. Dielectric measurements carried out for the cooling cycle confirm that SmC^*_{FI2} phase exists over a higher temperature range than Sm*C** phase. The phase sequence SmC^*_α - SmC^*_{FI2} - $SmC*$ was observed in pure 10OHF as well as its ODA-SWCNT nanocomposites. Both SmC* and SmC^*_{FI2} are monotropic i.e they exist only during the cooling mode. The dielectric permittivity increases with increasing concentration of ODA-SWCNT. The dielectric measurement carried out at an applied voltage of 1 volt confirms that the temperature range of SmC^*_{FI2} phase decreases in the

nanocomposites of 10OHF and ODA-SWCNT. For the sample with highest concentration of ODA-SWCNT, SmC^*_{FI2} almost disappears at 1 volt whereas at 5 volt there is no change in the temperature range of SmC^*_{FI2} phase.

In addition to the calamitic LC molecules, the columnar phases exhibited by discotic LCs are also very interesting. The discotic liquid crystal (DLC) in columnar phase can be considered as an organic semiconducting material. In chapter 8, the study on dielectric permittivity and conductivity of the thermotropic columnar liquid crystalline phases formed by triphenylene based DLC and its zinc sulfide (ZnS) nanoparticle nanocomposites is presented. The conductivity changes effectively after the addition of nanoparticles in the pure DLC system. The addition of ZnS nanoparticles enhance the dielectric constant of DLC. The electrical conductivity of these nanocomposites was observed to be enhanced by ~ 90% compared to the pure DLC. The in-plane charge transport mechanism for LC sample was studied by recording *I-V* (current- voltage) curve at different temperatures.

9.2 Future scope

In this thesis we have presented the results of experimental studies on nanocomposites of LC. We have carried out dielectric and electro-optical studies on functionalized CNT and nanoparticles doped LC systems. In addition to these experimental studies of the nanocomposites of LC, other experimental techniques (static and dynamic XRD, surface anchoring, photoluminescence spectroscopy) on these systems would reveal more detailed and important information about physical parameters of the LC samples. Our recent research indicates that the functionalized CNT as an alignment layer can be exploited for improved optical LC based display devices. We investigated that the TiO_2 nanoparticles doped 5PCH exhibits enhanced dielectric anisotropy as compared to pure 5PCH. These nanocomposites of 5PCH with TiO_2 nanoparticles can further be studied for the optical response time. The effect of mixture of TiO_2 nanoparticles and PI as an alignment layer on the physical properties and response time of LC can also be studied. The nematic phase of LCs has been exploited so far for imparting the orientational order onto nanomaterials. In addition to the nanocomposites of NLC, the study of nanocomposites of discotic LC is also of great interest. The Langmuir-Blodgett (LB) film of discotic LC can be transferred from air-water interface to solid substrate. The LB film of such nanocomposites can be employed for the fabrication of organic solar cell and the performance of the device can be studied under the

influence of various physical parameters. We believe that this research will lead to great improvement in understanding the fundamentals of self-assembly phenomena of nanomaterials in LC, and can be useful for potential applications, such as faster response LC display devices and photovoltaic application.

List of publications

Publications in international journals

1. Fast response in TN liquid crystal cells: effect of functionalised carbon nanotubes
   Jitendra Kumar, V. Manjuladevi, R. K. Gupta, S. Kumar, *Liquid Crystals* (*Taylor & Francis*), **43**, 488-496 (2016).
2. Effect of octadecylamine-functionalised SWCNTs on the elastic constants and electro-optic response of a liquid crystal
   Jitendra Kumar, V. Manjuladevi, R. K. Gupta, S. Kumar, *Liquid Crystals* (*Taylor & Francis*), **42**, 361-369 (2015).
3. Transparent ITO films for liquid crystal display application
   V. Manjuladevi, Jitendra Kumar, R. K. Gupta, *Rev. Adv. Sci. Eng*. *American Scientific Publishers (ASP),* **2**, 305-312 (2013).
4. Morphological transformation in Langmuir-Blodgett films of stearic acid due to change in orientational direction of substrate normal relative to compression direction
   K. Choudhary, J. Kumar, V. Manjuladevi & R. K. Gupta (*Communicated*)
5. Effect of ODA-SWCNT on the dielectric property of a chiral smectic liquid crystal
   J. Kumar, V. Manjuladevi, R. K. Gupta, S. Kumar (*Communicated*)

Publications in conferences

1 Electro-optic and dielectric studies on quantum dot doped nematic liquid crystal
   Jitendra Kumar, R. K. Gupta, S. Kumar, V. Manjuladevi, *Macromolecular Symposia (Wiley)*, **357**, 47-51 (2015).

2 Reduction of threshold electric field on doping nematic liquid crystal with functionalized CNT, Jitendra Kumar, R. K. Gupta, Manjuladevi V., *AIP conference proceedings,* **1536**, 693-694 (2013).

3 Effect of functionalized CNT on nematic anchoring
   Jitendra Kumar, R. K. Gupta, S. Kumar, Manjuladevi V., *Proceedings of International Liquid Crystal Conference,* 5551-0449, held at Mainz during August 19-24 (2012).

4. Functionalized CNT and Liquid Crystal
   Manjuladevi.V, Jitendra Kumar, R. K. Gupta, *National Conference on Condensed Matter Physics*, **2**, 30-35 (2012).

List of Presentations

1. **Poster presentation in National Conference on Liquid Crystal (NCLC-22**) at DIT university, 21-24 Dec. 2015, "Electro-optic switching studies on functionalized SWCNT nanocomposites of Octyl cyanobiphenyl".
2. **Poster presentation in International Conference on Soft Materials (ICSM 2014) ,held at MNIT Jaipur** During 6^{th}-10^{th} Oct 2014, "Electro-optic and dielectric studies on quantum dot doped nematic liquid crystal".
3. **Poster presentation in International Conference on Applied Physics and Material Science (RAM),** GCET Bikaner, Rajasthan which was held on Feb 1-2 2013, in "Reduction of Threshold Electric Field on Doping Nematic Liquid Crystal with Functionalized CNT".
4. **Poster presentation in International Conference on Nanomaterials & Nano technology (ICNANO)** at university of Delhi New Delhi, India, 18 - 21 December 2011, "Effect of functionalized carbon nanotube on electro-optic and dielectric properties of a nematic liquid crystal"
5. **Poster presentation in the National Conference on Condensed Matter Physics, BITS Pilani campus** , Pilani, Feb 24-25, 2012 " Effect of Electrical Field on Liquid Crystal-Carbon Nanotube Dispersion".

BRIEF BIOGRAPHY OF THE CANDIDATE

Mr. Jitendra Kumar obtained his M.Sc. degree in physics from University of Rajasthan, Jaipur in 2011. He is currently pursuing Ph.D. from BITS, Pilani in the field of soft condensed matter physics (experimental) as "Effect of nanomaterial dopants on the physical properties of liquid crystals" since August 2011. His research interests include the physical and electro-optic properties of liquid crystals doped with nanomaterials. He has published three papers in international journals and some more papers are under communication. In addition to this, he has participated and presented his work in several national and international conferences of high repute.

BRIEF BIOGRAPHY OF THE SUPERVISOR

Prof. V. Manjuladevi has acquired her Ph.D. from Raman Research Institute, Bengaluru in the field of physical properties of thermotropic liquid crystals in the year 2004. She has carried out research in the field of ferroelectric liquid crystals as a post doctoral fellow in Trinity College, Dublin, Ireland from 2005–2006. She joined BITS Pilani in December 2006 and currently, she is an associate professor in the department of physics, BITS Pilani. Her main research interests are electro-optic switching measurement and dielectric studies on liquid crystals and their nanocomposites, thin films of liquid crystals and sensors. She has completed three DST funded research projects either as PI or Co-PI. She has published more than 30 papers in reputed international journals.